Model Development and Analysis of Distribution Feeders with High Penetration of PV Generation Resources

by

Adarsh Nagarajan

A Dissertation Presented in Partial Fulfillment
of the Requirement for the Degree
Doctor of Philosophy

Approved December 2014 by the
Graduate Supervisory Committee:

Raja Ayyanar, Chair
Gerald Heydt
George Karady
Vijay Vittal

ARIZONA STATE UNIVERSITY

May 2015

© 2015 by Adarsh Nagarajan
All Rights Reserved

ABSTRACT

An increase in the number of inverter-interfaced photovoltaic (PV) generators on existing distribution feeders affects the design, operation, and control of the distribution systems. Existing distribution system analysis tools are capable of supporting only snapshot and quasi-static analyses. Capturing the dynamic effects of the PV generators during the variation in the distribution system states is necessary when studying the effects of controller bandwidths, multiple voltage correction devices, and anti-islanding. This work explores the use of dynamic phasors and differential algebraic equations (DAE) for impact analysis of the PV generators on the existing distribution feeders.

The voltage unbalance induced by PV generators can aggravate the existing unbalance due to load mismatch. An increased phase unbalance significantly adds to the neutral currents, excessive neutral to ground voltages and violate the standards for unbalance factor. The objective of this study is to analyze and quantify the impacts of unbalanced PV installations on a distribution feeder. Additionally, a power electronic converter solution is proposed to mitigate the identified impacts and validate the solution's effectiveness through detailed simulations in OpenDSS.

The benefits associated with the use of energy storage systems for electric-utility-related applications are also studied. This research provides a generalized framework for strategic deployment of a lithium-ion based energy storage system to increase their benefits in a distribution feeder. A significant amount of work has been performed for a detailed characterization of the life cycle costs of an energy storage system. The objectives include - reduction of the substation transformer losses, reduction of the life cycle cost for an energy storage system, and accommodate the PV variability.

The distribution feeder laterals in the distribution feeder with relatively high PV generation as compared to the load can be operated as microgrids to achieve reliability, power quality and economic benefits. However, the renewable resources are intermittent and stochastic in nature. A novel approach for sizing and scheduling the energy storage system and microtrubine is proposed for reliable operation of microgrids. The size and schedule of the energy storage system and microturbine are determined using Benders' decomposition, considering the PV generation as a stochastic resource.

ACKNOWLEDGEMENTS

I express my sincere gratitude to my advisor Dr. Raja Ayyanar for his guidance and leadership throughout my graduate studies. This work would not be the same without his superior insight and knowledge. His commitment to education and research is an inspiration. I am grateful to Arizona Public Service and PSERC for its continued support through the duration of this work. Gratitude is also due to my graduate supervisory committee, comprising of Dr. Gerald Heydt, Dr. Vijay Vittal and Dr. George Karady, Dr. Daniel Tylavsky for their time and support.

I also take this opportunity to thank the distinguished faculty of the power engineering program at Arizona State University, for their many contributions towards my comprehensive growth over the period of my education here. Appreciations are also due to all my fellow students at Arizona State University for their support. I am also grateful for my entire family, my parents Mr. Srikantaiah Nagarajan and Mrs. Usha Rajan, and my brother Dr. Harsha Nagarajan.

TABLE OF CONTENTS

Page

LIST OF TABLES ix

LIST OF FIGURES xi

LIST OF SYMBOLS xvii

CHAPTER

1 INTRODUCTION 1

1.1 Dynamic Analysis of Distribution Feeders with High Penetration of PV Generators 5

1.1.1 Dynamic Phasor Analysis of Distribution Feeders in Transient Analysis Tools 6

1.1.2 Dynamic Analysis of Distribution Systems Using Differential Algebraic Equations 8

1.2 Analysis and Mitigation of Phase Unbalance 9

1.3 Incorporating Energy Storage Systems in Distribution Feeders 9

1.3.1 Bulk Energy Storage 10

1.3.2 Microgrid Support Services 11

1.4 Literature Review 12

1.4.1 Dynamic Analysis of Distribution Feeders Using Dynamic Phasors 12

1.4.2 Dynamic Analysis of Distribution Systems Using Differential Algebraic Equations 14

1.4.3 Deployment of Bulk Energy Storage Systems in a Distribution Feeder 16

1.4.4 Energy Storage Sizing in Microgrids Based on Benders' Decomposition 18

CHAPTER Page

1.5 Modeling Needs for High Penetration PV Studies 18
1.6 Thesis Organization 24
2 DYNAMIC PHASOR ANALYSIS OF DISTRIBUTION FEEDERS IN TRANSIENT ANALYSIS TOOLS 25
2.1 Introduction 25
2.2 Dynamic Phasor Model Development in Tools without Inbuilt Solvers 26
2.2.1 Properties of the Fourier Coefficients 29
2.3 Proposed Technique 31
2.3.1 Analogy between Distribution Feeders and Trees 32
2.3.2 Modeling the Reduced Feeder 32
2.4 Proposed Algorithm for Network Reduction 33
2.4.1 Procedure of the Algorithm 34
2.5 Algorithm for Model Development in Transient Analysis Tool 36
2.6 Results and Validation 38
2.6.1 Results and Verification of Network Reduction 38
2.6.2 Results and Verification of the Transient Model 45
3 DYNAMIC ANALYSIS OF DISTRIBUTION SYSTEMS USING DIFFERENTIAL ALGEBRAIC EQUATIONS 55
3.1 Introduction 55
3.2 Proposed Approach 56
3.3 Average Model of Three-phase Inverter 57
3.3.1 Approach for Inverter Control 60
3.4 Dynamic Analysis Based on Differential Algebraic Equations 62
3.5 Simulation Results for Dynamic Analysis 63

CHAPTER Page

3.5.1 Performance of Fault Current Limiter in PV Generators 64
3.5.2 Impact of PV Generator Controller Bandwidth 65
3.5.3 Impact of Control Interaction 66
4 ANALYSIS AND MITIGATION OF PHASE UNBALANCE 69
4.1 Introduction 69
4.2 Model of the Test Distribution Feeder 70
4.2.1 Distribution Feeder Model in OpenDSS 71
4.2.2 Metric to Measure the Phase Voltage Unbalance 73
4.3 Phase Unbalance in Distribution Feeders 75
4.3.1 Sensitivity of Nodes in a Distribution Feeder 75
4.3.2 Effects of PV Unbalance on VUF and Neutral Currents 76
4.4 Mitigation of Phase Unbalance in Distribution Feeders 86
4.4.1 Active Power Filter Design to Mitigate Phase Unbalance in OpenDSS 88
5 DEPLOYMENT OF ENERGY STORAGE SYSTEMS IN A DISTRIBUTION FEEDER 95
5.1 Introduction 95
5.2 Detailed List of Data Required for Modeling 97
5.3 Model of the Test Distribution Feeder 100
5.4 Description of the Optimization Model 105
5.4.1 Minimization of Transformer Losses Based on Power Drawn from the Grid 106
5.4.2 Life Cycle Costs Associated with the BESS 106
5.4.3 Model Formulation 107

CHAPTER Page

5.4.4 Calculation of Penalty Factors k and C_t^z 108
5.4.5 Results of the BESS Schedule 108
5.5 Cost Savings as a Result of BESS 110
5.6 Impact of BESS Dispatch on Substation Transformer Losses 111
5.7 Optimal Dispatch of BESS with PV Solar Generation 113
5.7.1 Energy Shifting Scenario 114
5.7.2 Solar Smoothing Scenario 115
6 DESIGN AND SCHEDULING OF MICROGRIDS 118
6.1 Introduction 118
6.1.1 PV Generation as Stochastic Resource 122
6.1.2 Microturbines 122
6.1.3 Energy Storage Systems 123
6.1.4 Grid Support and Demand 124
6.2 Case Studies 124
6.3 Description of Problem Formulation 127
6.3.1 Mathematical Formulation of Master Problem 131
6.3.2 Mathematical Formulation of Subproblem 133
6.3.3 Energy Storage System Scheduling 135
6.4 Results of Case Studies 137
6.4.1 Energy Storage System and Microturbine Sizing for All Cases 138
6.4.2 Case 1 - Energy Storage Scheduling for 24 Hours of Microgrid Operation without Support from the Grid 140
6.4.3 Case 2 - Energy Storage for Microgrid Scheduling during Peak Hours of the Feeder 140

CHAPTER Page

6.4.4 Case 3 - Energy Storage Scheduling Based on the Mean Outage Reported from the Historical Data 143

7 SUMMARY AND CONCLUSIONS 145

7.1 Distribution System Modeling and Analysis 145

7.2 Analysis and Mitigation of Phase Unbalance 147

7.3 Microgrid Analysis and Design 148

7.4 Deployment of Energy Storage Systems in a Distribution Feeder . . . 149

REFERENCES 152

LIST OF TABLES

Table		Page
1.1	Detailed Component List of the Test Bed	19
2.1	Effect of Network Reduction on the Distribution Feeder	39
2.2	Performance Details of Network Reduction on the Distribution Feeder	40
2.3	Comparison of Power System Quantities (Voltages and Currents) from MATLAB/Simulink with those from CYMDIST	49
4.1	List of the Components for the Distribution Feeder	70
4.2	List of Nodes Arranged in Descending Order Based on the VUF	79
4.3	Neutral Currents, VUF and Phase Currents at the Most Sensitive Nodes of the Test Feeder with 25% PV Penetration	81
4.4	Neutral Currents, VUF and Phase Currents at the Most Sensitive Nodes of the Test Feeder with 50% PV Penetration	82
4.5	Neutral Currents, VUF and Phase Currents at the Most Sensitive Nodes of the Test Feeder with 100% PV Penetration	83
4.6	Neutral Currents, VUF and Phase Currents at the Most Sensitive Nodes of the Test Feeder with 200% PV Penetration	84
4.7	Maximum VUF for Various Case Studies	85
5.1	Details of the Energy Storage System	99
5.2	Details of the Grid Interface Inverter	100
5.3	List of Parameters and Decision Variables	109
5.4	Cost Savings as a Result of Active Power Support from BESS	112
5.5	Values of Energy Loss at the Substation Transformer Over a Day (August Weekday Profile)	113
6.1	List of Parameters for the Master Problem	133
6.2	List of Parameters for the Subproblem	134

Table Page

6.3 List of Parameters and Variables in the ESS Scheduling Problem 136

6.4 Power Rating of the Energy Storage System and Microturbine for All the Three Cases 138

7.1 Detailed Comparison of the Proposed Methodologies for Distribution System Analysis - Part 1 150

7.2 Detailed Comparison of the Proposed Methodologies for Distribution System Analysis - Part 2 151

LIST OF FIGURES

Figure		Page
1.1	Timeframes of Various Events in Power Systems	3
1.2	Numerical Methods Proposed to Solve Distribution Feeders with High Penetration of PV Generators	7
1.3	Approach for Snapshot and Quasi-static Modeling in CYMDIST and OpenDSS	20
1.4	View of the Test Feeder as Modeled in CYMDIST	21
1.5	Measured and Simulated Values of the Line-neutral Voltage at DAS 4 from OpenDSS	22
1.6	Measured and Simulated Values of the Active Power at the Feeder Head from OpenDSS	23
2.1	Generalized Block Diagram for Modeling the Distribution Feeders from GIS Database in Quasi-static and Transient Analyses Tools	27
2.2	Block Diagram of a PV Generator Used in the Tools with Inbuilt Phasor Solvers	28
2.3	Pseudo-code Implemented in MATLAB Programming Tool for Network Reduction of a Distribution Feeder	35
2.4	Algorithm Used to Develop a Model of the Reduced Distribution Feeder in the Transient Analysis Tool	37
2.5	Feeder Diagram of the Original and the Reduced Distribution Feeder from CYMDIST	41
2.6	View of the Reduced Distribution Feeders Representing the Capability of the Proposed Network Reduction Algorithm to Perform Selective Retention of Laterals	42
2.7	Voltage Profiles of the Original and the Reduced Network from CYMDIST	43

Figure Page

2.8 Profiles of the Reactive Power for the Original and the Completely Reduced Network from CYMDIST 44
2.9 Phase-neutral Voltage and Current of the Phase A for a Sample IEEE 37 Bus Test Feeder with a Series of Transients, Voltage Sag from 0.1 sec to 0.2 sec Followed by a Three-phase Fault at 0.25 sec 46
2.10 View of the Test Feeder from a Quasi-static Analysis Tool with the Locations of the Measurements Points, Capacitor Banks, and the Three-phase PV Generators Highlighted 47
2.11 Impact on the Phase-neutral Voltage at Various Points of the Feeder with and without Voltage Regulation During Fast Changes in Solar Irradiance as a Random Signal between 0.4 and 1 (p.u.) 50
2.12 Impact on Capacitor Bank Switching with and without Reactive Power Support from One of the Three-phase PV Generator During Cloud Transients and Voltage Sag 51
2.13 Impact on the Phase-neutral Voltage at Various Points of the Feeder with and without Voltage Regulation During Cloud Transients and Voltage Sag 52
2.14 Impact of Controller Bandwidth on the Distribution Feeder During a Cloud Transient 53
2.15 Phase-neutral Voltages and Currents at Various Points Downstream and Upstream of the Three-phase Fault in the Distribution Feeder 54
3.1 View of the Switching Model of the Three-phase Inverter 57
3.2 View of the Average Model of the Three-phase Inverter 58

Figure Page

3.3 Model of the Three-phase Inverter which has been Used to Obtain the Model of the Inverter in the *dq* Frame 59
3.4 Block Diagram of the Average Three-phase Inverter with All the Controllers in *dq* Reference Frame 61
3.5 Implementation of the User-defined Model in OpenDSS 63
3.6 Comparison of the Dynamic Simulation Results Based on DAE with the Time-domain Simulation Results for an IEEE 37 Bus Feeder 64
3.7 Phase-neutral Voltages and Currents at Various Points Upstream of the Three-phase Fault in the Distribution Feeder Showing the Performance of the Fault Current Limiter 65
3.8 Impact of Controller Bandwidth on the Distribution Feeder During a Cloud Transient 67
3.9 Impact on the Phase-neutral Voltage at Various Points of the Feeder with and without Voltage Regulation During Voltage Sag 68
4.1 Geographical View of the Test Distribution Feeder 71
4.2 Plot of the Load Shapes Consisting of a Series of Hourly Multipliers . . . 73
4.3 Magnitude of Neutral Currents at Various Points on the Distribution Feeder for One Year 76
4.4 Magnitude of Neutral Currents of the Distribution Feeder for the Month of June 77
4.5 Variation of VUF for Different Load Conditions 77
4.6 Process Involved in Choosing the Nodes for the Study 78
4.7 A Simple Schematic of the Active Power Filter with Voltage Source Converter 88

Figure Page

4.8 A Flowchart of the Process Involved for the Calculation of Correction Currents 89
4.9 Active Power Filter Implemented as a Controlled Current Source in OpenDSS 90
4.10 Phase Currents at the Feeder Head with the Proposed Active Power Filter in Operation 91
4.11 Phase Currents at the Feeder Head Without the Proposed Active Power Filter 92
4.12 Correction Currents Injected by the User-defined Active Power Filter Model in OpenDSS 92
4.13 Neutral Currents at the Most Sensitive Node Before and After Realizing the Active Power Filter 93
4.14 Neutral Currents at the Feeder Head Before and After Realizing the Active Power Filter 93
5.1 Tool Chain at a Detailed Level 99
5.2 One Line Diagram of the Test Substation with the Energy Storage System 101
5.3 View of the Feeder in OpenDSS Highlighting the Spots for Studying the Impact of the Reactive Power Support from BESS 102
5.4 Load Profile for a Typical Weekday in the Months of May, June, July, August, September, and October 103
5.5 Load Profile for a Typical Weekday in Months of January, February, March, April, November, and December 103

Figure Page

5.6 Waveforms of Power Supplied by BESS, the Reduction in SOC of BESS, and the Load Supplied Through the Transformer 104
5.7 Plot Presenting the Line-neutral Voltage of Phase A at the Feeder Head While the BESS is Discharged 105
5.8 Algorithm Used to Identify the Value of the Parameter k in C++ Programming Language 110
5.9 Load at the Substation, Fuel Cost, Charge Rate and Discharge Rate of BESS, and Power Drawn from the Grid on a Typical Weekday in the Month of January 111
5.10 PV Generation Profiles on the Two Days with Different Levels of Clouds 114
5.11 Load at the Substation, Fuel Cost, Charge Rate and Discharge Rate of BESS, and Power Drawn from the Grid on a Typical Weekday in the Month of December with Energy Shifting Scenario 115
5.12 Load at the Substation, Fuel Cost, Charge Rate and Discharge Rate of BESS, and Power Drawn from the Grid on a Typical Weekday in the Month of December with Solar Smoothing Scenario 116
5.13 Plot Comparing the Grid Power and the SOC for the BESS of the Solar Smoothing Scenario with that of the Energy Shifting Scenario 117
6.1 View of the Components Involved in the Sizing of the Energy Storage System 119
6.2 View of the Chosen Microgrid from the Test Feeder 120
6.3 Detailed View of the Chosen Microgrid from the Test Feeder 121
6.4 Load Profile of the Microgrid for a Typical Winter Month and Typical Summer Month 121

Figure Page

6.5 Measured PV Generation Corresponding to the Five PV Scenarios Used in the Study . . . 122
6.6 Typical Load Profiles for the Entire Feeder and Time-of-use Operational Costs for the Electric Power Drawn from the Grid . . . 125
6.7 Overview of Case Studies Performed . . . 125
6.8 Histogram of the Duration of Sustained Faults from Five Years of Historical Data . . . 126
6.9 Histogram of the Time of the Sustained Fault Events from Five Years of Historical Data . . . 127
6.10 Flowchart of the Steps Involved in Sizing the ESS and Microturbine . . . 132
6.11 Results of the Energy Storage Sizing for Each of the Cases Listed . . . 139
6.12 Optimal Schedule of the Generation Resources of the Microgrid without the Main Grid (Case 1) for a Typical Summer Month (June) . . . 141
6.13 Optimal Schedule of the Generation Resources of the Microgrid without the Main Grid (Case 1) for a Typical Winter Month (January) . . . 142
6.14 Optimal Schedule of the Generation Resources of the Microgrid with the Main Grid (Case 2) for a Typical Summer Month (June) . . . 143
6.15 Optimal Schedule of the Generation Resources of the Microgrid without the Main Grid (Case 2) with Non-firm Trade for a Typical Summer Month (June) . . . 144
6.16 Optimal Schedule of the Generation Resources to Support the Outages in the Microgrid for a Typical Summer Month (June) . . . 144

LIST OF SYMBOLS

Abbreviations

APF	Active Power Filter
BESS	Battery Energy Storage System
BFS	Breadth First Search
DAE	Differential Algebraic Equations
DAS	Data Acquisition Systems
DFS	Depth First Search
DLL	Dynamic Linked Library
EPRI	Electric Power Research Institute
ESS	Energy Storage System
GIS	Geographic Information Systems
IDE	Integrated Development Environment
IEEE	Institute of Electrical and Electronics Engineers
IGBT	Insulated-gate Bipolar Transistor
Li-ion	Lithium-ion Based Energy Storage System
LP	Linear Program
LTC	Load Tap Changer
LVUR	Line Voltage Unbalance Rate
MILP	Mixed Integer Linear Program
MPPT	Maximum Power Point Tracker
MST	Minimum Spanning Tree
MT	Microturbine
NEMA	National Equipment Manufacturers Association
p.u.	Per Unit
PCS	Power Conversion System

PHEV	Plug-in Hybrid Electric Vehicle
PLL	Phase Locked Loop
PNNL	Pacific Northwest National Laboratories
PVUR	Phase Voltage Unbalance Rate
PV	Photovoltaic Systems
PWM	Pulse Width Modulation
SDT	Substation Distribution Transformer
VUF	Voltage Unbalance Factor

Mathematical symbols

A	Coefficient matrix for the vector of integer variables y
a	The letter a commonly used to designate the operator that causes a rotation of 120 degrees in counterclockwise direction, which is a complex number of unit magnitude with an angle of 120 degrees
B_{kW}^{ESS}	Individual block sizes chosen for ESS to decide the best mix of units with a unit of kW
B_{kW}^{MT}	Individual block sizes chosen for MT to decide the best mix of units with a unit of kW
c	Cost parameter for the variable x in the objective function
C_t^z	Cost coefficient associated with the life cycle costs of the battery - varied based on the requirement
C_t^{grid}	Cost of power from the grid
$C_{\$/kWh}^{ESS}$	Cost of energy storage system installation costs with a unit of \$/kWh
$C_{\$/kW}^{ESS}$	Cost of power conversion system for the ESS with the unit of \$/kW
$C_{\$/kW}^{gas}$	Cost of natural gas with a unit of \$/kW
$C_{\$/kW}^{MT}$	Cost of microturbine with a unit of \$/kW
ch_t	Rate at which the battery will be charged (kW)
D_t	Load at 15 minute interval t
ds_t	Rate at which the battery will be discharged (kW)

ϵ	A threshold value of 0.5% used to decide the convergence of the Benders' decomposition
d	Cost parameter for the variable y in the objective function
E	A coefficient matrix for the vector of continuous variables x
e	Represents the vector of the grid phase-neutral voltages $\begin{bmatrix} e_a \\ e_b \\ e_c \end{bmatrix}$
e_d	The d component of the grid voltage in the dq reference frame
e_q	The q component of the grid voltage in the dq reference frame
F	A coefficient matrix for the vector of decision variables y
$\bar{h}$	Allowed maximum SOC of the BESS
$\underline{h}$	Allowed minimum SOC of the BESS
$head[Q]$	The first element of the queue Q
i	Represents a vector of the inverter currents $\begin{bmatrix} i_a \\ i_b \\ i_c \end{bmatrix}$ in the abc reference frame
I_0	Zero sequence currents
I_1	Positive sequence currents
I_2	Negative sequence currents
$I_a^{'}$	Correction currents injected by the active power filter back to phase A at the node of interest
$I_b^{'}$	Correction currents injected by the active power filter back to phase B at the node of interest
$I_c^{'}$	Correction currents injected by the active power filter back to phase C at the node of interest
k	Cost coefficient associated with the transformer losses - varied based on the need
L	Represents the value of the grid inductance and the filter inductance of a three-phase inverter
$load[t]$	Load at 1 hour interval t
M	Big M value for P_{grid}
m	Number of B_{kW}^{MT} required
ms	Unit of time referred as mili second (10^{-3} second)

η_{ch}	Charge efficiency of BESS - 90%
η_{ds}	Discharge efficiency of BESS - 90%
n	Number of B_{kW}^{ESS} required
NIL	A variable which has a null value
$\pi[s]$	Parent of the edge s in the network
P_t^{grid}	Power drawn from the grid in kW
$PV_\omega[t]$	PV generation as a stochastic variable $\omega \in \{5scenarios\}$ with a unit of kW
Q	A queue of the all the edges present in the network
$Q1$	A queue of the all the edges present in the network
$Q2$	A queue of the all the edges present in the network
R	Represents the value of the resistance used in the filter of a three-phase inverter
r_{xfrm}	Resistance of the transformer windings - 1.54 Ω (0.414 pu)
S	Rating of the PCS in kW
s	An individual edge from the adjacency list of the network under analysis
SOC_t	State of charge of the battery calculated from ch_t and ds_t (kWh)
T	Transformation matrix used to transform the quantities in the abc reference frame to the dq frame
t	Individual 1 hour intervals during a day
t_n	The set of independent variables in an ordinary differential equation
t_{n+1}	The set of independent variables in an ordinary differential equation
$\bar{v}_{AN}(t)$	Averaged values of the phase A voltages applied to the filter components
$\bar{v}_{BN}(t)$	Averaged values of the phase B voltages applied to the filter components
$\bar{v}_{CN}(t)$	Averaged values of the phase C voltages applied to the filter components
$\widehat{u}^p$	The dual variable for a constraint in the master problem

v	Represents the vector of inverter terminal phase-neutral voltages $\begin{bmatrix} v_a \\ v_b \\ v_c \end{bmatrix}$
V_A	Generally used as axis labels in the figures. Phase-neutral voltages for phase A
V_B	Generally used as axis labels in the figures. Phase-neutral voltages for phase B
V_C	Generally used as axis labels in the figures. Phase-neutral voltages for phase C
V_c	Control reference signal to the Pulse Width Modulation (PWM) block
V_d	DC link voltage which will be assumed as a constant value for the model
v_d	The d component of the inverter terminal voltage in the dq reference frame
v_q	The q component of the inverter terminal voltage in the dq reference frame
V_1	Positive sequence voltages
V_2	Negative sequence voltages
V_{ab}	Line-line voltages between phases A and B
V_{bc}	Line-line voltages between phases B and C
V_{ca}	Line-line voltages between phases C and A
$\widehat{x_m}$	Parameter in the subproblem representing the choice of the block m of the microturbine
$\widehat{x_n}$	Parameter in the subproblem representing the choice of the block n of the ESS
$\widehat{y}$	A parameter for the subproblem which has been fixed by the master problem
x	A vector of continuous variables
x_a	Electrical quantity of phase A having the form $X_m\ sin(\omega t)$
x_b	Electrical quantity of phase B having the form $X_m\ sin(\omega t - \frac{2\pi}{3})$
x_c	Electrical quantity of phase C having the form $X_m\ sin(\omega t - \frac{4\pi}{3})$
x_m	Binary variable to choose the block n of the ESS
x_n	Binary variable to choose the block m of the microturbine

y	A vector of integer variables
$y[t]$	Binary variable used to connect/disconnect the grid
y_{n+1}	The set of dependent variables in an ordinary differential equation which will be calculated based on y_n
y_n	The set of dependent variables in an ordinary differential equation which can either be an initial value or the previously calculated state
Z_t^+	Expected battery replacement cost as a function of depth of discharge from time t-1 to t in kW; calculated from the ch_t and ds_t
Z_{lower}	A dummy variable included to aid the solution of the master problem
Z_{upper}	The sum of the objectives of the master and the subproblem

Chapter 1

INTRODUCTION

Renewable energy standards in most of the states provide impetus for the adoption of large-scale renewable energy generation both at the bulk transmission level and at the distribution system level [1, 2]. A rapid increase in the penetration level of distributed renewable resources imposes a paradigm shift in the design, operation, protection, and control of the distribution systems. As the penetration level of interconnected PV systems increases on a distribution system there is an increasing need for both accurate models of the solar resource and advanced distribution system analysis tools to evaluate high penetration PV system impacts.

With the continued growth of the PV market, and the increasing penetration of PV resources in the distribution grids, the modeling tools must begin to incorporate support for PV. In order to investigate the distribution feeders with high penetration of distributed renewable resources, different types of analyses are needed, including snapshot, quasi-static, and transient analyses.

Snapshot analysis can be used for analyzing the voltage profiles along the feeder length. Voltage profiles are obtained by solving the powerflow of a distribution feeder, under scenarios of particular interest such as peak load with low PV generation and low load with high PV generation. In contrast, quasi-static analysis is preferred for extending the distribution system analysis for over a day, month, or year. This method is referred to as quasi-static simulation because it involves a series of steady-state solutions and omits the dynamic effects between each solution. The quasi-static analysis solves the system powerflow multiple times with step changes in PV generation, loads, and substation voltage. The focus of the quasi-static analysis is

the voltage levels at various nodes of interest, operation of the capacitor banks, and changes in the load-tap changing transformers.

There have been efforts recently in developing distribution system analysis tools with an emphasis on distributed renewable generation and smart grid initiatives. Some of the tools for distribution systems are CYMDIST, OpenDSS, and GridLab-D [3, 4].

The CYMDIST is representative of the state-of-the-art distribution system analysis tool commercially available, whereas the OpenDSS and GridLab-D are open-source tools. Existing distribution system analysis tools (CYMDIST, OpenDSS, and GridLab-D) are capable of supporting snapshot and quasi-static analysis. As mentioned, the quasi-static simulation focuses on simulating a series of steady-state solutions, omitting the dynamic effects between each solution. However, capturing the dynamic effects of the PV generators during the variation in the distribution system states is necessary when studying the effects of controller bandwidths, multiple voltage correction devices, and anti-islanding. An effective method of performing transient analysis is needed; however, performing transient analysis on a distribution system with high penetration of PV generators is extremely time consuming and impractical. Figure 1.1 presents a comparison of the time frames for quasi-static and transient analyses along with other power system events.

This study analyzed the impacts of high penetration levels of PV resources interconnected onto the distribution system. Research efforts under this study include:

- Development of distribution and PV system models required to evaluate the impacts of high penetration PV

- Development of analytical methods, especially methods for transient analysis, for determining the impacts of high penetration PV

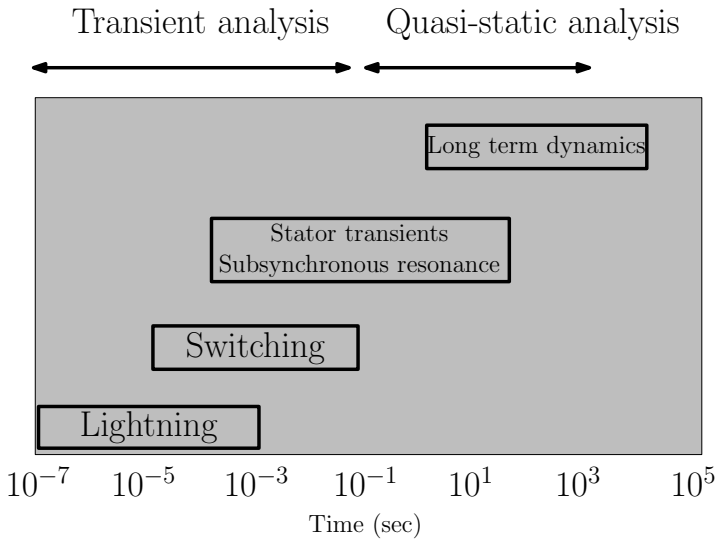


Figure 1.1 – Timeframes of Various Events in Power Systems

- Development of high penetration PV impact mitigation strategies including energy storage, microgrid mode of operation and active power filters for unbalance mitigation, and optimization for their design.

Novel mathematical techniques capable of capturing the necessary long-term transients using reduced computations were proposed in this project. This work focused in detail on the use of dynamic phasors and differential algebraic equations (DAE) for dynamic analysis of the existing distribution feeders. The advantages to using the dynamic phasor-based solver rather than the conventional time-domain simulations are illustrated. The implementations were conducted in MATLAB/Simulink. The network reduction techniques involving graph search algorithms were used to obtain a reduced feeder model. In addition, a nonheuristic network flow technique designed to automate the implementation of the distribution feeder in a transient analysis tool such as Simulink/SimPowerSystems was developed.

An additional approach for performing the dynamic analysis was based on differential algebraic equations. Because the focus of the project was to analyze the

impacts of high penetration of PV generators, solving the dynamic model of a complete feeder was not necessary. The dynamic models of the PV generators could be retained, with the remainder of the distribution feeder reported as a set of algebraic equations. The user-defined models were developed in OpenDSS to connect the solution of the dynamic models with the powerflow. This work considered various modeling and analysis techniques to capture the necessary transients injected due to the high PV penetration in the distribution feeder. The implementation details and verification of the implemented techniques are provided in the following chapters.

A significant challenge with the increasing penetration levels of the PV systems is the phase unbalance created by an unequal distribution of the customer-owned PV systems among the three phases. Because the utility has little control over the placement of the customer-owned PV systems, a large mismatch in the number and ratings of distributed PV generators connected to each of the three phases may occur. This PV induced unbalance may further exacerbate the existing unbalance due to load mismatch. The PV induced unbalance can change constantly as the injected power varies with the solar insolation. In addition, the PV induced unbalance is affected by the different orientations of the solar panels.

The phase unbalance can lead to various problems in the operation of a power distribution system. An increased phase unbalance significantly adds to the neutral currents leading to unnecessary tripping or possible loss of protection coordination. This study was designed to analyze and quantify the impact of unbalanced PV installations on a distribution feeder. Additionally, the scope of the study included design of a power electronic converter solution for mitigating the identified impacts and validating the solution's effectiveness through detailed simulations.

The benefits associated with the use of energy storage systems for electric-utility-related applications were also studied. Some of the benefits studied include

electric energy time-shift, voltage support, renewable energy time-shift, and renewable capacity firming. A multiobjective optimization with a quadratic objective and linear constraints was proposed in order to optimally schedule an energy storage system. An energy storage system based on lithium-ion technology with a capacity of 1,500 kWh, 500 kW was chosen for this study. Other than energy price arbitrage and substation transformer loss reduction, life cycle costs of an energy storage system was also modeled.

Microgrids have the potential to enhance the value of distributed generation such as solar PV. A microgrid is usually served by a combination of multiple micro resources such as PV generators and microturbines (gas/diesel). However, the renewable resources are intermittent and stochastic in nature. A potential solution to accommodate the variability of renewable resources is to use an energy storage system. In this thesis, a novel approach for optimally sizing and scheduling the energy storage system with the microturbine was proposed. The size and schedule of the energy storage system were determined using Benders' decomposition. The PV generation was considered as a stochastic resource. In addition, a nonfirm trade allowing the microgrid to interrupt the power delivery to the main grid was also considered. The formulated problem was implemented in the IBM ILOG CPLEX optimization studio (CPLEX).

1.1 Dynamic Analysis of Distribution Feeders with High Penetration of PV Generators

The existing distribution system analysis tools (CYMDIST/OpenDSS) are capable of supporting snapshot and quasi-static analysis. However, capturing the dynamic effects of the PV generators during the variation in the distribution system states was

necessary to study the effects of controller bandwidths, multiple voltage correction devices, and anti-islanding.

Using a test distribution feeder as the basis, this work implemented novel mathematical techniques to capture the necessary transients for analyzing the distribution feeder using reduced computations. This work is a detailed exploration of the use of dynamic phasors and differential algebraic equations for impact analysis of high PV penetration on the test feeder. Figure 1.2 presents the set of methodologies implemented in this work.

1.1.1 Dynamic Phasor Analysis of Distribution Feeders in Transient Analysis Tools

Performing transient analysis on a distribution system with high penetration of PV generators is time consuming. In a typical transient analysis tool, the system of interest is modeled as a set of ordinary differential equations and solved using numerical integration techniques. Due to the presence of high-bandwidth controllers in the model of PV generators, the numerical integration technique used small time steps leading to substantial computation times. Hence, the use of dynamic phasors, or time-varying phasors, was proposed for this project [5–8]. The main idea behind this method was to represent the periodical or nearly periodical system quantities by their time-varying Fourier coefficients (dynamic phasors). The programming tool MATLAB/Simulink was extensively used for this purpose.

A typical distribution feeder contains a primary three-phase line, which runs through the complete feeder; numerous single-phase laterals branch out of the primary three-phase line and eventually connect to the load centers. Typically, the utilities prefer to use underground cables as the single-phase laterals, which might sometimes span tens of miles. Devising a detailed modeling of the three-phase lateral in a distribution feeder was crucial; however, the modeling of each single-phase

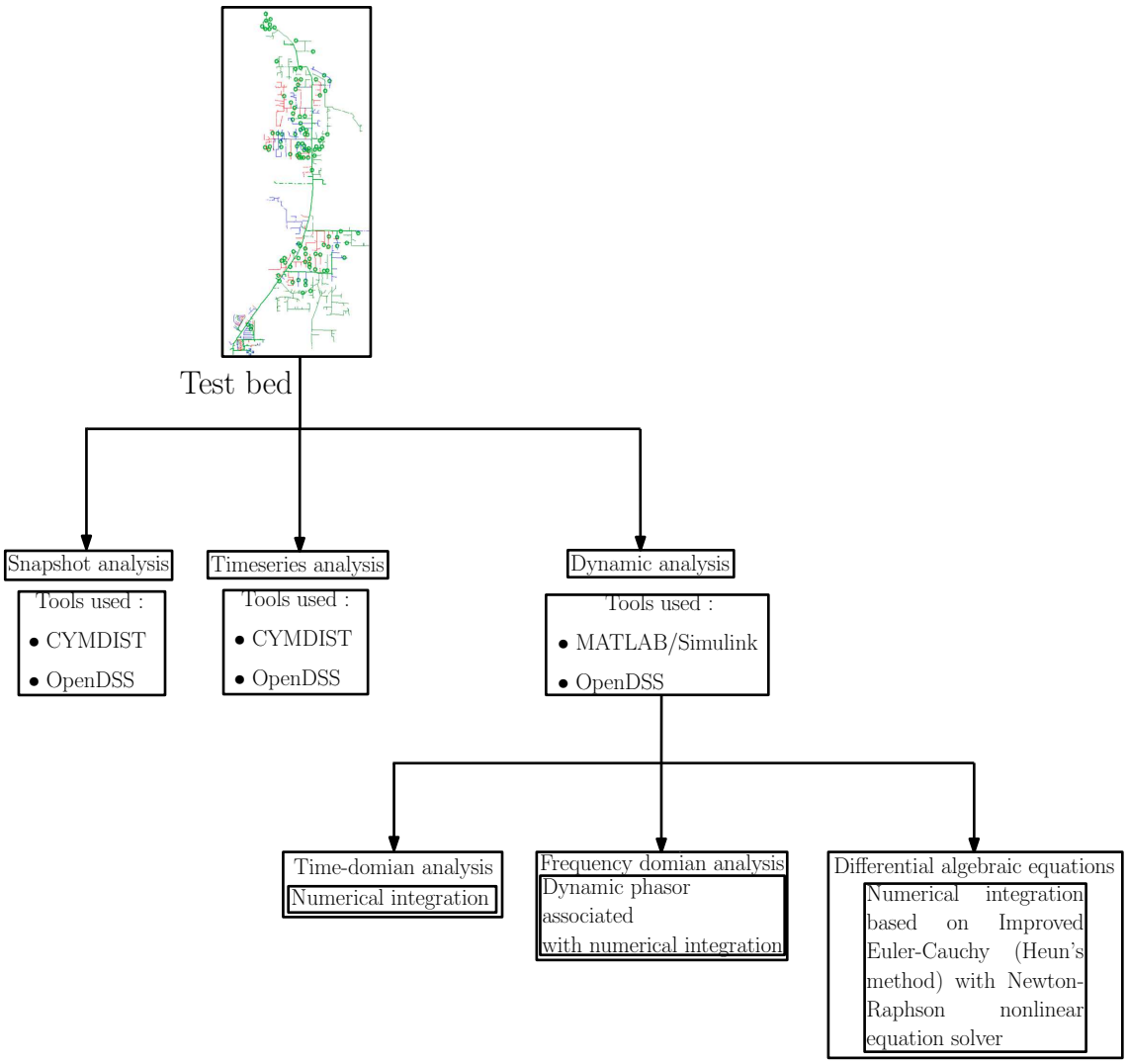


Figure 1.2 – Numerical Methods Proposed to Solve Distribution Feeders with High Penetration of PV Generators

lateral contributed complexity and time for the electromagnetic transient program. The network reduction proposed in this research is capable of selectively retaining the laterals of interest, thus enabling dynamic analysis on customers tens of miles down the laterals. Further, underground cables have relatively high cable capacitance when compared with overhead lines. The proposed network reduction technique accommodates the reactive power generation from cable capacitance to the loads.

1.1.2 Dynamic Analysis of Distribution Systems Using Differential Algebraic Equations

In addition to the dynamic phasor, the use of differential algebraic equations was proposed in this work for conducting the dynamic analysis on the distribution feeders. The use of differential algebraic equations for the dynamic analysis involved selectively modeling the states of interest using differential equations, with the rest of the distribution system written as algebraic equations.

To achieve this framework, the open source tool from EPRI, OpenDSS, was used. This work is one of the first studies to implement the approach of differential algebraic equations for solving a distribution feeder with 3,000 nodes. The capability of OpenDSS was extended to achieve the objective

The native tool of OpenDSS can perform only snapshot analysis and quasi-static simulations. Quasi-static simulation involves a series of steady-state solutions, which omits the dynamic effects between each solution. Capturing the dynamic effects of the PV generators during the variation in the distribution system states is necessary when studying the effects of controller bandwidths, multiple voltage correction devices, and anti-islanding.

This work extends the capability of the tool by developing a user-defined model for PV generators as a dynamic linked library (DLL). The mathematical solution was based on differential algebraic equations. Selective states, such as the electric currents of PV generators, were solved using differential equation solvers, whereas the rest of the distribution system was solved using three-phase powerflow solutions.

1.2 Analysis and Mitigation of Phase Unbalance

Phase unbalance can lead to various problems in the operation of a power distribution system. An increased phase unbalance significantly adds to the neutral currents, leading to unnecessary tripping or possible loss of protection coordination. Further, phase unbalance leads to unequal loading of transformer windings and distribution cables. Increased phase unbalance makes it difficult to meet voltage unbalance factor (VUF) standards and causes problems with the sensitive three-phase equipment.

The objective of this study was to analyze and quantify the impact of unbalanced PV installations on a distribution feeder. Additionally, the scope of the project included the design of a power electronic converter solution for mitigating the identified impacts and validating the solution's effectiveness through detailed simulations. A model of a typical distribution circuit was developed, analyzed, and simulated extensively using a distribution system analysis tool (OpenDSS). The impact of adding large-scale PV installations was studied in terms of neutral current, voltage unbalance, and transformer and line loading. Chapter 4 provides the details of the test distribution feeder used for this study.

1.3 Incorporating Energy Storage Systems in Distribution Feeders

Energy storage systems mediate between variable sources and variable loads. This work incorporated the use of Li-ion battery-based energy storage systems (BESS). Li-ion batteries are versatile in module size and discharge time, compared to other technologies. Additionally, the Li-ion battery technology is widely implemented in various areas of grid services. Energy storage systems can be used for various purposes as listed below:

- Bulk energy services
  - Electric energy time-shift (arbitrage)
  - Electric supply capacity
- Ancillary services
  - Regulation
  - Spinning,non-spinning, and supplemental reserves
  - Voltage support
- Transmission infrastructure services
  - Transmission upgrade deferral
  - Transmission congestion relief
- Distribution infrastructure services
  - Distribution upgrade deferral
  - Accommodate PV variability
  - Voltage support
  - Microgrid support services.

This research explored the use of energy storage systems in a distribution feeder under two domains - bulk energy storage and microgrid support services.

1.3.1 Bulk Energy Storage

The use of a pre-sized energy storage system (1,500 kWh, 500 kW) for energy price arbitrage and substation transformer loss reduction was studied. This study

provided a generalized framework for strategic operation of the lithium-ion based battery energy storage system (BESS) to increase their benefits in a distribution feeder. An optimal schedule for the BESS was proposed based on the technical and economic variables using a novel quadratic objective convex optimization problem. The multiple objectives of the proposed optimization problem were as follows:

- Reduce substation transformer losses
- Reduce the cost of energy delivered from the grid
- Reduce life cycle costs of the energy storage system
- Accommodate variability of renewable energy resources

1.3.2 Microgrid Support Services

The installation of PV generators in the distribution feeders can occur either as a roof-top single-phase installation or as a utility-scale three-phase installation. The laterals in the distribution feeder with relatively high PV generation compared to the load can be operated as microgrids to achieve economic benefits. Since renewable resources are the primary source for the microgrids, the variability needs to be accommodated by using an energy storage system and microturbines.

Energy storage systems are fast-response devices that add flexibility to the control of the microgrids as well as achieve additional economic benefits. Further, energy storage systems can store energy during times of lower electric prices and use the stored energy at times of high electric prices. Energy storage systems can be used for load following, peak load management, power quality improvement, and deferral of upgrade investments. However, energy storage systems must be optimally sized in order to prevent over or under utilization. Because sizing of energy storage devices

largely depends on the variability of the renewable resources, the stochasticity of the renewable resource was considered in this research.

A mathematical approach based on optimization techniques was used for this purpose. The complete problem of unit sizing and unit scheduling was decomposed into three stages. The first two stages involved sizing of the kW/kWh rating of the energy storage system and the kW rating of the microturbine. In order to manage the computational complexity, the first two stages were coupled using Benders' decomposition. The third stage provided an optimal schedule for the microturbine and the energy storage system. The life-cycle cost of the energy storage system was considered in determining the optimal schedule. Based on the outputs of the first two stages, the third stage was solved as an independent problem. The formulated problem was implemented in the IBM ILOG CPLEX optimization studio (CPLEX).

1.4 Literature Review

The work proposed in this thesis comprises of five parts: dynamic phasor analysis on distribution feeders, dynamic solutions based on differential algebraic equations, analysis and mitigation of phase unbalance, use of energy storage systems as bulk storage devices, and energy storage sizing for the operation of microgrids. The existing research relevant to these topics is discussed in this section.

1.4.1 Dynamic Analysis of Distribution Feeders Using Dynamic Phasors

The topic of dynamic analysis using the dynamic phasors has three subsidiary topics as follows:

- Framework for an automated model development in MATLAB/Simulink
- Network reduction of the distribution feeder

- Reduced order model of the PV generators for analysis based on the dynamic phasors

1.4.1.1 Framework for an Automated Model Development in MATLAB/Simulink

A methodology for developing an automated distribution feeder model for the dynamic analysis in MATLAB/Simulink from the GIS database was proposed. As part of the model development in a transient analysis tool, a graph-search algorithm based on the depth-first search (DFS) approach was extensively used. To date, very few published studies can be found on the topic of modeling the distribution feeders for dynamic analysis. Section 2.5 presents a novel approach proposed for an automated development of the distribution feeder in MATLAB/Simulink.

1.4.1.2 Network Reduction of the Distribution Feeder

Studies on the topic of network reduction are old and frequently visited. Even though a detailed work on the reduction of a network was published in the year 1949 [9], the topic of network reduction has been revisited at regular intervals over time [10–12]. Most of these seminal reduction techniques are heuristic (experience-based) or semi-heuristic in nature. These methods have been developed for transmission systems with multiple, physically distant synchronous generators. However, this work concentrated on distribution systems and involved the modeling of large numbers of distributed PV generators. Use of power electronics-based converters makes the PV generators impossible to aggregate, compared to synchronous generators. Therefore, different techniques have been explored for distribution network reduction with inverter-interfaced systems.

Ischenko, Jokic, Myrzik, and Kling [13] provided an approach for dynamic reduction of the distribution networks with wind systems and neglected the PV generators.

Le, Tran, Devaux, Chilard, and Caire [14], in contrast, focused on the synchronous generators and disregarded the participation of the power electronics interfaced renewable sources for system studies.

A technique similar to the proposed technique was described by Oh [15], involving a network reduction algorithm based on the grouping of nodes. The distinction between the referred study and the current study is that the grouping in Oh's [15] study was decided based on congestion studies. Yun, Chu, Kwon, and Song [16] proposed a technique for network reduction, but the study was confined to reduction in solving times, and the proposed technique was predominantly heuristic and data specific.

1.4.1.3 Reduced Order Model of PV Generators Compatible with Dynamic Phasors

This study presents a customized model of the PV generator for transient tools with an inbuilt dynamic phasor solver. This reduced order model is based on the PV generator model developed by Mao and Ayyanar [17]. In addition to replacing the switches with its cycle-by-cycle average, the high-bandwidth controller was assumed to have an ideal operation. The phase-locked loop was redesigned specifically for the phasor mode. The model of the PV generator implemented an incremental conductance theorem with a voltage controller acting as a maximum power point tracker. The PV generator also contained a low bandwidth voltage controller for the DC link voltage, along with a PLL.

1.4.2 Dynamic Analysis of Distribution Systems Using Differential Algebraic Equations

The use of differential algebraic equations for solving a transmission system with multiple nodes is a relatively old topic [18–20]. However, until now the distribution

feeders were analyzed using snapshot and quasi-static analysis. The increased penetration of PV generators in the distribution feeder has imposed a need for conducting dynamic analysis. However, none of the existing distribution system analysis tools supports dynamic analysis. Implementing an explicit fixed-step integration method with a sequential solution of the differential and algebraic equations is a novel approach to manage a distribution system.

The use of power system analysis tools for performing the dynamic analysis on the distribution feeder is not recommended. The powerflow analysis of a typical distribution system varies to a great extent, when compared with the powerflow analysis methods used for a transmission system. The key differences in distribution systems include higher R/X ratios, unbalanced loads, and untransposed lines. Hence, the distribution system analysis tools necessarily implement a three-phase powerflow solution.

The many tools which can be classified as distribution system analysis tools include PSS Adept by Power Technologies; WindMil by Milsoft Integrated Solutions; CYMDIST by CYME International; Technical 2000 by EDSA Micro Corporation; SynerGEE Electric by Advantica Stoner; Dapper Demand Load Analysis by SKM Systems Analysis; OpenDSS by EPRI; GridLab-D by PNNL; Power System Toolbox (PST) by Rensselaer Polytechnic Institute; ABB Feederall by ABB; Power Tools for Windows from SKM Systems Analysis, Inc.; PowerWorld Simulator by Power-World Corporation; EuroStag by Tractebel; DigSilent PowerFactory by DigSILENT; and NEPLAN by BCP-Suiza.

This work extends the capability of an open-source distribution system analysis tool, OpenDSS. OpenDSS was chosen for the feature of solving differential equations and algebraic equations sequentially with the open-source tool. This study is one of the first works to simulate a complete dynamic model of the three-phase PV gen-

erator, along with multiple controllers in conjunction with the algebraic equations of a distribution system. A user-defined DLL defining the dynamic model of the three-phase PV generator was built using the Object Pascal programming language in Delphi, an integrated development environment (IDE) [21].

1.4.3 Deployment of Bulk Energy Storage Systems in a Distribution Feeder

This study proposes the use of a multiobjective optimization to dispatch the BESS with a goal of minimizing the following objectives:

- Loading of the substation transformer
- Cost incurred for delivering power from the substation
- Life cycle costs associated with BESS

The objectives were combined to frame a convex optimization problem with a quadratic objective and linear constraints. Similar to this work, the U.S. Department of Energy (DOE) has funded multiple projects in collaboration with local utilities [22, 23]. Authors in the reference [24] report similar studies performed in Australia. However due to the incipient stage of the these projects, the papers/reports do not yet provide a generalized approach to determine the dispatch schedule of the energy storage system.

Sandia National Laboratories has performed a detailed study on the benefits associated with the use of energy storage systems for electric-utility-related applications [25, 26]. Report prepared by Sandia National Laboratories estimates the benefit through a simple storage dispatch algorithm, without utilizing a convex optimization based approach. Authors in the reference [25] present an approach which can also be referred to as a greedy approach or brute force algorithm. In general, the brute force

algorithm is computationally intensive and also lacks in modeling the astute details required for life cycle costs of the energy storage system.

An exhaustive search among the existing publications have been conducted to compare the proposed approach with the existing methods [27–29]. The referred publications proposed load levelling as an approach for utilizing the BESS in order to minimize the losses. Since the network losses is a square function of the current, shifting the load from peak to off-peak periods was observed as a common thread among all the publications in line with this work. However, none of the references considered a direct study on the reduction of substation transformer losses, detailed modeling of the BESS life cycle costs, and accommodated the fast variations of PV generation resources.

A significant amount of work has been performed in this research for detailed analysis and modeling of the life cycle costs of the BESS along with reducing the substation transformer loses. A fair number of publications/reports can be found on accurate modeling of the batteries present in the PHEV [30, 31]. Electric Power Research Institute (EPRI) has performed an exhaustive work in this regard [32]. The element which distinguishes this work from the existing work on PHEV battery packs is the energy rating of the BESS and its interaction with the distribution system. In similar lines, a fair number of publications can be found on the integration of energy storage systems with distribution systems [33–36]. The key contribution of this study compared to be above work is again the detailed modeling of the life cycle costs of BESS and the inclusion of substation transformer losses in the optimization. The characteristics modeled in the objective and constraints of the convex optimization as a part of this work are as follows:

- Refrain from letting the energy storage system at high state of charge for long durations - the life cycle of the battery is affected

- Avoid charging-discharging the energy storage system at the high rates
- Frequent variation in the rate of charge/discharge is avoided
- Avoiding the charge/discharge twice a day - Charge/discharge cycles multiple times a day does not impact the life cycle, but the calendar life would be reduced by 50% due to two-fold increase in daily cycling

1.4.4 Energy Storage Sizing in Microgrids Based on Benders' Decomposition

Benders' decomposition is a well-researched and often utilized decomposition technique for integer and mixed-integer linear programs [37]. Instead of solving one large complex problem, the problem is decomposed into smaller component parts to be solved individually. Some of the initial applications of the Benders' decomposition occurred as early as 1984 [38], focusing on generator unit sizing. Since then, Benders' decomposition has been widely used for multiple areas of unit commitment and transmission expansion planning [39–43].

An energy storage has always been a primary method to overcome the variability of renewable generation [44]. Some of the initial work involved the integration of energy storage systems for wind farms in transmission systems [45]. With increased renewable penetration at the distribution level, energy storage systems were proposed [44, 46, 47]. The current study is one of the first to use Benders' decomposition for sizing energy storage systems in distribution systems. This work considered the PV generation as a stochastic variable with five scenarios obtained from the year 2013.

1.5 Modeling Needs for High Penetration PV Studies

An extensive study was performed on the subject of model development and analysis of the distribution feeders with various levels of detail. The analysis and

Table 1.1 – Detailed Component List of the Test Bed

Feeder length	9 miles
Peak load	7MW
Capacity	13 MW
Customers	Residential - 3000
	Commercial - 300
Primary segments	1809
Transformers	921
Capacitor banks	3
Number of residential PV	107
Residential PV generation	300 kW
Utility-scale PV generator 1	400 kW
Utility-scale PV generator 2	500 kW

modeling performed in this work were based on a test bed distribution feeder. The test distribution feeder was modeled in CYMDIST, OpenDSS, and MATLAB/Simulink for conducting various studies. The view of the test distribution feeder in CYMDIST is shown in Figure 1.4. Details of the feeder are listed in Table 1.1. The instantaneous PV penetration, defined as the ratio of PV generation to the total load at a given time, reached as high as 40% for the modeled feeder. The initial part of this work focused on developing a novel framework for modeling a distribution feeder starting from the GIS information found in multiple distribution system analysis tools, such as CYMDIST and OpenDSS. The modeled distribution feeder was validated with extensive field measurements. The details of the implementation are furnished in Figure 1.3.

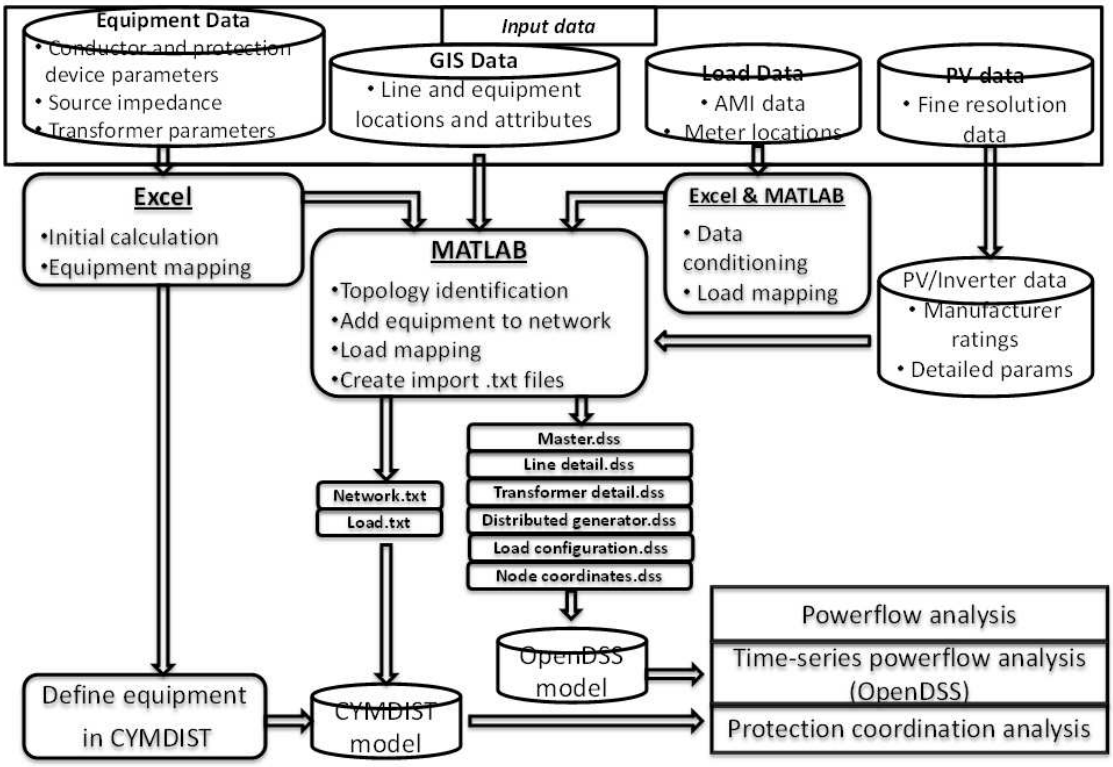


Figure 1.3 – Approach for Snapshot and Quasi-static Modeling in CYMDIST and OpenDSS

The model of the feeder developed in OpenDSS was verified with the field measurements. Figures 1.5 and 1.6 show the comparison of the measured and the simulated values of line-neutral voltages and the active power values. The quasi-static simulation for the varying load and PV generation profiles was performed in OpenDSS for a duration of 24 hours with a time resolution of one minute. The largest voltage deviation of the simulated values from the field measured values was 2%. Figure 1.5 shows the comparison between the measured and the simulated line-neutral voltages of phase A at data acquisition system (DAS) 3 of the distribution feeder. The simulated voltage values closely followed the measured data, as shown in the Figures 1.5 and 1.6.

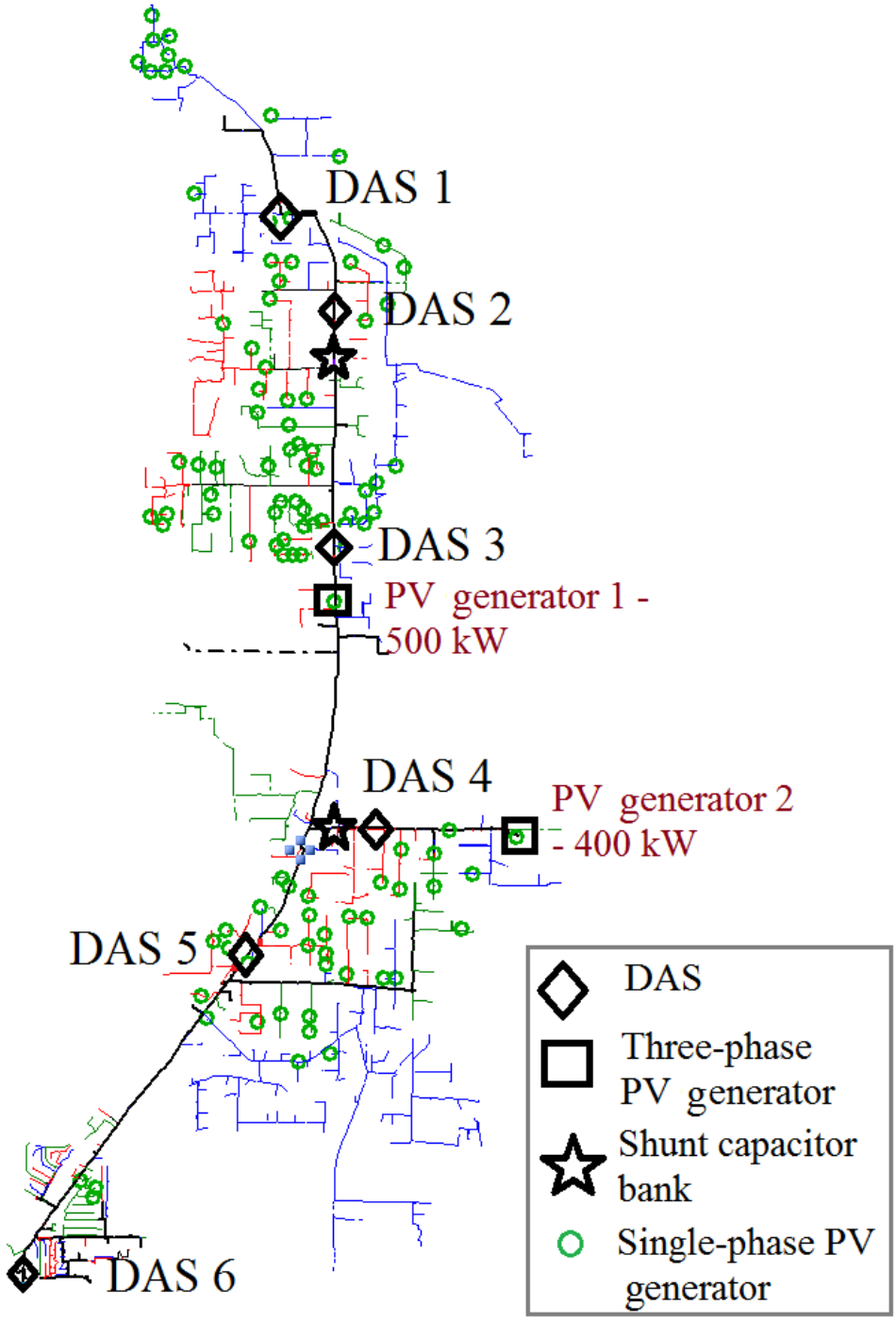


Figure 1.4 – View of the Test Feeder as Modeled in CYMDIST

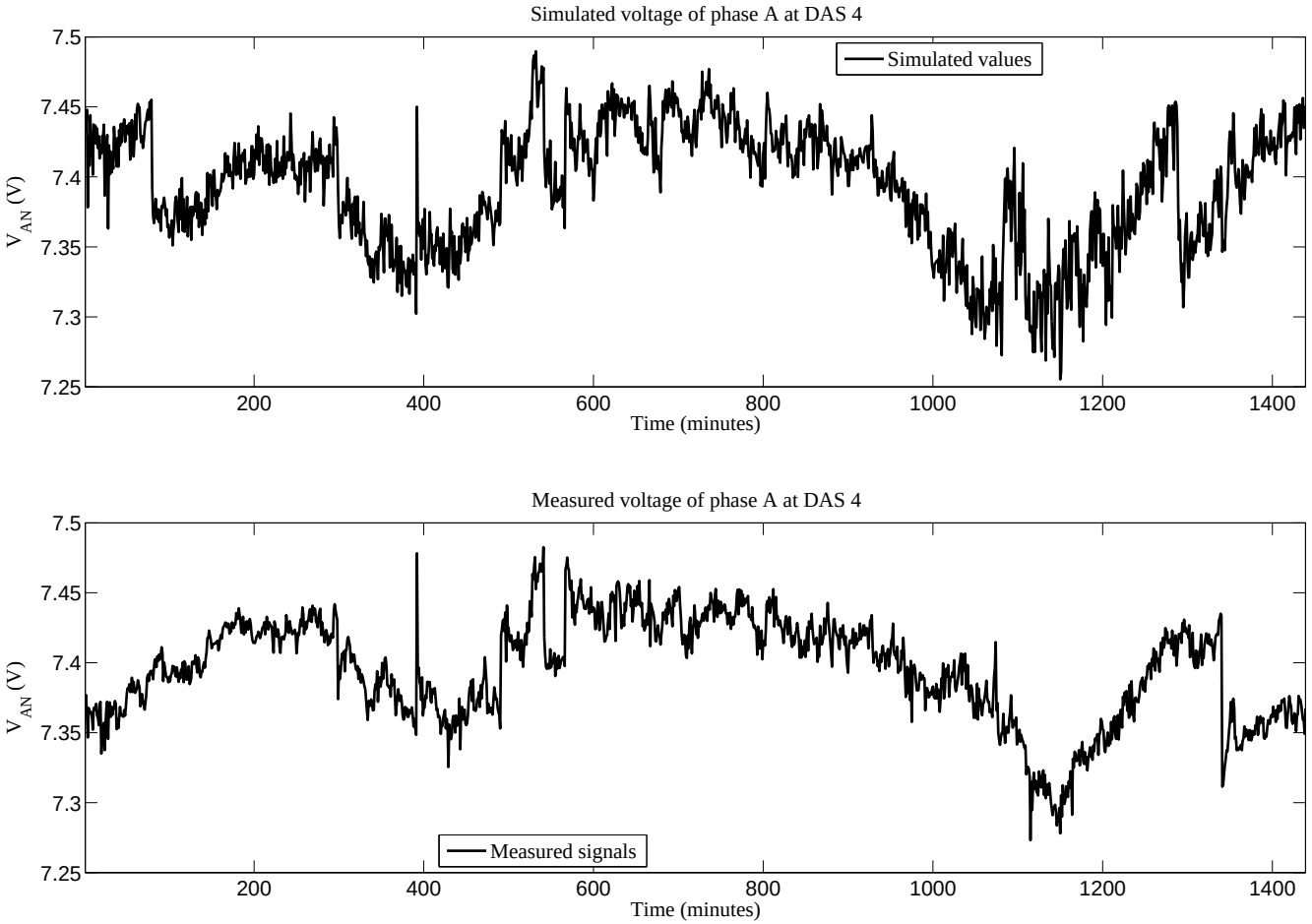


Figure 1.5 – Measured and Simulated Values of the Line-neutral Voltage at DAS 4 from OpenDSS

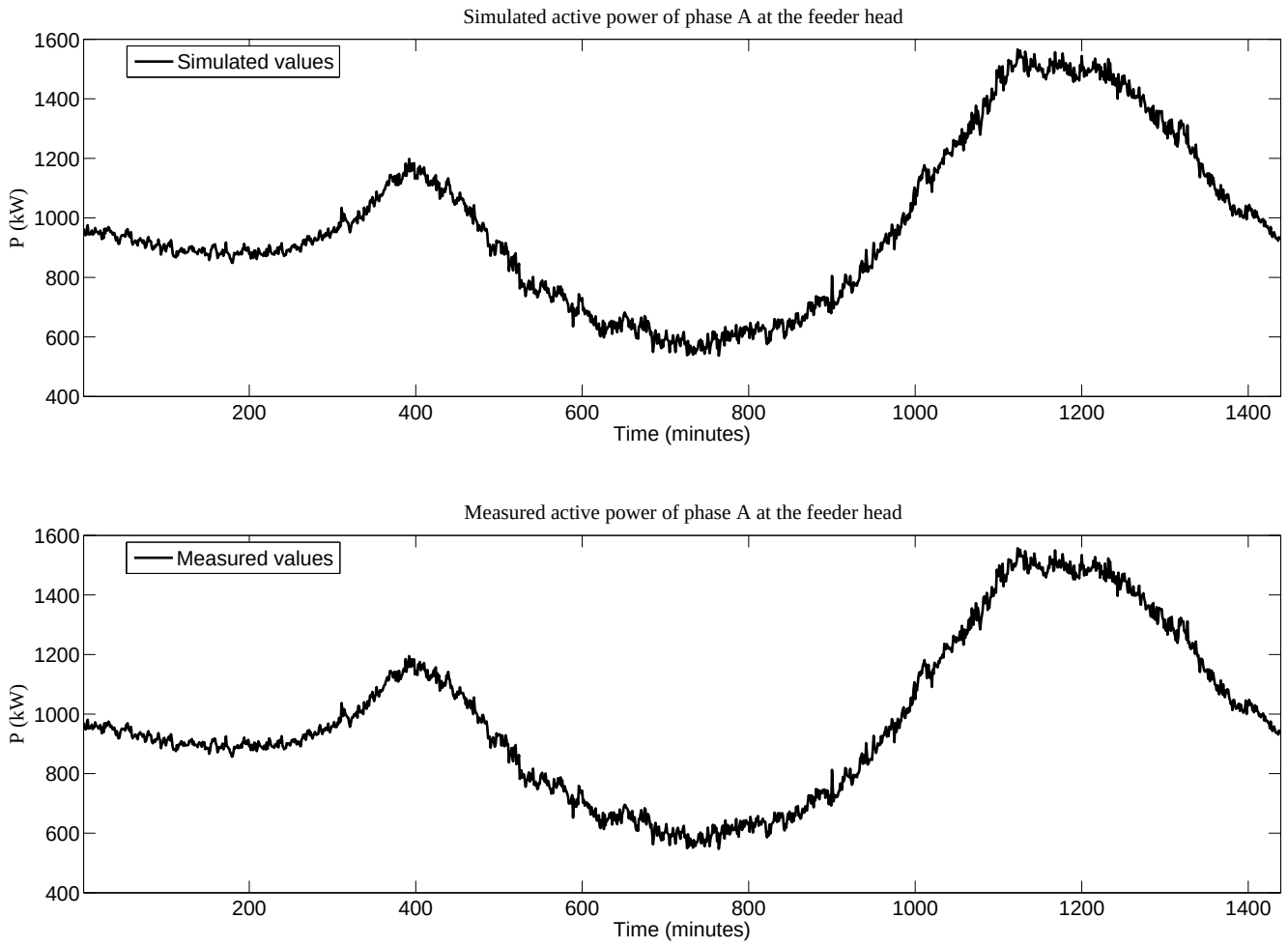


Figure 1.6 – Measured and Simulated Values of the Active Power at the Feeder Head from OpenDSS

1.6 Thesis Organization

The work proposed in this thesis comprises of five parts: dynamic phasor analysis on distribution feeders, dynamic solutions based on differential algebraic equations, analysis and mitigation of phase unbalance, use of energy storage systems as bulk storage devices, and energy storage sizing for the operation of microgrids. The details of the modeling framework was presented in Chapter 1. A review of the existing literature on the topics discussed in this thesis was presented in Chapter 1.

Chapter 2 elucidates the detailed steps involved in conducting the dynamic phasor analysis on distribution feeders and their implementation and validation using MATLAB/Simulink. Chapter 3 presents a novel method for performing dynamic analysis based on the DAE. The complete framework for performing dynamic analysis based on DAE is programmed in an open source tool from EPRI, OpenDSS.

Chapter 4 analyzes and quantifies the impact of unbalanced PV installations on a distribution feeder. In addition, a power electronic converter solution is proposed for mitigating the identified impacts and to validate the solution's effectiveness through detailed simulations.

The benefits associated with the use of energy storage systems for electric-utility-related applications are studied in Chapter 5. A multiobjective optimization with a quadratic objective and linear constraints is proposed in order to optimally schedule an energy storage system. The laterals in a distribution feeder with relatively high PV generation compared to the load can be operated as microgrids when required, to achieve economic benefits. Chapter 6 presents the use of Benders' decomposition to determine the size and schedule of the energy storage system and microturbine for their use in microgrids.

Chapter 2

DYNAMIC PHASOR ANALYSIS OF DISTRIBUTION FEEDERS IN TRANSIENT ANALYSIS TOOLS

2.1 Introduction

Performing transient analysis on a distribution system with high penetration of PV generators is computationally intensive. A typical transient analysis tool models the distribution feeder as a set of differential equations and solves the problem using numerical integration techniques. Due to the presence of high-bandwidth controllers in the modeling of PV generators, the numerical integration technique uses small time steps, leading to substantial computation time. To reduce this computation time, the use of dynamic phasors or time-varying phasors was proposed for performing dynamic analysis on the distribution feeders [5–7]. The main idea behind this method was to represent the periodical or nearly periodical system quantities by their time-varying Fourier coefficients (dynamic phasors). The concept of dynamic phasors is based on a Fourier approximation of system quantities. MATLAB/Simulink was extensively used for this purpose. The tool MATLAB/Simulink contains an inbuilt dynamic phasor mode for solving a power system.

The network reduction proposed in this study could selectively retain the laterals of interest, thus enabling dynamic analysis on customers tens of miles down the laterals. Additionally, the reactive power generated from the capacitance of the underground cables was considered during the network reduction. The proposed network reduction technique accommodates the reactive power generation of the reduced

single-phase laterals at the loads. The development of the distribution feeder in the transient analysis tool mainly used three algorithms as follows:

- Topology identification
- Network reduction
- Modeling in the transient analysis tool

The complete procedure for performing the dynamic phasor analysis is diagrammatically displayed in Figure 2.1. The algorithms for network reduction and modeling in the transient analysis tool were developed from the inception.

Figure 2.1 presents a generalized framework of the modeling process. The modeling process starts from the GIS database. The proposed algorithm reads the GIS database, explores the structure of the feeder, and provides input as required for the transient analysis tool. The graph search algorithm will be extensively used for these purposes.

The final model was developed in MATLAB/Simulink using the SimPowerSystems toolbox. The model of the PV generator presented in Figure 2.2 was used. The model of the PV generator implemented the incremental conductance theorem acting as a maximum power point tracker with a voltage controller. The PV generator also contained a low bandwidth voltage controller for the DC link voltage along with a phase locked loop (PLL). The main idea behind this work was the development of a non-heuristic network flow technique to model a large distribution system in the transient analysis tool.

2.2 Dynamic Phasor Model Development in Tools without Inbuilt Solvers

Phasor representation of a sinusoidal signal is a powerful tool for analyzing the steady state behavior of voltages and currents. The phasors are used for the

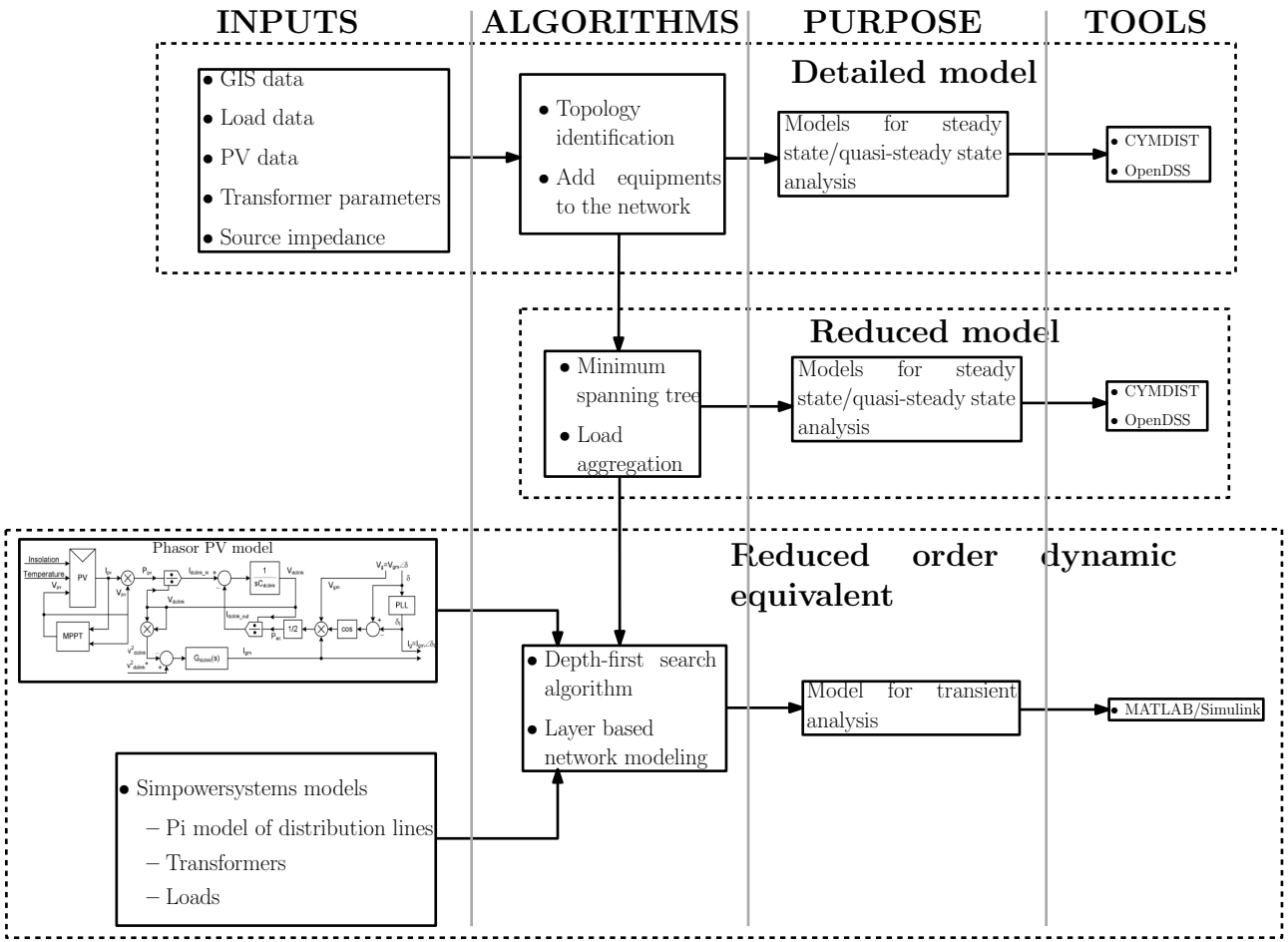


Figure 2.1 – Generalized Block Diagram for Modeling the Distribution Feeders from GIS Database in Quasi-static and Transient Analyses Tools

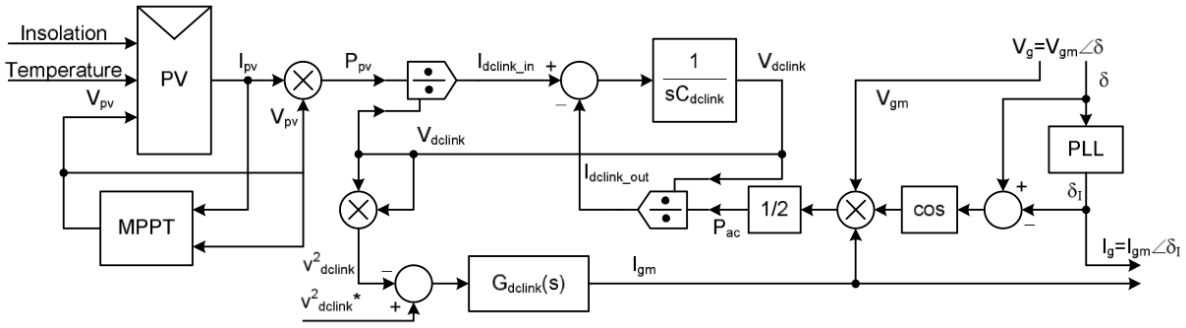


Figure 2.2 – Block Diagram of a PV Generator Used in the Tools with Inbuilt Phasor Solvers

analysis of power systems in a stationary sense. Phasor representation is a class of mathematical transformation to eliminate the fundamental frequency component in the calculation. A single-phase signal can be represented as

$$x(t) = X(t)cos(\omega t + \delta(t)), \tag{2.1}$$

where $x(t)$ is a time varying signal which is periodic with a frequency ω. The phasor representation links $\hat{x}(t)$

$$\hat{x}(t) = X(t)\ e^{j\delta(t)} = X(t)\angle\delta(t), \tag{2.2}$$

with the modulated signal $x(t)$. In other words, the original signal $x(t)$ is related to its phasor $\hat{x}(t)$ by

$$x(t) = Re(\hat{x}(t)e^{j\omega t}). \tag{2.3}$$

With these fundamentals the dynamic phasor method is based on the fact that a waveform $x(\bullet)$ can be decomposed into its individual frequency components on the time interval $(t-T, t]$ to arbitrary accuracy with a Fourier series representation of the form

$$x(t - T + \tau) = \sum_k \langle x \rangle_k (t)\, e^{jk\omega(t-T+\tau)} \tag{2.4}$$

where the sum is over all integer values of k, $\tau \in (0, T]$, $\omega = 2\pi/T$, and the $\langle x \rangle_k (t)$ are the complex Fourier coefficients. These Fourier coefficients are functions of time. The interval under consideration for the Fourier coefficient slides as a function of time. The k-th coefficient is calculated using

$$\langle x \rangle_k (t) = \frac{1}{T} \int_0^T x(t - T + \tau)\, e^{-jk\omega(t-T+\tau)}\, d\tau. \tag{2.5}$$

The analysis computes the time-evolution of the Fourier series coefficients as the window of length T slides over the actual waveform. The kth Fourier coefficient of a time-domain signal $x(t)$ is represented as $\langle x \rangle_k\ (t)$. For the purpose of convenience (t) is dropped for rest of the work. As the $\langle x \rangle_k$ is a complex quantity, except the dc-coefficient ($\langle x \rangle_0$); a typical kth Fourier coefficient can be rewritten in terms of real and imaginary parts as

$$\langle x \rangle_k = \langle x \rangle_k^R + j\ \langle x \rangle_k^I \tag{2.6}$$

where the superscripts R and the I represent the real and the imaginary components of a Fourier coefficient.

2.2.1 Properties of the Fourier Coefficients

A differential equation which considers a time-varying sinusoidal carrier signal can be rewritten as a time-invariant differential equation by replacing all the derivatives using the differentiation rule. The new set of equations being in the complex phasor domain are of twice the original dimension of the system. The trajectory of the transients can be directly interpreted in terms of the envelop variation using the dynamic phasor formulation.

2.2.1.1 Differentiation with Respect to Time

The time derivative of the first order for the kth coefficient was computed as follows

$$\frac{d}{dt}\langle x\rangle_k = \left\langle \frac{d}{dt}x \right\rangle_k - jk\omega \langle x\rangle_k . \tag{2.7}$$

The time derivative of the second order for the kth coefficient is computed as

$$\frac{d^2}{dt^2}\langle x\rangle_k = \left\langle \frac{d^2}{dt^2}x \right\rangle_k - k^2\omega^2 \langle x\rangle_k . \tag{2.8}$$

In case ω is time varying the varying nature of the frequency should be accommodated into the equations.

2.2.1.2 Linear Elements

The branch variables for a linear resistive element are related by Ohm's law. The Ohm's law for the k-th coefficient will be

$$\langle e\rangle_k = R\ \langle i\rangle_k \tag{2.9}$$

where e represents voltage applied across the resistor, R is the resistance and the i is the current flowing through the resistor.

2.2.1.3 The Dynamic Phasor Equations for Capacitor Voltage and Inductor Current

The current i_C flowing through a capacitor C with a terminal voltage e can be represented by

$$\langle i_C\rangle_k = C\ \frac{d}{dt}\langle e\rangle_k + j\ \omega\ C\ \langle e\rangle_k \tag{2.10}$$

Similarly with the voltage $e(t)$ across an inductor, L, a current of $i_L(t)$ is flowing through can be represented by

$$\langle e \rangle_k = L \frac{d}{dt} \langle i_L \rangle_k + j \ \omega \ L \ \langle i_L \rangle_k \tag{2.11}$$

2.3 Proposed Technique

The purpose behind network-reduction is to develop a reduced distribution system to facilitate dynamic analysis of the feeder with high penetration of PV generators. Starting from the GIS database network topology was identified [48]. After the identification of network topology, the network reduction proposed in this thesis was performed. The reduced distribution feeder was modeled in a quasi-static tool and the dynamic analysis tool for the purpose of validation. This study proposes a network-reduction technique by using the minimum spanning tree (MST) algorithm. The highlights of the proposed technique are as follows:

- The algorithm identifies the nearest three-phase section for each load and PV generator.
- Aggregates all the loads for each phase and links the loads to the nearest three-phase section.
- Selectively retains the laterals, without reduction, such that dynamic analysis on the customers tens of miles down the laterals can be performed
- Retains all the loads which have PV generators associated. The PV generators are retained because the goal is to study the dynamic impact of PV inverters on the distribution system.
- The proposed network reduction technique accommodates the reactive power generation from cable capacitance to the loads.

2.3.1 Analogy between Distribution Feeders and Trees

The analysis of the structure of a distribution feeder can be skillfully performed using network-flow algorithms [49]. Basic components of a graph include edges and vertices. An edge is equivalent to a section and a vertex is analogous to a bus/node in a distribution system. Since data for large distribution systems are shared in the format of GIS databases, application of graph algorithms for understanding the structure of the distribution system is direct and necessary.

2.3.2 Modeling the Reduced Feeder

The data for a distribution feeder have been stored as GIS data (geodatabase format), providing the locations and details of the equipment, rating for the lines, and information about other devices on the feeder. Each distribution system analysis tool has individual modeling specifications, for example CYMDIST (Cooper Power Systems) requires the feeder details be in terms of section numbers, where as the GridLab-D (from PNNL) requires feeder details specific to the nodes. For this study, the principle used for identifying the topology from the GIS data was derived from the reference [48]. After identification of the network topology the network was reduced per the proposed algorithm in this section. The reduced network was modeled in CYMDIST and MATLAB/Simulink. Rebuilding the reduced distribution system for modeling a distribution system in CYME required an understanding of the technical specifications of the distribution system analysis tool. For modeling a distribution system in CYMDIST the files and the associated details are as follows (the text in the parentheses depict the data type)

- Bus coordinates configuration - node number (integer), x-coordinate (float), y-coordinate (float)

- Section configuration - section number (integer), from node (integer), to node (integer), phase of section (string)
- Line configuration - section number (integer), conductor details (string), line length (float)
- Load configuration - section number (integer), load name, load kVA (float), load power factor (float), load phase (string)
- Distributed generator configuration - section number (integer), name (string), active power generation (float), power factor (float)
- Transformer configuration - section number (integer), transformer device number (string), transformer rating (float), transformer phase (string)

After the network reduction all the details as listed above needed to be retained or regenerated for rebuilding the feeder in the quasi-static analysis tool (CYMDIST). For modeling the feeder in MATLAB/Simulink a graph-search algorithm based on a depth first search was used. The proposed algorithm and the process of rebuilding the feeder from the reduced adjacency list are described in the following section.

2.4 Proposed Algorithm for Network Reduction

A network flow algorithm was applied for the purpose of network reduction. Minimum spanning tree (MST) was used for this endeavor [50, 51]. This work implemented Prim's MST algorithm [49]. Prim's algorithm is a special case of the generic MST algorithm, based on a breadth-first search. Operation of Prim's algorithm is similar to the use of Dijkstra's algorithm for finding the shortest paths in a graph.

Typically distribution feeders are radial in structure, and a single source exists for all the loads. Thus, applying the MST algorithm to a radial distribution feeder

results in identifying the existing single path. The tree starts from an arbitrary load section (edge) and grows until the tree spans all the edges in the lateral. In the process of spanning, all the loads and the PVs were identified and analyzed. Loads without any PV generators for each phase and each lateral were aggregated; the loads with the PV generators were retained. This algorithm used a first-in-first-out queue, operating completely based on the edges.

2.4.1 Procedure of the Algorithm

The algorithm in Figure 2.3 presents the pseudo code implemented in MATLAB programming tool for network reduction of a distribution feeder. The procedure of the algorithm is as follows. Lines 1-3 set the parent of every edge to be NIL. Line 4 initialized Q to the queue just containing the edge u; thereafter Q always contained the set of edges to be read in subsequent iterations. The main loop of the program was defined in lines 5-26. The loop iterated as long as there remained unread edges, which were discovered edges that had not yet had their adjacency lists fully examined. Line 6 determined edge s at the head of the queue Q. The for loop in lines 7-18 considered each edge v in the adjacency list of s. If the edge v was not a load section, not a PV generator section, and not a three-phase section, then it was enqueued at the tail of the queue Q. Subsequently, s was recorded as its parent. The algorithm was designed to explore the single-phase laterals and keep track of loads and PV generators. The algorithm was followed by rebuilding the reduced-order distribution system in a quasi-static and dynamic analysis tool for validation. Because the x-coordinates and the y-coordinates for the aggregated loads were unknown, an algorithm for the calculation of x-coordinates and y-coordinates was developed. The key steps were as follows:

- The three-phase components retain the details of bus coordinate configuration, section configuration, line configuration.

```
1  while Q ≠ ∅ do
2      s ← head[Q]
3      foreach v ∈ Adj[s] do
4          if v ∉ Q & v ∉ L & v ∉ P & v ∉ s_three_phase then
5              π[v] ← s
6              Enqueue(Q, v)
7          end
8          if v ∈ L then
9              Enqueue(L_test, v)
10         end
11         if v ∈ P then
12             Enqueue(P_test, v)
13         end
14     end
15     foreach v ∈ Adj[s] do
16         if v ∈ s_three_phase then
17             [v] ∈ s_three_phase
18         end
19         Enqueue(junction_section, s)
20     end
21     Dequeue(Q)
22 end
```

Figure 2.3 – Pseudo-code Implemented in MATLAB Programming Tool for Network Reduction of a Distribution Feeder

- Loads without associated PV generators - create a new entry for distribution transformer (entries should appear in bus coordinate configuration), create a new entry for the aggregated load.

- Loads with an associated PV generator - update the previously existing x-coordinate, y-coordinate entries for the distribution transformer, load and the PV generator.

This network reduction algorithm substantially reduced the number of transformers and single-phase laterals. Hence, the losses which resulted due to the transformers and the single-phase laterals were irretrievable. For example, if the feeder had no PV generators, the reduced network would have as many loads as the number of the single-phase taps from the primary three-phase trunk line.

2.5 Algorithm for Model Development in Transient Analysis Tool

This section details the approach for modeling a distribution feeder in a transient analysis tool. A depth-first search algorithm was used for this purpose.

The connectivity of the original graph was available as an incidence list. The list of adjacent edges was extracted from the incidence list. The pseudo code presented in Figure 2.4 was implemented in MATLAB programming language to develop the feeder in the transient analysis tool (Simulink). The procedure for developing the model in Simulink is as follows. Lines 2-6 initialized the parent for each section to NIL and reset the queues $Q1$ and $Q2$. Lines 7-10 checked each section in the distribution feeder and if the section was not present in the queue, $Q1$ called the recursive subroutine SUB DFS(s).

The functionality of the subroutine SUB DFS(s) is as follows. The edges were explored from the most recently discovered edge that still had unexplored edges leav-

```
1  MAIN DFS
2  foreach section s do
3  |  π[s] ← NIL
4  end
5  Q1 = ∅
6  Q2 = ∅
7  foreach section s do
8  |  if s ∉ Q1 then
9  |  |  SUB DFS(s)
10 |  end
11 end
12 SUB DFS(s)
13 Enqueue(Q1, s)
14 foreach v ∈ Adj[s] do
15 |  if v ∉ Q1 then
16 |  |  π[v] ← s
17 |  |  SUB DFS(v)
18 |  end
19 |  Enqueue(Q2, s)
20 end
```

Figure 2.4 – Algorithm Used to Develop a Model of the Reduced Distribution Feeder in the Transient Analysis Tool

ing it. In the process of exploring all the edges leaving the parent s, the parent was enqueued into $Q1$. After all the edges were explored, the parent edge was enqueued into $Q2$. Line 13 enqueued s to $Q1$. Enqueuing the section s in the queue $Q1$ avoided re-entry of data in the final adjacency list.

The procedure for developing the model in Simulink was entirely automated. SimPowerSystems toolbox was used for this purpose. The overall modeling procedure was performed based on a multilayer approach. The first layer involved the implementation of the distribution lines along with the source. Subsequent to the modeling of the distribution lines, loads were modeled as part of the second layer. As a third layer, PV generators were included in the transient model (see Figure 2.2)

2.6 Results and Validation

This section presents the results from the implemented model in MATLAB/Simulink. The results are categorized in two subsections - results and verification of the network reduction and case studies of the verified transient model.

2.6.1 Results and Verification of Network Reduction

The results verifying the proposed network reduction algorithm are presented in this section. The details of the test feeder before and after the application of the network reduction algorithm are shown in Table 2.1. Significant reduction in the number of nodes, sections, transformers and loads can be observed from the values in Table 2.1. PV generators were retained while the network was reduced, thus supporting the study of the impact from PV generators on the feeder.

The test feeder under consideration showed the majority of the three-phase segments as overhead lines and the single-phase laterals as underground cables. The network reduction algorithm significantly reduced the single-phase laterals, thus af-

fecting the reactive power profile of the reduced feeder. Therefore, the network reduction algorithm accommodated the kVAr consumption of the underground cables in the loads. Based on the values shown in Table 2.2, the network reduction technique clearly retained a majority of the critical feeder details.

Figures 2.5a through 2.6b furnish the view of the test feeder in CYMDIST for various cases of the network reduction. A view retaining only the three-phase laterals is shown in Figure 2.5b. The circles in Figures 2.5a and 2.5b depict the PV generators located in the test feeder. The network reduction proposed in this study is capable of selectively retaining the single-phase lateral of interest, thus enabling the dynamic analysis on customers tens of miles down the lateral. Figures 2.6a and 2.6b present the view of the distribution feeder with selected laterals retained.

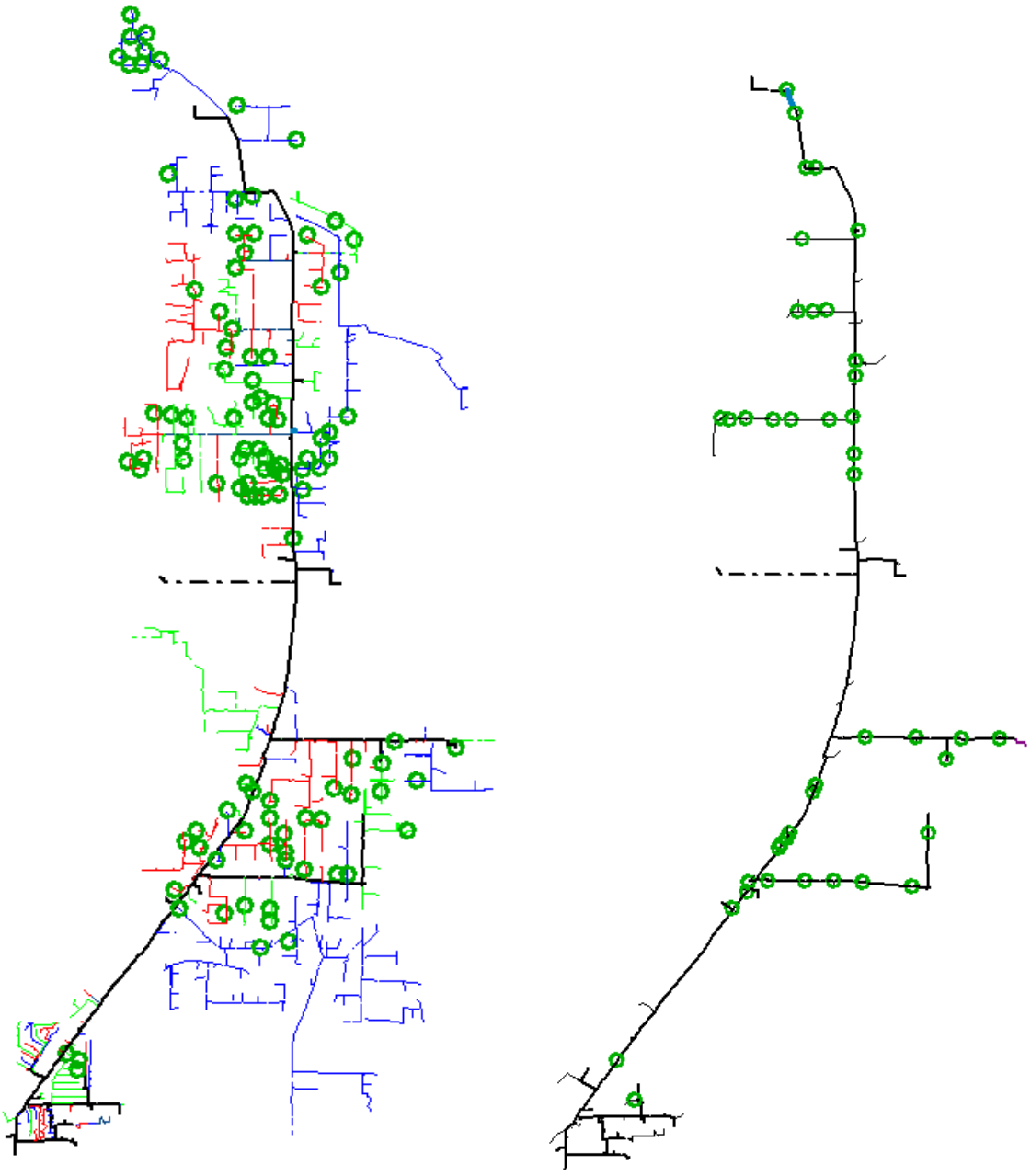
Table 2.1 – Effect of Network Reduction on the Distribution Feeder

Feeder details	**Original network**	**After network reduction**
Number of nodes	3032	738
Number of sections	4094	1142
Number of transformers	929	174
Number of PV generators	107	107
Number of loads	921	287

The test feeder under consideration has majority of the three-phase segments as overhead lines and the single-phase laterals as underground cables. The network reduction algorithm significantly cuts down the single-phase laterals, thus affecting the reactive power profile of the reduced feeder. Therefore, the network reduction algorithm accommodates the kVAr consumption of the underground cables in the

Table 2.2 – Performance Details of Network Reduction on the Distribution Feeder

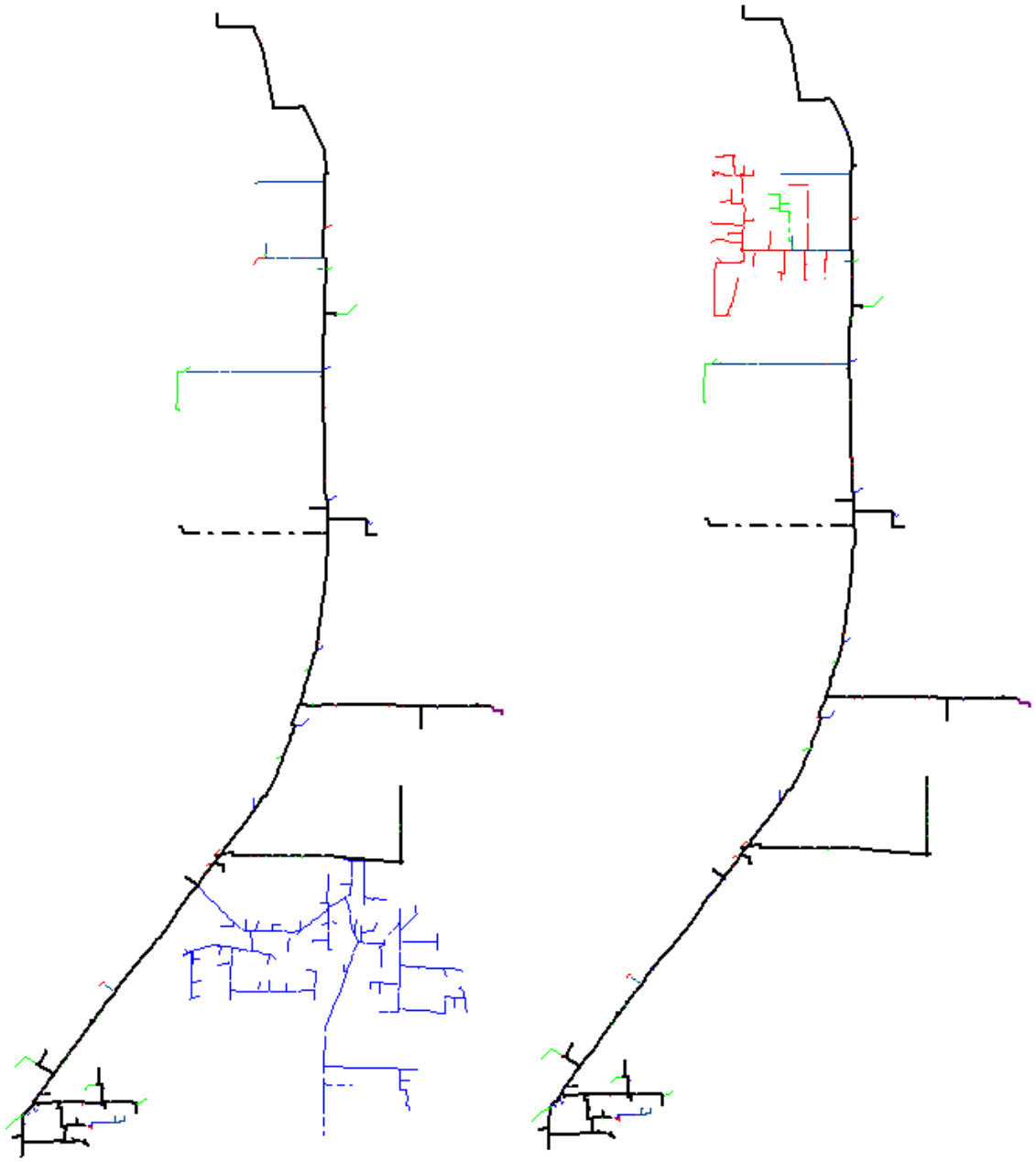
Feeder details	**Original network**	**After network reduction**
Current drawn from the substation (Amps)	226.9 (phase A), 284.9 (phase B), 246.1 (phase C)	231.7 (phase A), 281.8 (phase B), 251 (phase C)
Total load (kW)	5350	5350
Total load (kVAr)	430.58	90.01
Line losses (kW)	119.97	118.07
Cable losses (kW)	4.74	3.27
Transformer losses (kW)	57.29	40.55
Line losses (kVAr)	310.66	309.52
Cable losses (kVAr)	2.93	2.19
Transformer losses (kVAr)	108.18	120.34
kVAr consumption in line (capacitive)	16.63	12.80
kVAr consumption in cable (capacitive)	340.74	55.27



(a) Feeder diagram of the original feeder

(b) Feeder diagram after applying the network reduction algorithm

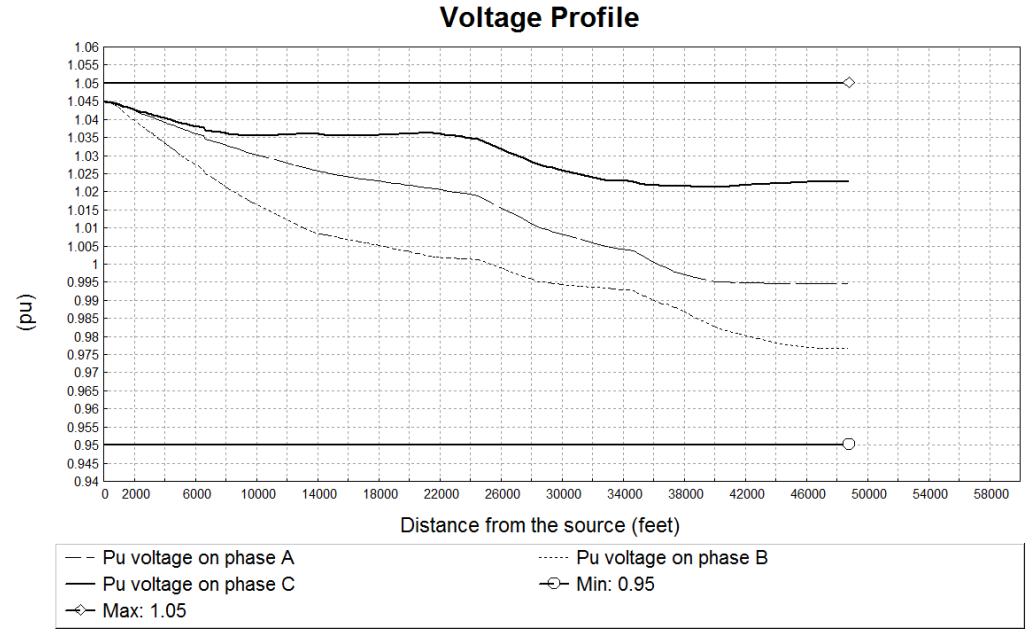
Figure 2.5 – Feeder Diagram of the Original and the Reduced Distribution Feeder from CYMDIST



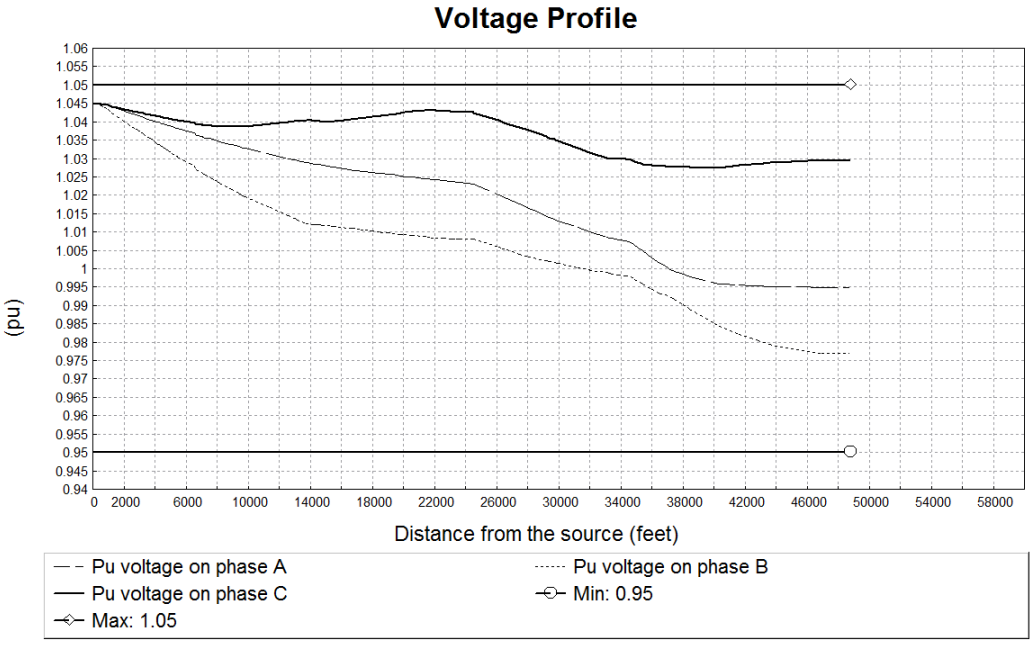
(a) Feeder diagram with a specific lateral of interest retained

(b) Feeder diagram with a specific lateral of interest retained

Figure 2.6 – View of the Reduced Distribution Feeders Representing the Capability of the Proposed Network Reduction Algorithm to Perform Selective Retention of Laterals

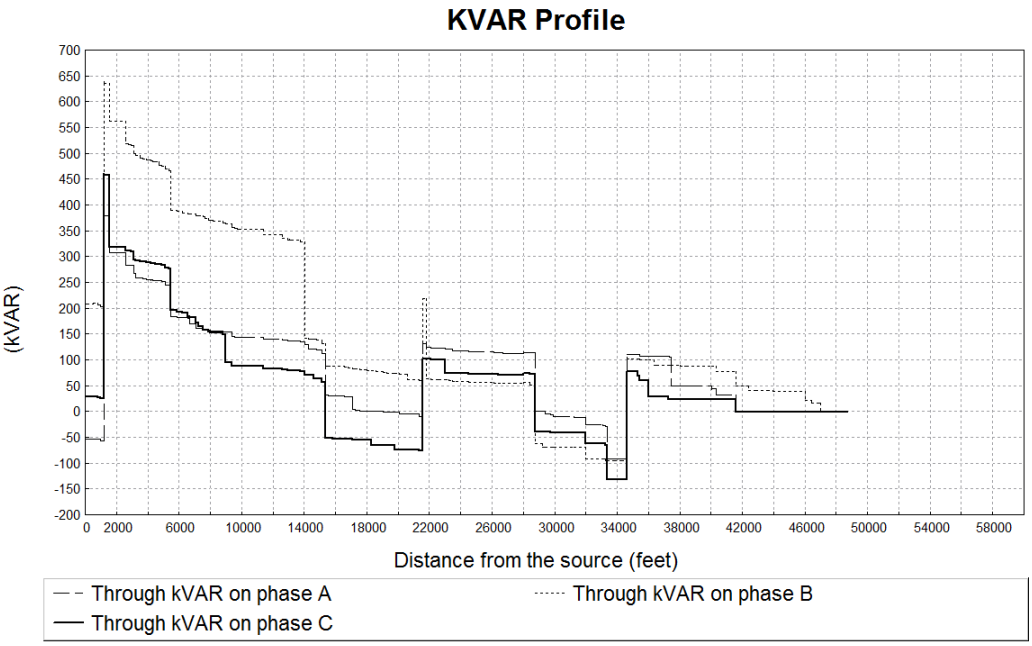


(a) Voltage profile for the original network

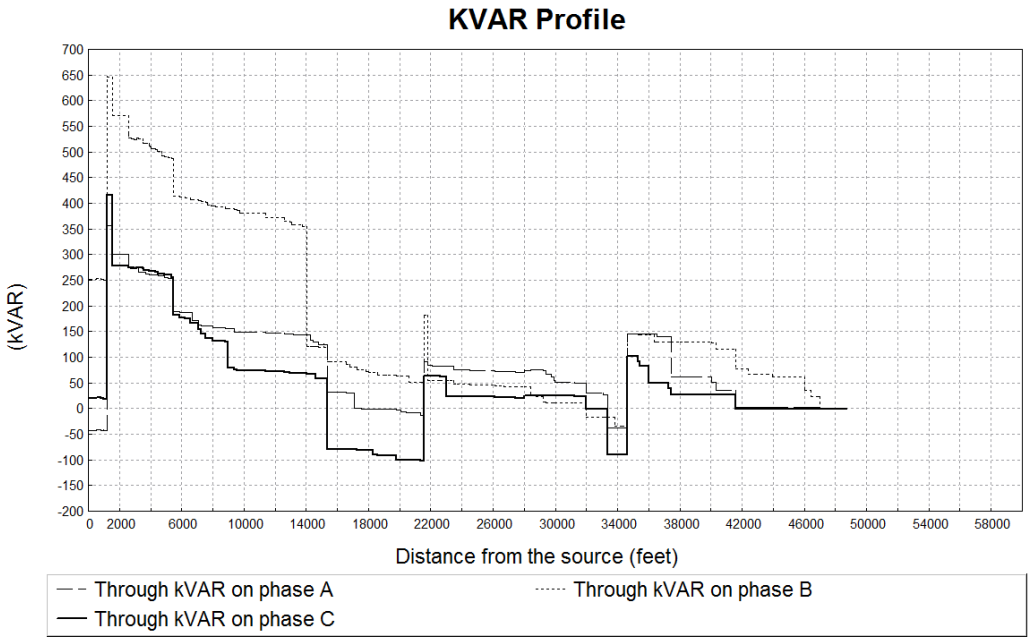


(b) Voltage profile for the reduced network

Figure 2.7 – Voltage Profiles of the Original and the Reduced Network from CYMDIST



(a) Reactive power profile for the original network



(b) Reactive power profile for the reduced network

Figure 2.8 – Profiles of the Reactive Power for the Original and the Completely Reduced Network from CYMDIST

loads. Based on the values in Table 2.2, it can be clearly observed that the network reduction technique retains majority of the critical feeder details.

Figures 2.7a and 2.7b provide the voltage profile of the original and the reduced network respectively. Figures 2.8a and 2.8b provide the reactive power profile of the original and the reduced network respectively. The voltage profiles and the reactive power profiles of the reduced network are in complete agreement with the original feeder.

The main purpose of the network reduction was to assist the modeling of the distribution feeder in a transient analysis tool. The reduced network was modeled in MATLAB/Simulink and the inbuilt phasor solver was used for solving the test feeder. The accuracy of the dynamic model in MATLAB/Simulink was verified with the model in the quasi-static analysis tool (CYMDIST).

2.6.2 Results and Verification of the Transient Model

The original feeder (Figure 2.5a) after the network reduction (Figure 2.5b) was modeled in MATLAB/Simulink based on the algorithm previously defined. The developed model was simulated for various scenarios and the results are presented in the following sections. This section also verified the dynamic phasor solver available in the MATLAB/Simulink by comparing the results with the conventional time domain solver for an IEEE 37 bus test feeder [52]. Solving the reduced feeder (Figure 2.5b) in the time domain solver was impractical, hence the IEEE 37 bus feeder was chosen. Figure 2.9 furnishes the voltages and currents of the IEEE 37 bus radial feeder in the conventional time domain mode as well as in the dynamic phasor mode. Figure 2.9 shows that the results from the phasor domain enveloped the sinusoidal waveforms obtained from the conventional time domain solver. Figure 2.9 shows that the dynamic phasor mode was not successful in capturing the high frequency transients.

Hence, dynamic phasor based solvers were efficient in analyzing the impact of the long-term transients rather than impact of the switching transients.

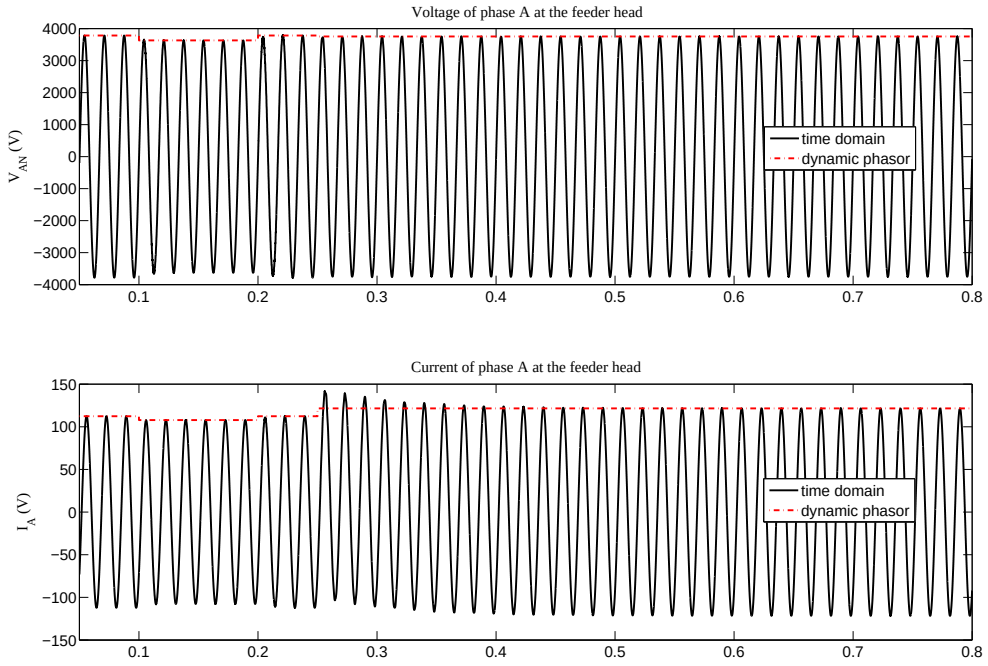


Figure 2.9 – Phase-neutral Voltage and Current of the Phase A for a Sample IEEE 37 Bus Test Feeder with a Series of Transients, Voltage Sag from 0.1 sec to 0.2 sec Followed by a Three-phase Fault at 0.25 sec

Throughout this section, the reduced network feeder presented in Figure 2.5b was used. The reduced feeder is presented in Figure 5.3, showing the legends useful for verifying the transient model. For the purpose of the verification, the feeder under study was identified with six measurement points. The measurement points were named and numbered DAS 1 to DAS 6 in order from the tail of the feeder and highlighted with rectangular boxes in Figure 5.3. The feeder had three fixed shunt capacitor banks two based on voltage set point and one based on current set point. The two voltage-controlled capacitor banks, highlighted as circles in Figure 5.3, were considered for the study of control interaction. The test feeder had two utility-scale

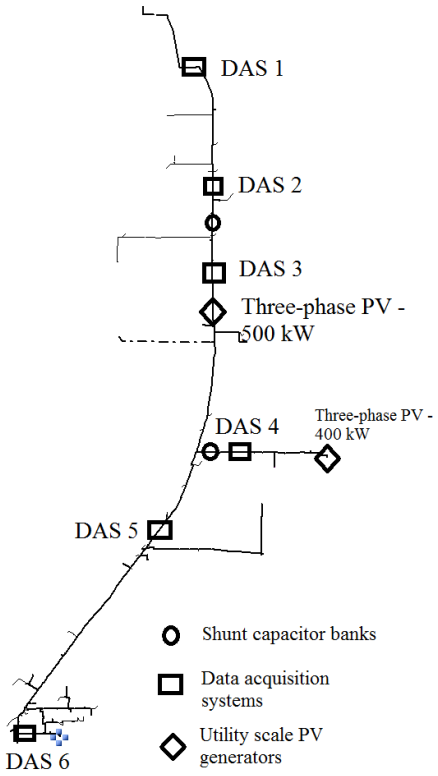


Figure 2.10 – View of the Test Feeder from a Quasi-static Analysis Tool with the Locations of the Measurements Points, Capacitor Banks, and the Three-phase PV Generators Highlighted

three-phase PV generators, highlighted with rectangles in Figure 5.3. The two utility-scale three-phase PV generators were considered to provide reactive power support.

2.6.2.1 Verification of the Transient Model

Table 2.3 shows a comparison of the values of the voltages and currents for the test feeder in the transient analysis tool with those of the quasi-static analysis tool (CYMDIST). The comparison was performed at various points on the feeder. The physical locations of the measurement points are highlighted in Figure 5.3. The voltages and currents were observed to deviate as follows: (@Feeder head = phase A

: 1.06%, phase B : 1.5%, and phase C : 0.23%), and (@End of the feeder = phase A : 3.4%, phase B : 1.8%, and phase C : 1.7%).

2.6.2.2 Impact of Fast Changes in Solar Irradiance

Figure 2.11 presents the voltage for phase A at different points on the feeder with and without voltage support from the PV generator. Further, this case study highlighted the possibility of performing long-term transient analysis using dynamic phasors. The model required 45 minutes to complete the simulation in the phasor mode, whereas the simulation for 20 ms in the conventional time-domain mode required five days.

The solar irradiation for the two utility-scale PV generators varied as a random number between 1 (clear sky) and 0.4 (cloudy sky). The PV generators accommodated the varying solar irradiation by generating the required reactive power, as shown in Figure 2.11. The model was simulated for a duration of 5 minutes by using the dynamic phasor solver in MATLAB/Simulink. The lines seen in the voltage plots of Figure 2.11 are the peak values of the voltages. Although the transient model was a complete three-phase model, only the voltage for phase A is furnished. The reactive power controller adjusted the generation to accommodate the variation in the voltages caused by the fast-changing solar irradiation.

2.6.2.3 Impact of Control Interaction

The results of the dynamic model for a scenario of control interaction are presented. A control interaction involves a correction attempt made at the same instant from multiple correction devices. In this case, for a voltage sag, the shunt capacitor bank and voltage support of the three-phase PV generator acted simultaneously. This case study simulated a voltage sag starting at the 30th second (Figure 2.12), forcing

Table 2.3 – Comparison of Power System Quantities (Voltages and Currents) from MATLAB/Simulink with those from CYMDIST

DAS number	**CYME**						**MATLAB/Simulink**					
	Voltage l-n (kV)			**Current (A)**			**Voltage l-n (kV)**			**Current (A)**		
	A	**B**	**C**	**A**	**B**	**C**	**A**	**B**	**C**	**A**	**B**	**C**
Feeder head	7.2	7.2	7.2	189.4	251.5	209.1	7.2	7.2	7.2	187.38	247.5	208.6
DAS 6	7.2	7.1	7.2	172.7	229.2	174.4	7.2	7.16	7.2	167.93	215.2	178.2
DAS 5	7	6.9	7.1	91.4	103.4	58.6	7.04	7	7.15	97.4	110.4	65.3
DAS 4	7	6.9	7.2	9.4	9.4	12.9	6.999	7	7.2	8.48	8.5	8.13
DAS 3	6.9	6.8	7.1	77.7	54.1	72	6.9	6.89	7.1	75	55.05	77.7
DAS 2	6.8	6.7	7	55.6	49.9	19.6	6.8	6.7	7.05	52.32	53.98	21
DAS 1	6.8	6.6	7	1.3	26.2	0.2	6.79	6.6	7	1.414	33.9	0.67

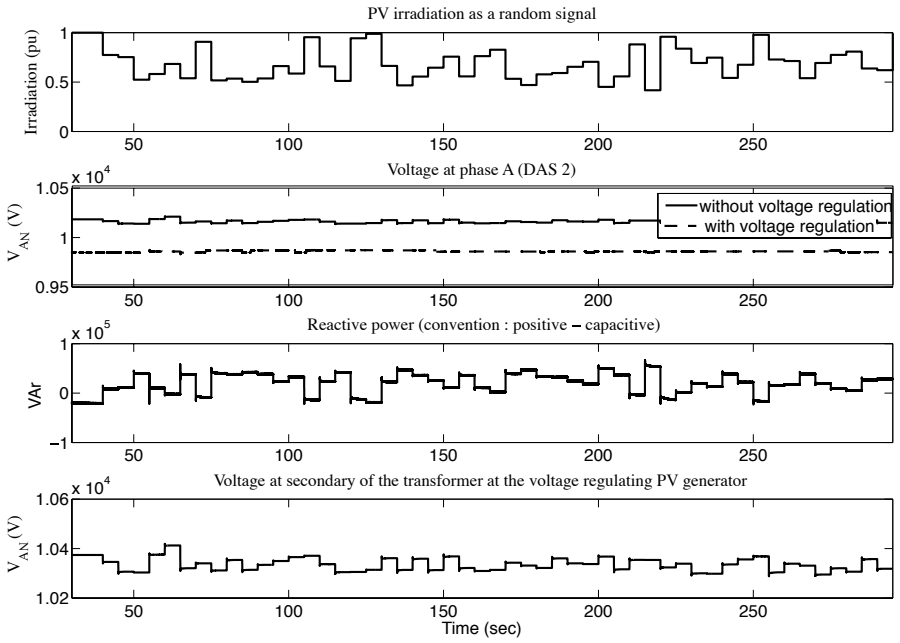


Figure 2.11 – Impact on the Phase-neutral Voltage at Various Points of the Feeder with and without Voltage Regulation During Fast Changes in Solar Irradiance as a Random Signal between 0.4 and 1 (p.u.)

the turn-on of the two voltage-controlled shunt capacitor banks. The voltage sag was set to end at the 65th second. During the duration of the voltage sag, a few cloud transients at the 35th, 45th, and 55th seconds were simulated (Figure 2.12).

The impacts of voltage sag with cloud transients were studied, alternatively including and omitting the presence of reactive power support from the three-phase PV generator. Figure 2.12 presents the transientsthat is, the voltage sag, the variation of solar irradiation, and the status of the shunt capacitor banks. The voltage support from the three-phase PV generator eliminates the switching of the shunt capacitor bank. Figure 2.13 shows the impact of the voltage support from the three-phase PV generator on the voltages, measured at multiple points on the feeder.

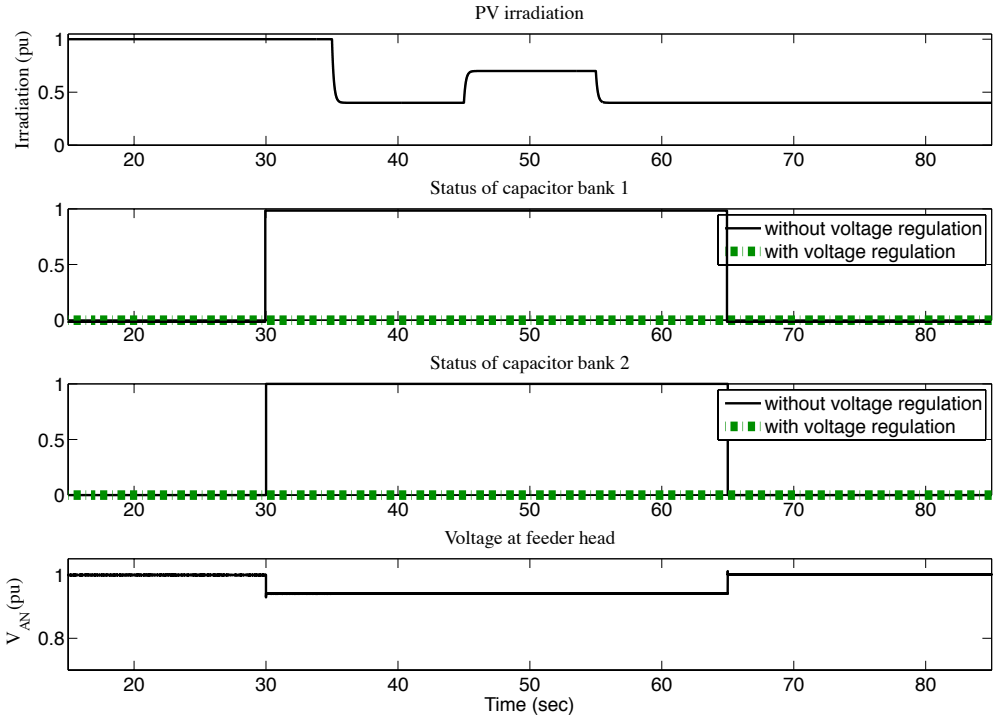


Figure 2.12 – Impact on Capacitor Bank Switching with and without Reactive Power Support from One of the Three-phase PV Generator During Cloud Transients and Voltage Sag

2.6.2.4 Impact of PV Generator Controller Bandwidth on the Feeder Response

The controllers of state-of-the-art inverters have multiple stages of inner and outer control loops with different control bandwidths. Typically, PV inverter manufacturers use proprietary methodologies to design the controllers. The quasi-static analysis was not useful for capturing the dynamics developed by these controllers. Hence, the simulation used dynamic phasors to capture the dynamics.

Figure 2.14 shows that the dynamics originating from the PV generators penetrated throughout the distribution feeder. The simulation modeled a cloud transient that reduced the PV generation capacity by 100 kW at the 45th second. The test

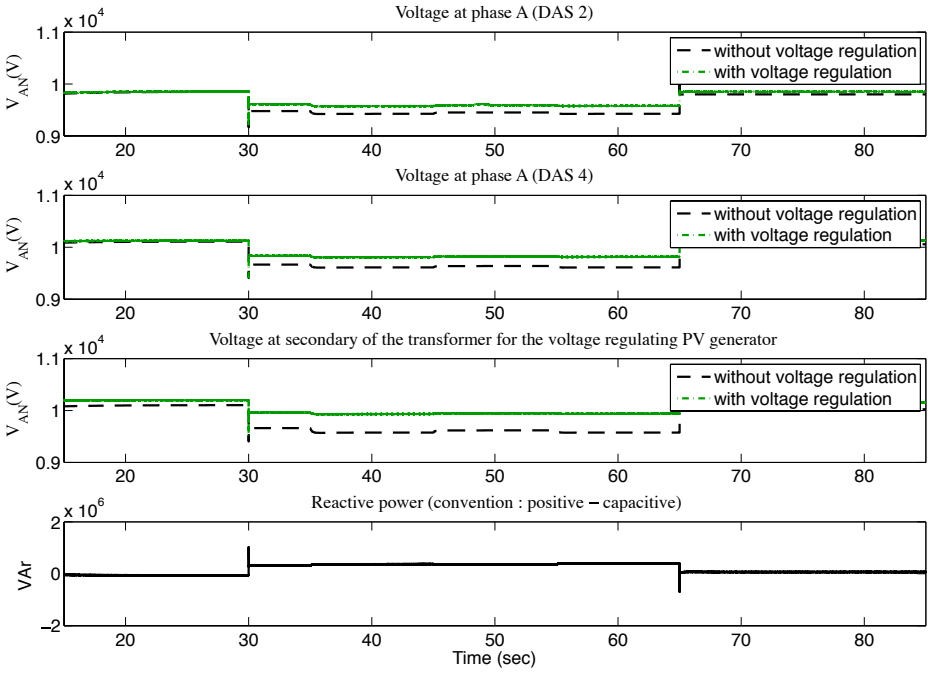


Figure 2.13 – Impact on the Phase-neutral Voltage at Various Points of the Feeder with and without Voltage Regulation During Cloud Transients and Voltage Sag

feeder was simulated twice for different controller bandwidth configurations. Figure 2.14 shows the voltages at various points on the feeder during a cloud transient, occurring in the 45th second of the simulation. The voltages for phase A at the DAS 2, the voltage at the transformer secondary of the 400 kW PV generator, and the DC link capacitor of the 500 kW PV generator are evident. The cloud cover caused a drop in the DC link voltage, which was corrected by the DC link voltage controller. The transient originating from the DC link controller affected the voltage of the feeder in different ways, depending on the controller specifications.

2.6.2.5 Simulation of a Transient Fault in the Feeder

An important application of the transient models is in the study of system faults and inverter response to the faults. This section presents the voltages and currents at

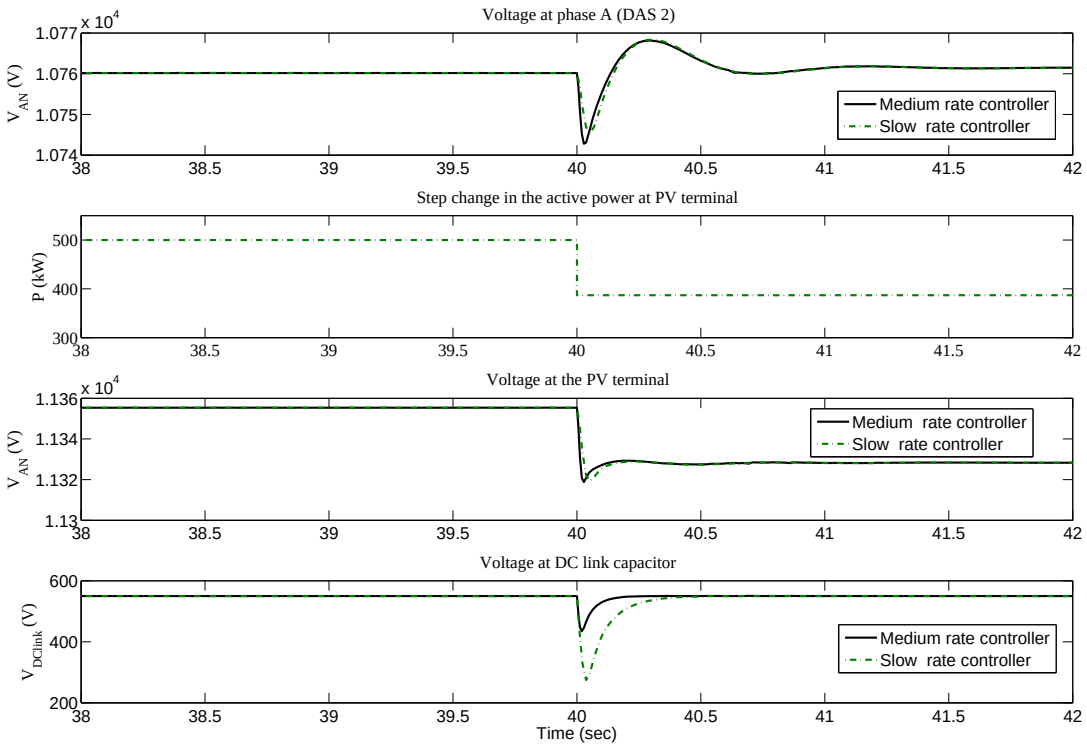


Figure 2.14 – Impact of Controller Bandwidth on the Distribution Feeder During a Cloud Transient

various points of the feeder during a three-phase fault halfway from the feeder head (inbetween DAS 3 and DAS 4).

Figure 2.15 presents the voltages and currents at the feeder head (upstream of the fault), DAS 4 (downstream of the fault), and the terminal of the voltage-controlled PV generator (upstream of the fault). The PV generator has a voltage regulation in place along with a current limiter. The voltage regulation loop of the PV generator attempts to follow the dropping voltage by forcing the current output to rise in order to follow the active power reference. The current limiter restricts the current reference of the controller from rising above the threshold.

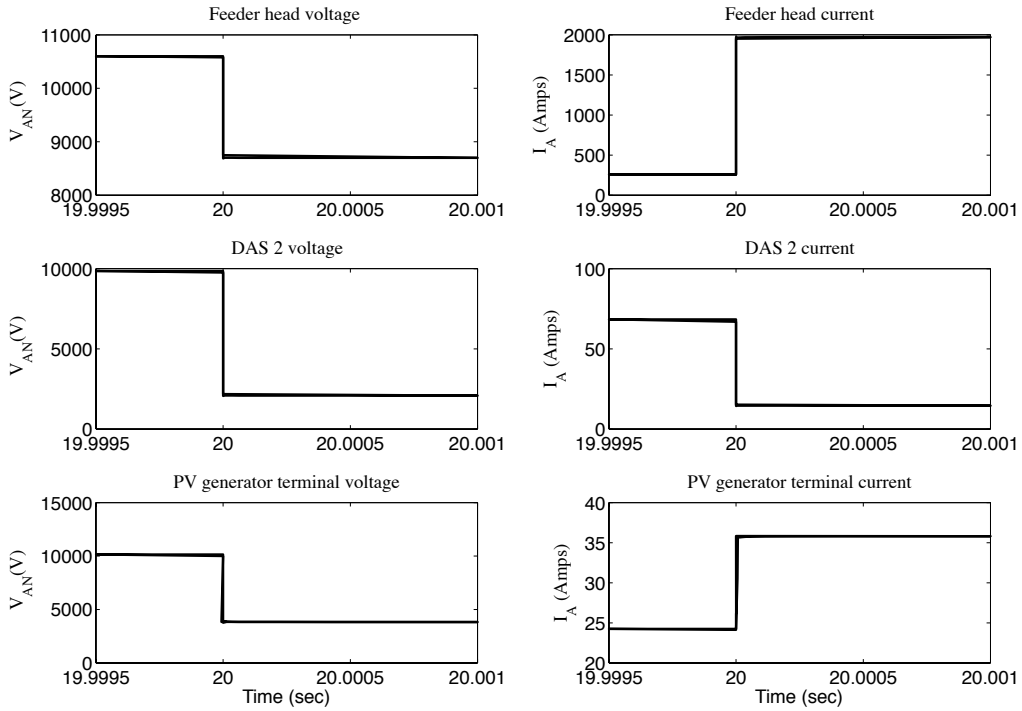


Figure 2.15 – Phase-neutral Voltages and Currents at Various Points Downstream and Upstream of the Three-phase Fault in the Distribution Feeder

Chapter 3

DYNAMIC ANALYSIS OF DISTRIBUTION SYSTEMS USING DIFFERENTIAL ALGEBRAIC EQUATIONS

3.1 Introduction

The variability of PV generators in distribution systems may lead to voltage fluctuations in the feeder, excessive tap-changer operations, or excessive capacitor-switching operations. These effects can be simulated and analyzed with a tool that runs a series of powerflows with short time-steps, following variable load and generation profiles. Running a sequence of powerflows is referred to as a quasi-static simulation, which involves a series of steady-state solutions that omit the dynamic effects between each solution. This method has been used for several years to simulate the effects of variable wind and solar power on energy distribution systems [53].

Capturing the dynamic effects of PV generators is necessary to analyze the impacts of controller bandwidths, voltage correction devices, and anti-islanding methods. Because the aim of this work was to analyze distribution feeders for dynamic properties, an efficient mathematical method needed to be developed. In this chapter, the use of an open source distribution system analysis tool, OpenDSS, was proposed for conducting the dynamic analysis. The mathematical solution was based on differential algebraic equations (DAE). The proposed application of the DAE modeled the selected states as differential equations, with the remaining distribution system shown as algebraic equations.

3.2 Proposed Approach

The implementations in this chapter were performed in OpenDSS, because the model of the field-verified test feeder already existed in OpenDSS, which is an open source tool. States such as PV generator electric currents were modeled using differential equations, and the rest of the distribution system was written as algebraic equations. In this study, the differential equations modeled two utility-scale PV generators. The improved Euler-Cauchy, or Heuns, method was used to solve the ordinary differential equations in OpenDSS. The improved Euler-Cauchy method is a predictor-corrector method, because the predicted value shown in (3.1) is corrected in (3.2). Equations (3.1) and (3.2) present the improved Euler-Cauchy method,

$$y^*_{n+1} = y_n + h\ f(t_n, y_n), \tag{3.1}$$

$$y_{n+1} = y_n + \frac{h}{2}\left[f(t_n, y_n) + f(t_{n+1}, y^*_{n+1})\right], \tag{3.2}$$

where, t_n, t_{n+1} are the independent variables, y_n, y_{n+1} are the dependent variables, y_n is either the initial value or the previously calculated state, and y_{n+1} is the unknown state that needs to be calculated. The hierarchy of the solution is as follows:

1. Formulate the algebraic equations and the ordinary differential equations separately

$$y' = f(t, y), \tag{3.3}$$

$$0 = g(t, y). \tag{3.4}$$

2. Solve the ODE using the numerical integration technique $y' = f(t, y)$

3. From the calculated state of y, solve the algebraic equations $g(t, y) = 0$

4. Increase the time-step and repeat the steps 2 and 3 until the final time specified.

The previously listed steps were implemented in OpenDSS by developing a user-defined dynamic linked library (DLL). The use of a DLL for the dynamic model of the PV generator had an additional advantage of protecting the technology vendors' proprietary information.

3.3 Average Model of Three-phase Inverter

The test feeder consisted of two utility-scale PV generators with a capacity of 400 kW and 500 kW shown at the highlighted locations in Figure 1.4. The dynamic models for two utility-scale PV generators were used for this study. In this section, the process for obtaining the dynamic model of an average three-phase PV generator and its controller is explained. A view of a complete switching model of a typical three-phase PV generator is shown in Figure 3.1. This study used the average model of a three-phase inverter, because switching of semiconductor devices occurs at high frequencies of the order of kilohertz (kHz).

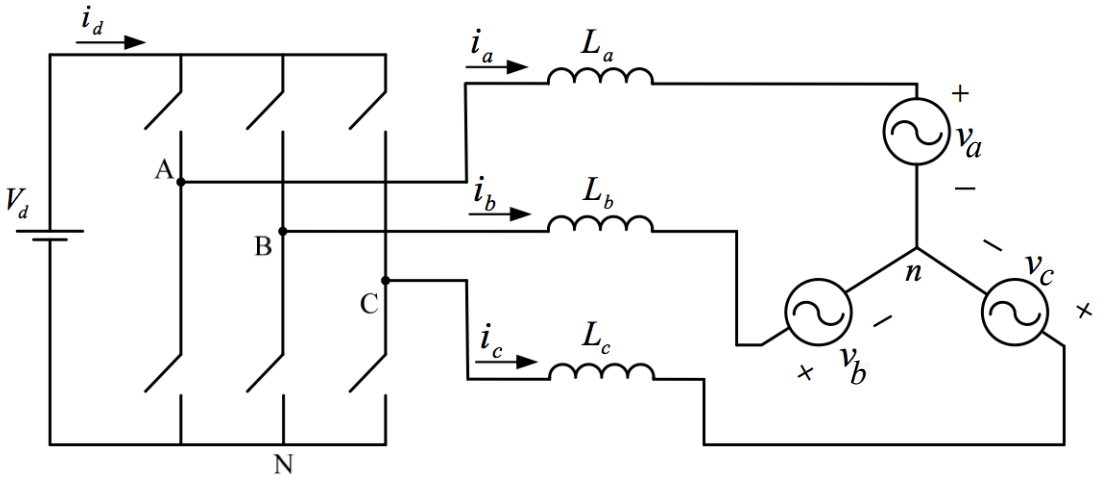


Figure 3.1 – View of the Switching Model of the Three-phase Inverter

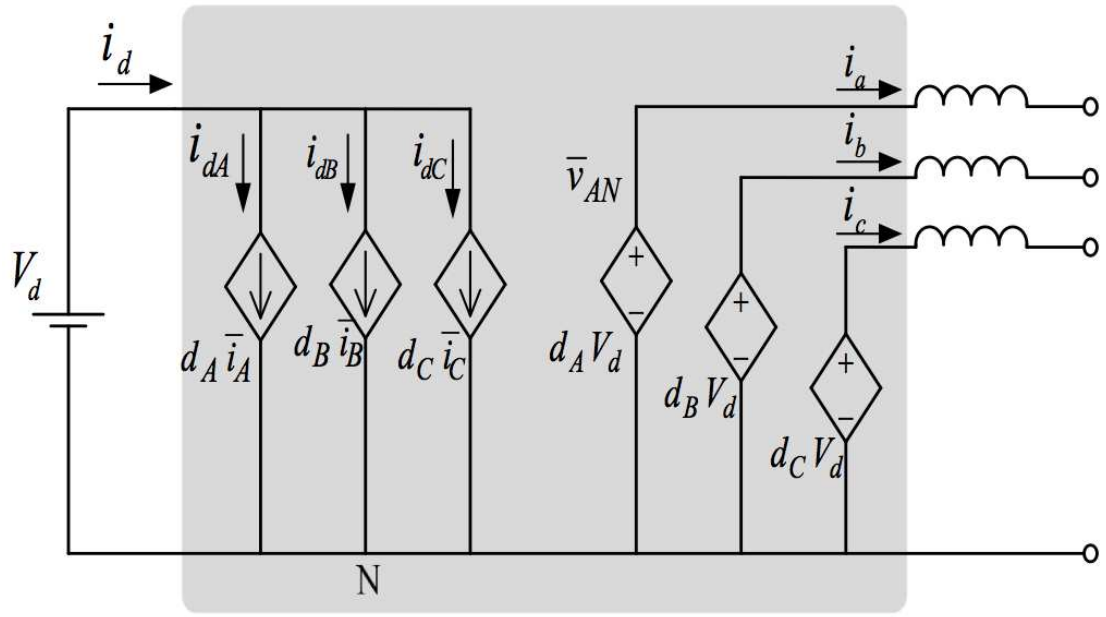


Figure 3.2 – View of the Average Model of the Three-phase Inverter

With reference to Figure 3.2, the analytical equations for the average model of the three-phase inverter can be written as

$$\bar{v}_{AN}(t) = \frac{V_d}{2} + \frac{V_d}{2} V_c sin(\omega t), \tag{3.5}$$

$$\bar{v}_{BN}(t) = \frac{V_d}{2} + \frac{V_d}{2} V_c sin(\omega t - 120^o), \tag{3.6}$$

$$\bar{v}_{CN}(t) = \frac{V_d}{2} + \frac{V_d}{2} V_c sin(\omega t + 120^o), \tag{3.7}$$

where, $\bar{v}_{AN}(t)$, $\bar{v}_{BN}(t)$, and $\bar{v}_{CN}(t)$ were the averaged values of the voltages applied to the filter components, V_d was the DC link voltage assumed to be a constant value for the model, and V_c was the control reference signal to the pulse width modulation (PWM) block. The control reference, V_c, for the PWM block was generated from the controller. The PWM block determined the steady state performance, quality of waveform and efficiency, whereas the controller determined the dynamic performance.

This work designed the controller based on the synchronous reference frame (dq control). Equations (3.8) and (3.9) show the matrices used to transform the values

of electrical voltages and currents from the *abc* frame to the *dq* frame and vice-versa respectively.

$$\begin{bmatrix} x_d \\ x_q \end{bmatrix} = \frac{2}{3} \begin{bmatrix} sin(\omega t) & sin(\omega t - \frac{2\pi}{3}) & sin(\omega t - \frac{4\pi}{3}) \\ -cos(\omega t) & -cos(\omega t - \frac{2\pi}{3}) & -cos(\omega t - \frac{4\pi}{3}) \end{bmatrix} \begin{bmatrix} x_a \\ x_b \\ x_c \end{bmatrix} \tag{3.8}$$

$$\begin{bmatrix} x_a \\ x_b \\ x_c \end{bmatrix} = \begin{bmatrix} sin(\omega t) & -cos(\omega t) \\ sin(\omega t - \frac{2\pi}{3}) & -cos(\omega t - \frac{2\pi}{3}) \\ sin(\omega t - \frac{4\pi}{3}) & -cos(\omega t - \frac{4\pi}{3}) \end{bmatrix} \begin{bmatrix} x_d \\ x_q \end{bmatrix} \tag{3.9}$$

where, x_a, x_b, and x_c were the electrical quantities in the *abc* reference frame, x_d, and x_q were the electrical quantities in the *dq* reference frame. The electrical quantities x_a, x_b, and x_c were assumed to be $X_m\ sin(\omega t)$, $X_m\ sin(\omega t - \frac{2\pi}{3})$, and $X_m\ sin(\omega t - \frac{4\pi}{3})$ respectively, where X_m was the peak value of the sinusoidal waveform. With reference

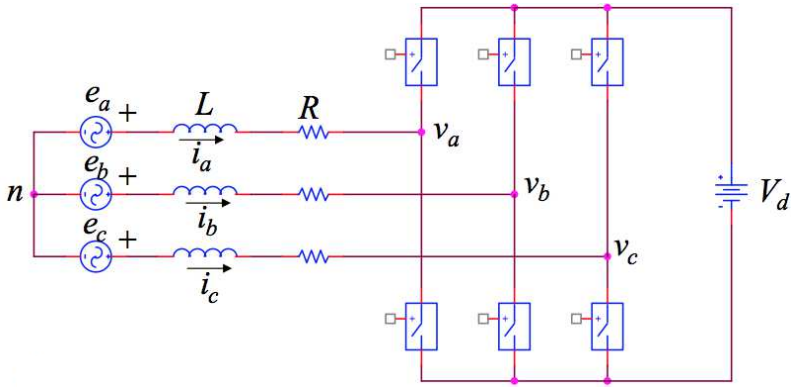


Figure 3.3 – Model of the Three-phase Inverter which has been Used to Obtain the Model of the Inverter in the *dq* Frame

to Figure 3.3 the equation for the grid voltage was written as,

$$e = L\frac{di}{dt} + Ri + v, \tag{3.10}$$

where, e represented the vector of phase voltages $\begin{bmatrix} e_a \\ e_b \\ e_c \end{bmatrix}$, i represented the vector of currents $\begin{bmatrix} i_a \\ i_b \\ i_c \end{bmatrix}$, v represented the vector of inverter voltages $\begin{bmatrix} v_a \\ v_b \\ v_c \end{bmatrix}$, R represented the value

of the resistance used in the filter and L represents the value of the grid inductance and the filter inductance of the three-phase inverter. The value of filter resistance and inductance for each phase was assumed equal. T represented the transformation matrix shown in (3.8), used to transform the quantities in the *abc* reference frame to the *dq* frame in (3.10),

$$Te = LT\frac{di}{dt} + RTi + Tv. \tag{3.11}$$

After the transformation of (3.11), all the terms in the *abc* reference frame were transformed into the *dq* reference frame as shown

$$L\frac{di_d}{dt} = e_d - Ri_d - v_d + \omega Li_d, \tag{3.12}$$

$$L\frac{di_q}{dt} = e_q - Ri_q - v_q - \omega Li_q, \tag{3.13}$$

where, ωLi_d and ωLi_q were the cross-coupling terms, v_d and v_q were the output of the average model of the three-phase inverter (equations (3.5) - (3.7)) in the *dq* reference frame, and e_d and e_q were the grid voltages in *dq* reference frame. The values of the v_d and v_q were calculated using a controller. The design of the controller is described in the following subsection.

3.3.1 Approach for Inverter Control

The model of a three-phase inverter in *dq* reference frame was derived in Section 3.3. The controllers for active power, reactive power, and voltage append the average three-phase inverter for the regular operation. A complete view of the average model of a three-phase inverter is shown in Figure 3.4. The inverter control was based on the synchronous reference frame. A dynamic model of a three-phase inverter as a DLL was appended to OpenDSS externally. The use of a DLL had an additional advantage of protecting the technology vendors' proprietary information.

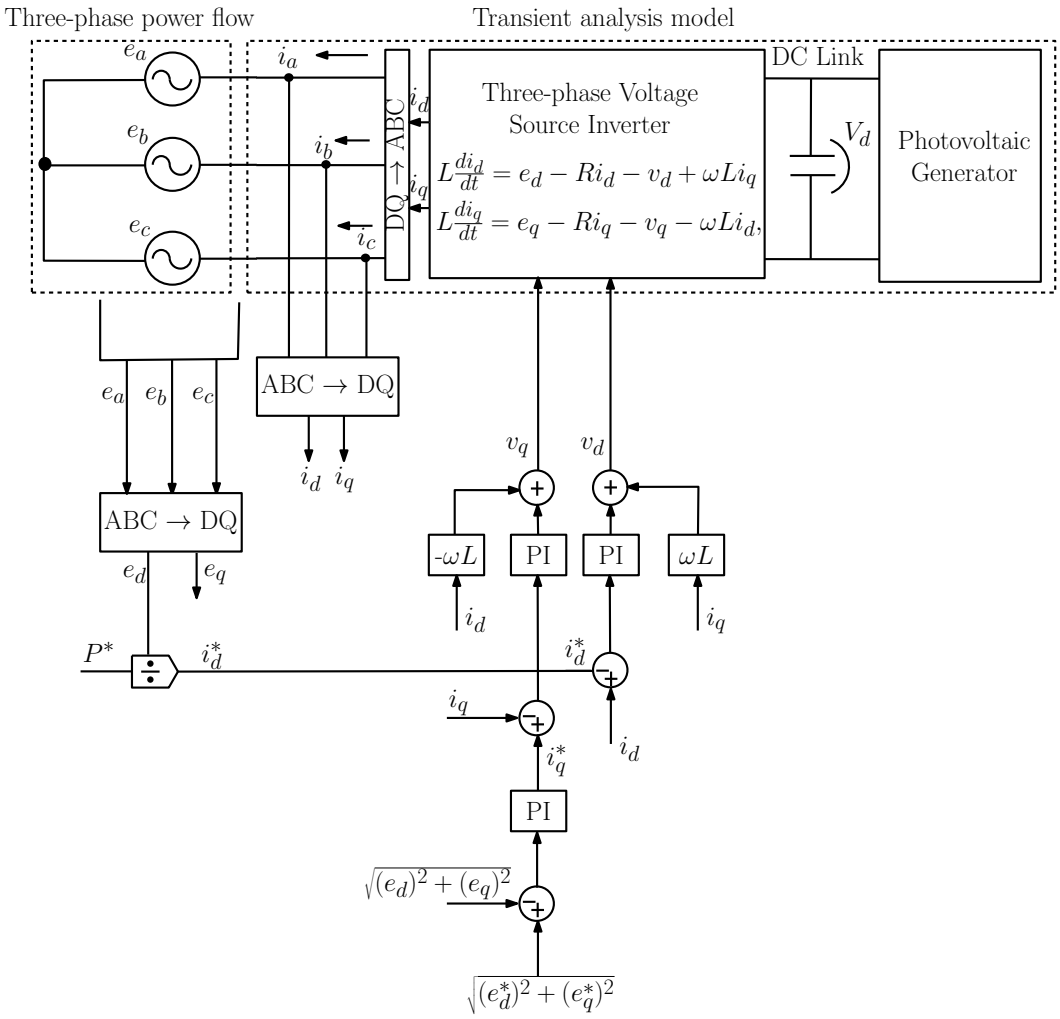


Figure 3.4 – Block Diagram of the Average Three-phase Inverter with All the Controllers in dq Reference Frame

Second order current controllers were designed for setting d axis and q axis currents. The view of the controllers in Laplace domain are as follows

$$G_{id} = \frac{K}{s}\frac{1+\frac{s}{\omega_p}}{1+\frac{s}{\omega_z}} \tag{3.14}$$

$$G_{iq} = \frac{K}{s}\frac{1+\frac{s}{\omega_p}}{1+\frac{s}{\omega_z}} \tag{3.15}$$

where G_{id} and G_{iq} are the controllers for d axis and q axis currents, s represents the Laplace transform, ω_p, and ω_z are the constants specific to the zero and pole of the

controllers. The behavior of a PV generator is governed using a sixth order ordinary differential equation.

3.4 Dynamic Analysis Based on Differential Algebraic Equations

The native tool of OpenDSS can perform only snapshot and quasi-static simulations. This work extended the capability of OpenDSS to run the dynamic simulations by developing a user-defined model for PV generators as a DLL. The user-defined DLL was developed in the same programming language as that used by OpenDSS. The source code of the OpenDSS, available online, was implemented in object Pascal (Delphi) programming language [54]. Embarcadero Delphi, an integrated development environment (IDE), was used to compile the DLL of the transient model for the three-phase inverter. The steps for creating the DLL are listed below:

- Define user input and output variables for the model.
- Supply input parsing, input editing, and output functions to be called from OpenDSS.
- Supply a Calc callback function:
  - Given the terminal voltage, calculate model current for powerflow, fault, dynamics, and other solution modes at each time-step.
  - Update internal model state variables, after each time-step.
- Supply an Init callback function, which initializes a dynamic solution from terminal voltage and current values.
- Supply an Integrate callback function, which performs predictor and corrector steps on state variables.

Figure 3.5 presents the overall view of the process for creating a DLL. The new() function instantiates a PV generator object. At every time-step (less than 1 ms), the Integrate() function was called, followed by the Calc() function. The Init() function was called to initialize the values for the first time-step. The values of the voltages at the point of interconnection were obtained from GetVariable() prior to calling Integrate(). Based on the voltages at the point of interconnection, the value of the electric currents to be injected were calculated.

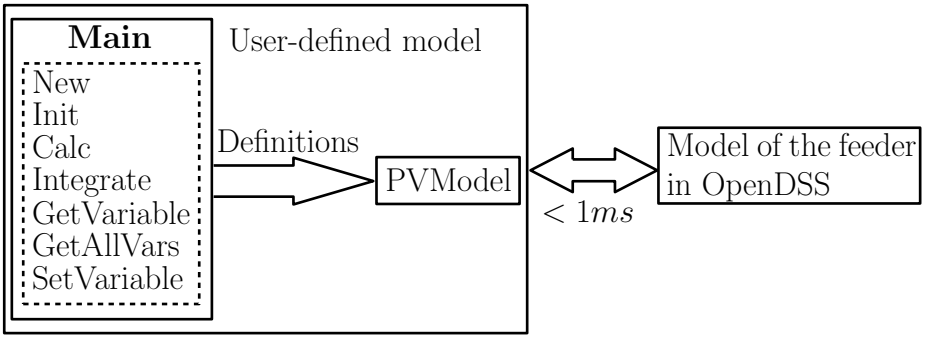


Figure 3.5 – Implementation of the User-defined Model in OpenDSS

3.5 Simulation Results for Dynamic Analysis

Figure 3.6 compares the DAE dynamic simulation with the time-domain simulation. The comparison was performed on a 37-node IEEE test distribution feeder, used as a standard platform [52]. The IEEE 37-node distribution system was modeled in MATLAB/Simulink to conduct the time-domain analysis. The systems in MATLAB/Simulink and OpenDSS were subjected to an identical cloud transient, as shown in Figure 3.6. At the 0.4 second mark in the simulation, the system experienced a fast-moving cloud cover, leading to a drop in solar irradiation from 1 p.u. to 0.8 p.u. Beginning at 0.5 second and continuing until the end of the simulation (0.8 second), a ramp rate increase in the solar irradiation was simulated. The peak values from

the dynamic simulation based on DAE closely encompassed the sinusoidal waveforms

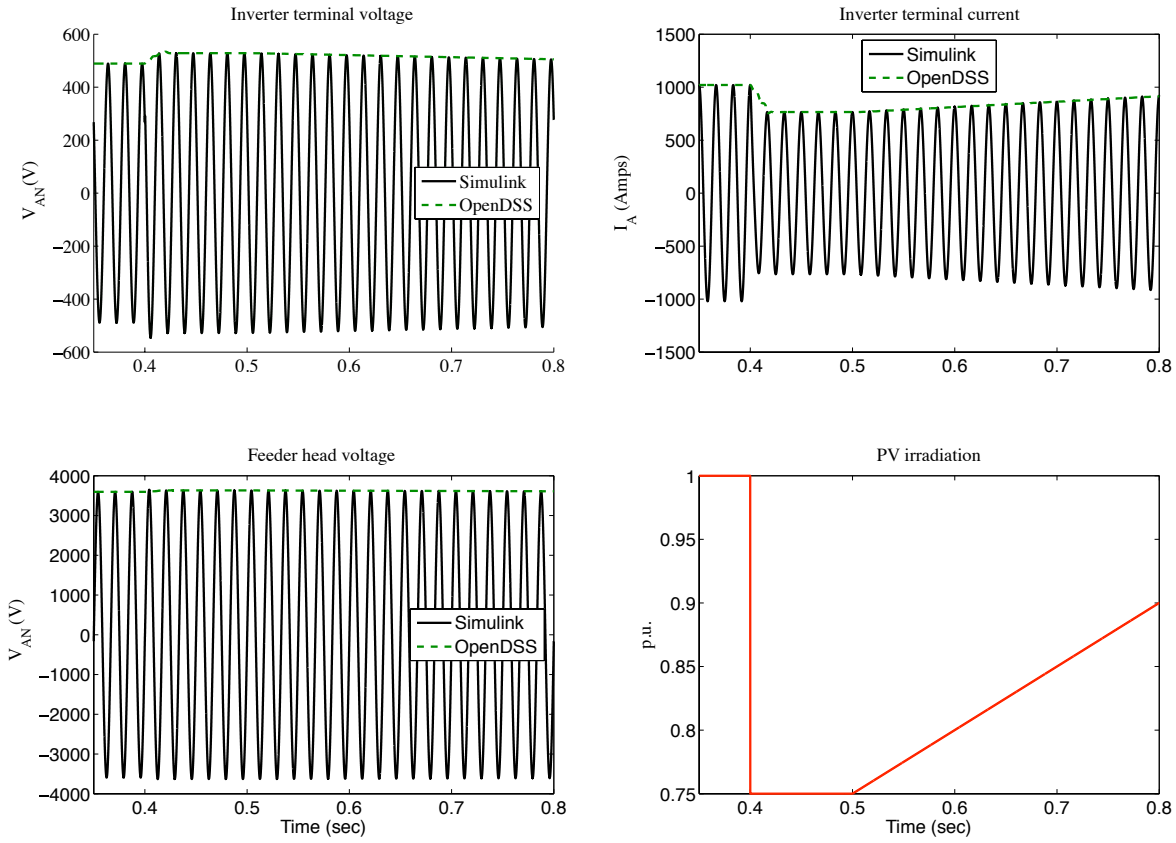


Figure 3.6 – Comparison of the Dynamic Simulation Results Based on DAE with the Time-domain Simulation Results for an IEEE 37 Bus Feeder

3.5.1 Performance of Fault Current Limiter in PV Generators

The dynamic model emphasizes the study of system faults. This section presents the phase-neutral voltages and currents at various points on the feeder during a three-phase fault at the end of the feeder (between DAS 1 and DAS 2). Figure 3.7 shows the electric voltages and currents at the feeder head (upstream of the fault), at DAS 2 (upstream of the fault), and at the terminal of the PV generator (upstream of the fault). The PV generator had a fault current limiter in place. The active power

controller of the PV generator, located upstream of the three-phase fault, attempted to follow the decreasing voltage forcing the electric current injection to rise. The current limiter restricted the current reference of the current controller from rising above the threshold (1.5 times the nominal value).

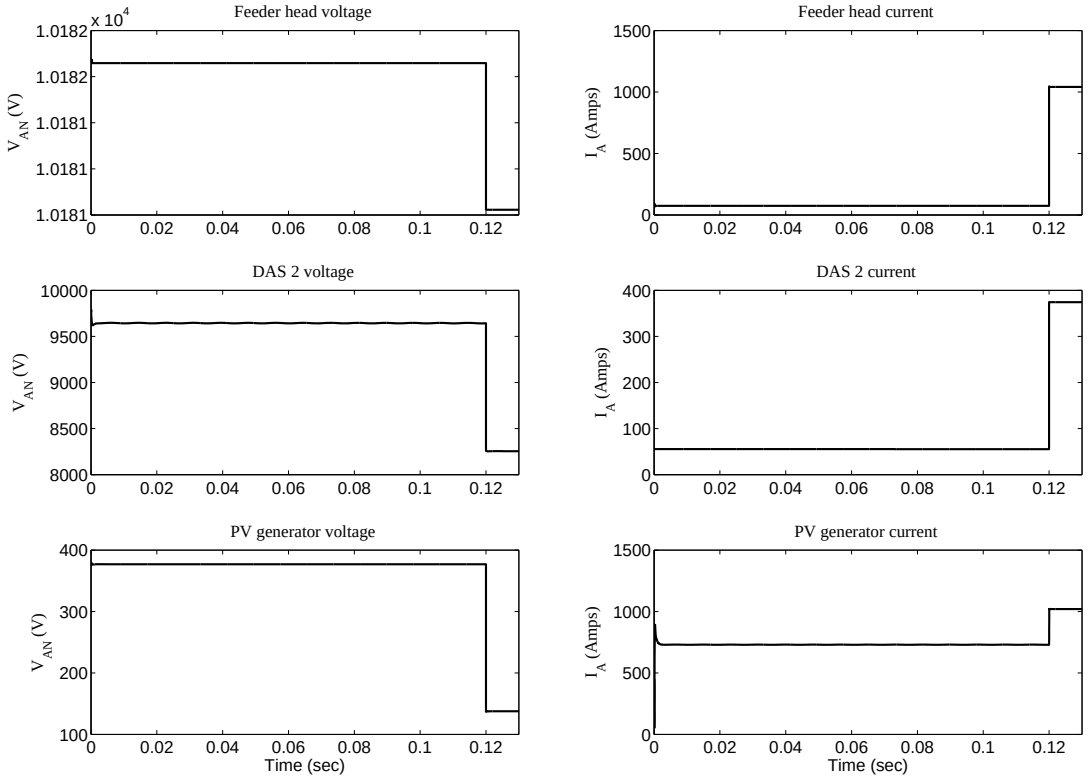


Figure 3.7 – Phase-neutral Voltages and Currents at Various Points Upstream of the Three-phase Fault in the Distribution Feeder Showing the Performance of the Fault Current Limiter

3.5.2 Impact of PV Generator Controller Bandwidth

The controllers of state-of-the-art inverters have multiple stages of inner and outer control loops with different control bandwidths. Typically PV inverter man-

ufacturers use proprietary methodologies to design the controllers. The dynamic simulation proposed in the chapter had an additional advantage of protecting the technology vendors' proprietary information.

Figure 3.8 shows that the dynamics originating from the PV generators penetrated throughout the distribution feeder. The simulation was performed for an identical cloud transient at 0.1 second with a varying current controller bandwidth. Figure 3.8 shows the phase-neutral voltages and currents at various points in the feeder during a cloud transient occurring at 0.1 second of the simulation. Figure 3.8 shows the phase-neutral voltages for phase A at the feeder head, for DAS 2, and for voltage at the transformer secondary of PV generator 2. The cloud cover caused a drop in the current injection from the PV generator, which the substation fulfilled. The transient originating from the current controller affected the currents of the feeder in different ways depending on the controller specifications.

3.5.3 Impact of Control Interaction

Control interaction involves multiple correction devices acting simultaneously. In this case, for a voltage sag, the shunt capacitor bank and the voltage support of the three-phase PV generator acted simultaneously. This case study simulated a voltage sag starting at 0.12 second (Figure 3.9) forcing the turn-on of the two shunt capacitor banks with a voltage set point. Although the capacitor banks typically have a delay, after which they begin to operate, for this simulation, the operation of the capacitor banks were modeled to be instantaneous (without delays).

The capacitor banks turned on during the voltage sag, provided that the reactive power support from the three-phase PV generator was not present. The voltage support from the three-phase PV generator eliminated the switching of the shunt capacitor bank. Figure 3.9 furnishes the phase-neutral voltages and currents at mul-

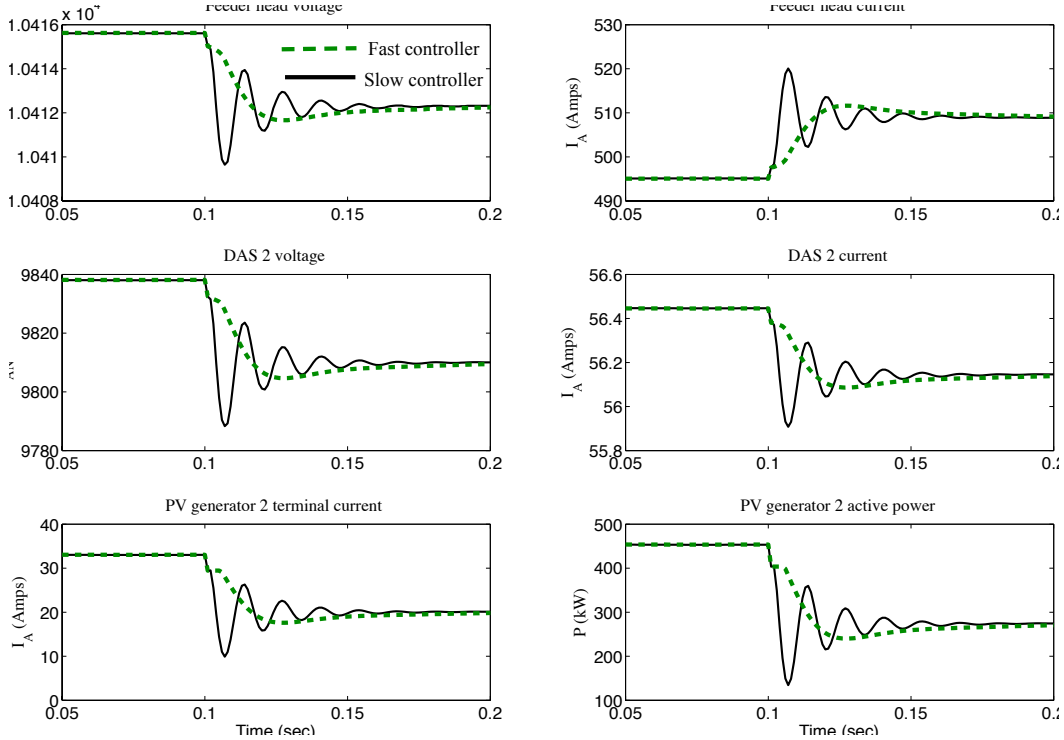


Figure 3.8 – Impact of Controller Bandwidth on the Distribution Feeder During a Cloud Transient

tiple measurement points on the feeder. The electrical voltages and currents at the feeder head and at DAS 2 measurement are presented. Additionally, the voltage at the terminal of one of the voltage regulated PV generator is presented. The event of voltage sag required additional reactive power to maintain the voltage at the PV generator terminals from crossing the limits.

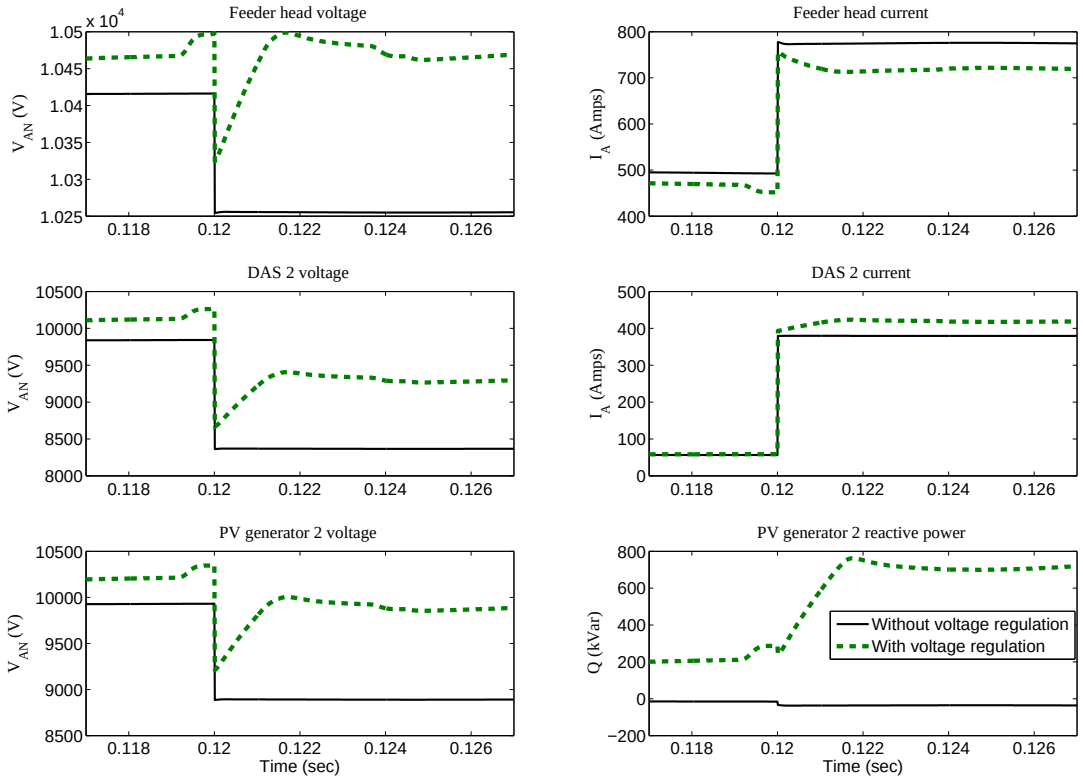


Figure 3.9 – Impact on the Phase-neutral Voltage at Various Points of the Feeder with and without Voltage Regulation During Voltage Sag

Chapter 4

ANALYSIS AND MITIGATION OF PHASE UNBALANCE

4.1 Introduction

Another significant challenge with the increasing penetration of PV systems is the phase unbalance created by an unequal distribution of the customer-owned PV systems among the three phases found in a typical power supply system. The unbalance induced by PV generators further exacerbates the existing unbalance caused by load mismatch. In addition, the unbalance induced by PV generators varies in conjunction with the constant variation of solar insolation.

The phase unbalance leads to various problems in the operation of a power distribution system. An increased phase unbalance significantly adds to the neutral currents, leading to unnecessary tripping or possible loss of protection coordination. Further, phase unbalance leads to unequal loading of transformer windings and distribution cables. Increased phase unbalance makes it difficult to meet the standards on unbalance factor and causes problems with sensitive three-phase equipment. Another key problem is excessive neutral-to-ground voltages.

The objective of this study was to analyze and quantify the impact of unbalanced PV installations on a distribution feeder. In addition, a power electronic converter solution was proposed for mitigating the identified impacts and to validate the solution's effectiveness through detailed simulations. A model of the test distribution circuit was developed, analyzed, and simulated extensively using a distribution system analysis tool. The effect of adding large-scale PV installations was studied in

terms of neutral current, voltage unbalance, voltage stability, and transformer and line loading.

Various case studies were performed at different levels of PV penetration and different levels of phase unbalances. The relationship between PV penetration levels and the effects was determined and documented, thus leading to the development of realistic specifications for the design of the phase unbalance mitigation solutions.

4.2 Model of the Test Distribution Feeder

A test distribution feeder was chosen for studying the impacts of increased rooftop PV installations. This distribution feeder was a three-phase 12 kV distribution circuit supplied through a substation distribution transformer (SDT). Table 4.1 lists the details of the test distribution feeder considered for this study. The GIS coordinates for the distribution feeder were not available; however, a preliminary model of the feeder in OpenDSS without the detailed location information was made available. The geographical map of the test distribution feeder is shown in Figure 4.1.

Table 4.1 – List of the Components for the Distribution Feeder

Number of nodes	2020
Number of loads	740
Peak load	4.6 MW
Shunt capacitor banks	2
PV generators	-
Maximum VUF (%)	0.1498

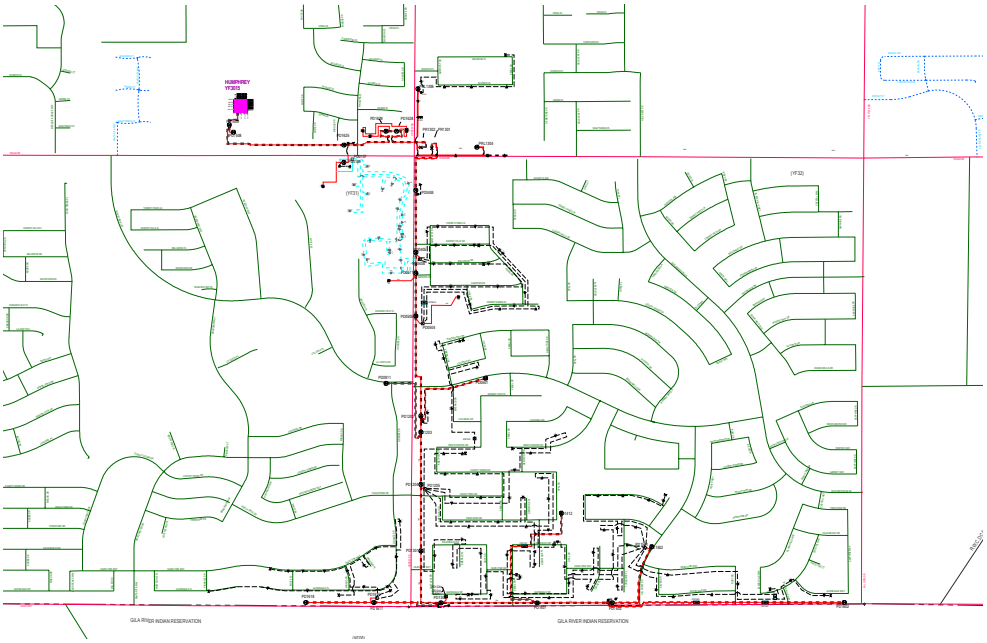


Figure 4.1 – Geographical View of the Test Distribution Feeder

4.2.1 Distribution Feeder Model in OpenDSS

The transmission side of the distribution system was modeled as a voltage source with a constant voltage 1.02p.u. and a zero-degree phase angle. The system impedances were calculated from a data file supplied by the utility.

The SDT's were rated at 67/12.47kV, 16.8MVA in capacity, with a high-side/low-side $\triangle$/Y grounded winding connection. The SDT had 8% reactance and 0.2% resistance. The SDT had five high-side taps. They were 70600, 68800, 67000, 65200, and 63400V taps; hence, the SDT was set at 68800V. The high-side tap was fixed under normal operation.

The load tap changers (LTCs) were installed at the low-sides of SDT. The LTCs could change low-side taps in the range of +/- 10%that is, 0.9 pu to 1.1 pu. There were 33 positions and 32 steps in total, nominal: 16 raise and 16 lower. LTC's are controlled by line-drop regulators, with 2.0% reactance and approximately 0.0%

resistance. The PTs used for these regulators had a ratio of 60; therefore, the band center was 122V, and the bandwidth was set as 3V. A 45-second time delay was set in the tap-change regulator. This time delay was measured between the time the regulator voltage strayed outside of the deadband and the time when the tap changing began. This time delay was used to coordinate multiple LTCs to determine which one would act first.

Both primary and secondary feeders were modeled as sectionalized lines in series in the OpenDSS code. Each line was defined by specifying the buses at both terminals, the number of phases, and the line parameters. The primary feeders left the SDT and terminate at distributed transformers, operating at 12kV. The sectionalized lines of primary feeders were modeled in OpenDSS as normal Pi circuits. The lines that belonged to the backbone portion were three-phase, while others were single-phase lines. The parameters required by OpenDSS in the input data file included positive-sequence series resistance and reactance in ohms per 1,000 ft and shunt capacitance in nF per 1,000 ft, as well as zero-sequence resistance, reactance, and capacitance. The length of the line was also given in multiples of 1,000 ft.

The customers were modeled as PQ loads connected to the secondary lines. The real power (P) and reactive power (Q) of each load were listed in an OpenDSS data file. The load shape consisted of a series of hourly multipliers, ranging from 0.0 to 1.0, which were applied to the base kW value of the load to yield the load at every hour for a year. Different load shapes were applied to various types of loadsfor example, residential or commercial loads. All the load shapes are plotted in Figure 4.2. During the off-peak period, the load multipliers ranged from 10% to 40% of the peak value.

Shunt capacitors were installed at appropriate locations along the three-phase backbone feeder as reactive power compensators. Each compensator was a three-phase capacitor bank, with fixed 1,200 kVAr capacity (i.e., 400 kVAr per phase).

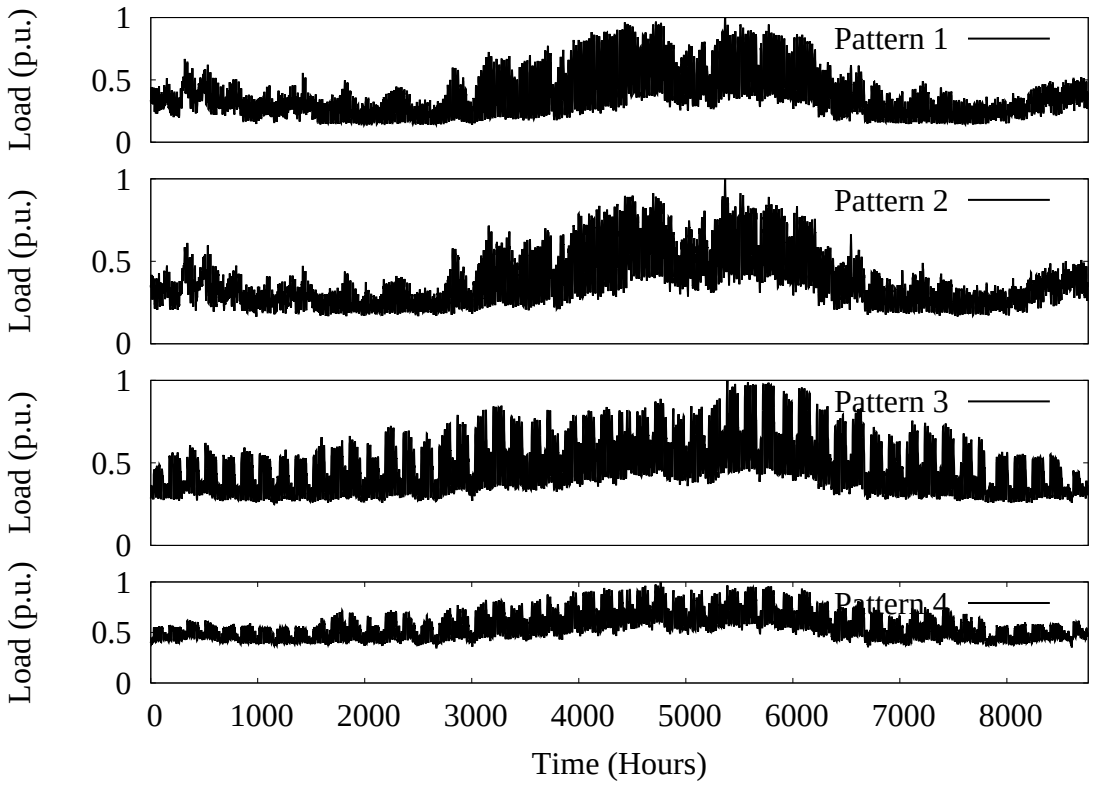


Figure 4.2 – Plot of the Load Shapes Consisting of a Series of Hourly Multipliers

4.2.2 Metric to Measure the Phase Voltage Unbalance

The unbalance in the distribution feeder was measured through the voltage unbalance factor (VUF) as a percentage. The three definitions of voltage unbalance are stated below.

NEMA (National Equipment Manufacturers Association). The NEMA definition assumes that the average voltage is always equal to the rated value, and because it works only with magnitudes, phase angles are not included. The NEMA definition [55] of voltage unbalance, also known as the line voltage unbalance rate (LVUR), is given by

$$\%LVUR = \frac{\text{maximum voltage deviation from the average line voltage}}{\text{average line voltage}} \times 100 \quad (4.1)$$

IEEE (Institute of Electrical and Electronics Engineers). The IEEE uses the same definition of voltage unbalance as NEMA; the only difference is that the IEEE uses phase voltages rather than line-to-line voltages. The IEEE definition [56] of voltage unbalance, also known as the phase voltage unbalance rate (PVUR), is given by

$$\%PVUR = \frac{\text{maximum voltage deviation from the average phase voltage}}{\text{average phase voltage}} \times 100 \tag{4.2}$$

General definition. Voltage unbalance is generally defined as the ratio of the negative sequence voltage component to the positive sequence voltage component [57], given by

$$VUF(\%) = \frac{\text{magnitude of negative sequence voltage}}{\text{magnitude of positive sequence voltage}} \times 100 \tag{4.3}$$

The positive and negative sequence voltage components were obtained by resolving three-phase unbalanced line-voltages V_{ab}, V_{bc}, and V_{ca} (or the phase voltages) into positive and negative sequence components, V_1 and V_2 respectively. The symmetrical components are given by

$$V_1 = \frac{(V_{ab} + aV_{bc} + a^2V_{ca})}{3} \tag{4.4}$$

$$V_2 = \frac{(V_{ab} + a^2V_{bc} + aV_{ca})}{3} \tag{4.5}$$

where $a = 1\angle 120$ and $a^2 = 1\angle 240$. This work used the general definition to identify the unbalanced nodes. Understanding the effects of phase voltage unbalance is important. In IEEE standard 241, impacts of phase voltage unbalance on three-phase motors and other electronic equipment have been presented. Some electronic equipment, such as computers may be affected by a phase voltage unbalance of more than 2% or 2.5% [56]. Hence, for this work, a VUF up to 2% was considered safe for operation.

4.3 Phase Unbalance in Distribution Feeders

The sensitivity of each node caused by the unbalanced PV generators varied based on the loading of the distribution feeder. Based on the load shapes presented in Figure 4.2, an hourly simulation for a year was performed, and neutral currents at two locations on the distribution feeder were captured. The neutral currents shown in Figure 4.3 and Figure 4.4 are from the nodes with the highest and the lowest magnitude of neutral currents. The feeder head happened to be the node with the lowest magnitudes of neutral current in the test distribution feeder. The currents in Figure 4.3 clearly show that the magnitudes of the neutral currents increases with the load. Moreover, the neutral currents and the loads peak at the 5,370th hour in the month of June. Figure 4.4 provides a closer view of the values of the neutral currents for the month around the 5,370th hour.

The voltage unbalance factor was also studied in detail at different loading conditions in time-series simulations. Figure 4.5 further confirms the variation of the VUF with loading conditions. The VUF for the chosen distribution feeder peaked at the 5,370th hour, as shown in Figure 4.5.

4.3.1 Sensitivity of Nodes in a Distribution Feeder

The impact of the unbalanced PV penetrations on the VUF largely depended on the selection of nodes in the distribution feeder. Hence, categorization of the nodes based on their sensitivity to VUF was important.

The distribution feeder consisted of single-phase, two-phase, and untransposed three-phase lines serving the unbalanced loads. The unbalanced loads led to unequal phase voltages, which affected the VUF. Figure 4.6 shows a systematic approach to categorize the nodes as most sensitive, intermediary sensitive, and least sensitive

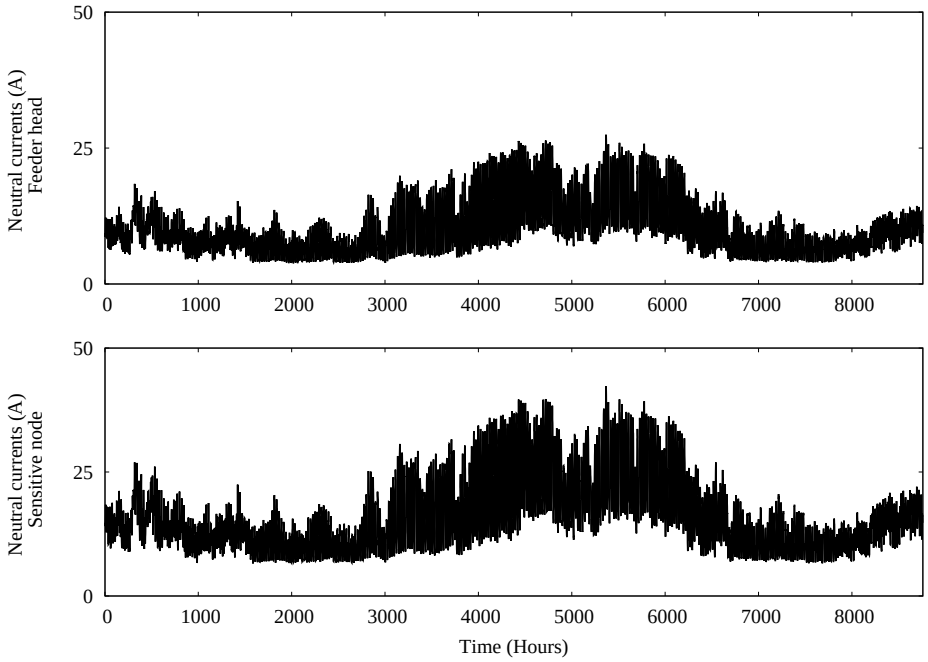


Figure 4.3 – Magnitude of Neutral Currents at Various Points on the Distribution Feeder for One Year

based on the VUF. Based on the process presented in Figure 4.6, the most sensitive, intermediary sensitive and least sensitive nodes were chosen. The PV generators were assumed to be installed at the most sensitive nodes in order to study the impacts of the large-scale penetration. Table 4.2 lists the most sensitive, intermediary sensitive, and least sensitive nodes along with the VUF identified from the process shown in Figure 4.6. In order to analyze the sensitivity of the nodes on the VUF, subsequently, PV generators were moved from the most sensitive nodes to the intermediary sensitive nodes and least sensitive nodes.

4.3.2 Effects of PV Unbalance on VUF and Neutral Currents

In order to study the unbalance induced by the PV generators, various case studies were examined. The level of PV penetration was increased in steps, and

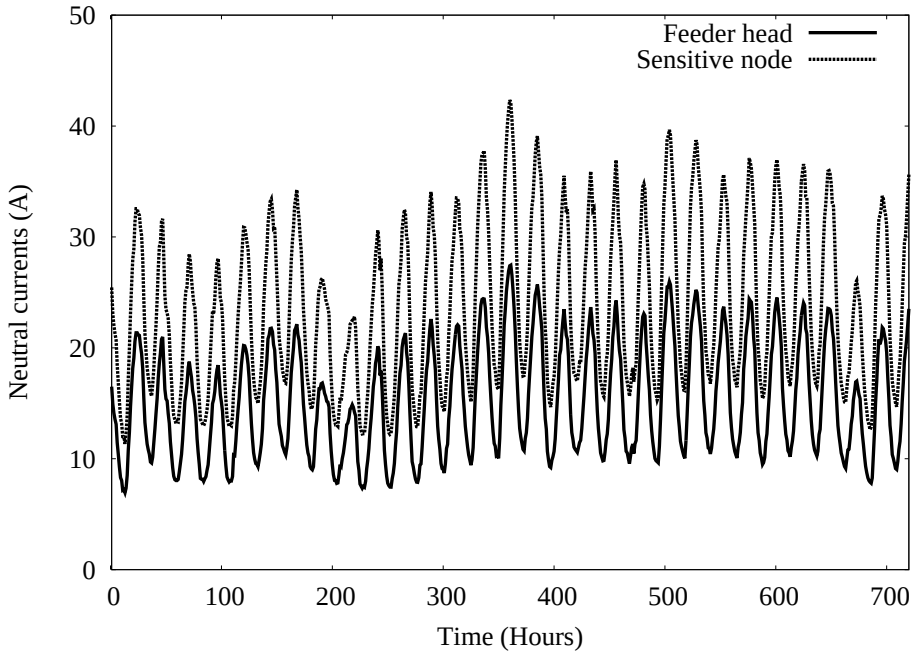


Figure 4.4 – Magnitude of Neutral Currents of the Distribution Feeder for the Month of June

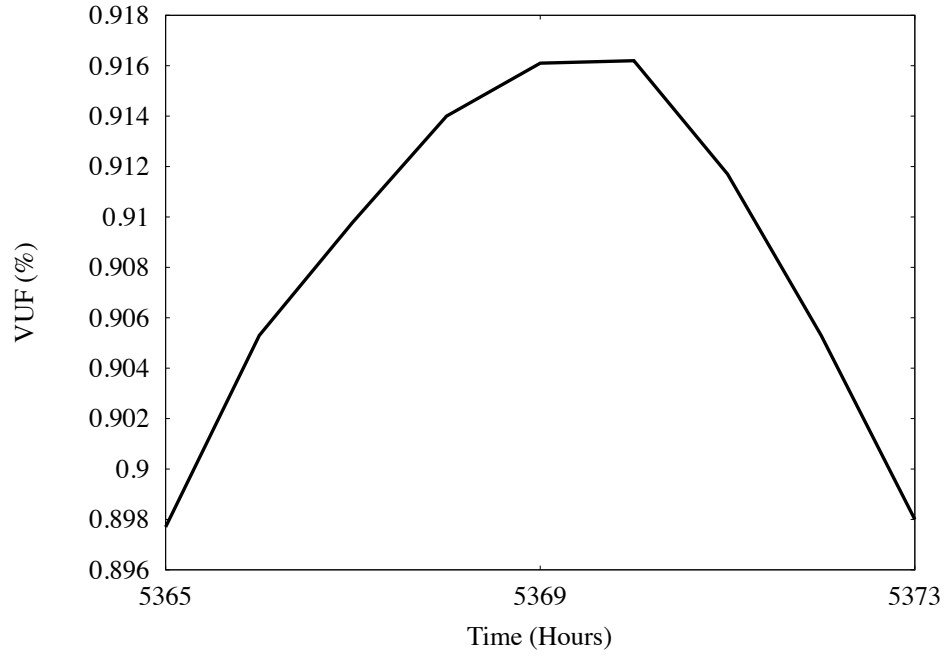


Figure 4.5 – Variation of VUF for Different Load Conditions

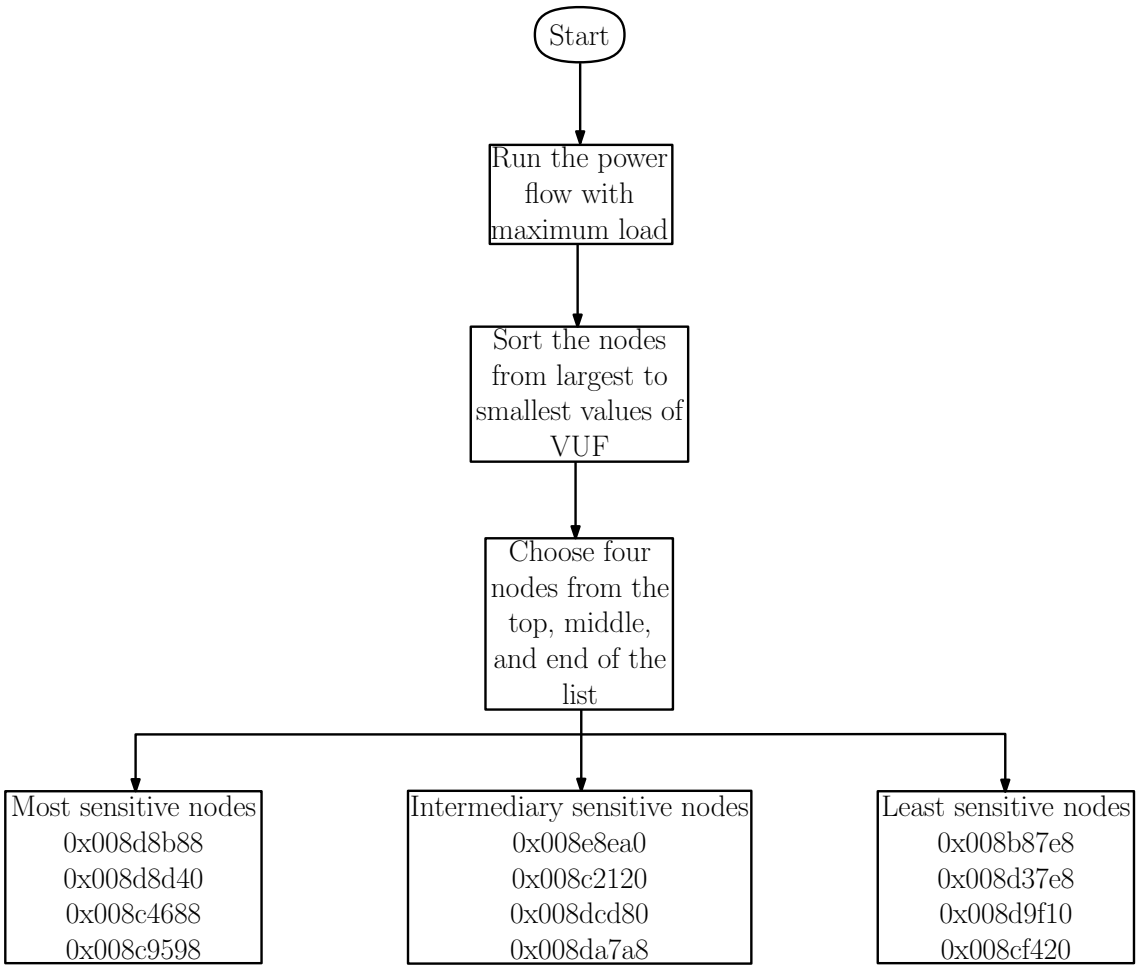


Figure 4.6 – Process Involved in Choosing the Nodes for the Study

the corresponding increases in the VUF and neutral currents were studied. The PV penetration was raised as a percentage of the maximum load (4,600 kW), from 25% to as high as 200% to determine the effects at very high penetration levels. The four penetration levels considered are as follows:

- 25%, 1150 kW
- 50%, 2300 kW
- 100%, 4600 kW

Table 4.2 – List of Nodes Arranged in Descending Order Based on the VUF

Set	**Nodes**	**VUF (%)**
Most sensitive nodes	0x008d8b88	0.1498
	0x008d8d40	0.1497
	0x008c4688	0.1494
	0x008c9598	0.1493
Intermediary sensitive nodes	0x008e8ea0	0.1307
	0x008c2120	0.1307
	0x008dcd80	0.1307
	0x008da7a8	0.1307
Least sensitive nodes	0x008b87e8	0.1049
	0x008d3fe8	0.1049
	0x008d9f10	0.1049
	0x008cf420	0.1049

- 200%, 9200 kW

The PV penetration was shared equally among the four most sensitive nodes. Different allocation of the total PV among the three phases found in a typical power supply system were considered to study the impact on VUF and neutral currents. The three scenarios considered were as follows:

- Equal allocation among the phases
- Phase A 20%, phase B 60%, phase C 20%

- Phase A 0%, phase B 100%, phase C 0%

Table 4.3 through Table 4.6 present the values of the neutral currents, phase currents and VUF for increasing values of the unbalanced PV penetration on the distribution feeder. An increase in the unbalanced PV penetration has adverse effects on the neutral currents and VUF. Choosing the most sensitive nodes for installing the PV generators results in violation of the VUF limit at 50% PV penetration. A larger PV penetration can be supported without VUF violation if the PV generators are installed at nodes with lower sensitivity.

In order to highlight the impact of the node sensitivity, the maximum VUF of the distribution feeder was studied with the PV generators located at various sets of nodes. The PV generators were added at four nodes each, from the most sensitive, intermediary sensitive, and least sensitive sets of nodes of the distribution feeder, and the maximum VUF for each case was obtained from OpenDSS.

Table 4.7 show the results corresponding to 50% PV penetrations, with the maximum VUFs for different locations of the PV generators. A reduction in the maximum VUF was observed with the PV generators in less sensitive nodes. A 40% reduction in the VUF was observed by placing the identical PV generators at less sensitive nodes. The results in Table 4.7 clearly show the importance of choosing an appropriate node for installing the PV generators in a distribution feeder. The distribution feeder can accommodate much higher penetration levels when installed at less sensitive nodes.

Table 4.3 – Neutral Currents, VUF and Phase Currents at the Most Sensitive Nodes of the Test Feeder with 25% PV Penetration

PV penetration(%)	**PV penetration (kW)**	**Per phase (kW)**			**Currents (Amps)**			**Neutral currents(A)**	**VUF (%)**
		A	**B**	**C**	A	B	C		
25	1150 (20%/60%/20%)	230	690	230	8.17	24.2	34.77	56.09	0.5217
					8.17	2402	31.7		
					8.17	24.2	34.77		
					8.17	24.02	31.7		
	1150 (100%/0%/0%)	1150	0	0	40.018	0	42.122	59.493	1.165
					40.018	0	39.04		
					40.018	0	42.122		
					40.018	0	39.04		

Table 4.4 – Neutral Currents, VUF and Phase Currents at the Most Sensitive Nodes of the Test Feeder with 50% PV Penetration

PV penetration(%)	**PV penetration (kW)**	**Per phase (kW)**			**Currents (Amps)**			**Neutral currents(A)**	**VUF (%)**
		A	**B**	**C**	A	B	C		
50	2300 (20%/60%/20%)	460	1380	460	16.15	47.86	28.02	70.8	0.9162
					16.15	47.86	25.04		
					16.15	47.86	28.02		
					16.15	47.86	25.04		
	2300 (100%/0%/0%)	2300	0	0	88.578	0	42.148	97.78	2.195
					88.578	0	39.065		
					88.578	0	42.148		
					88.578	0	42.148		

Table 4.5 – Neutral Currents, VUF and Phase Currents at the Most Sensitive Nodes of the Test Feeder with 100% PV Penetration

PV penetration(%)	**PV penetration (kW)**	**Per phase (kW)**			**Currents (Amps)**			**Neutral currents(A)**	**VUF (%)**
		A	**B**	**C**	A	B	C		
100	4600 (20%/60%/20%)	920	2760	920	42.77	94.32	31.99	87.65	1.956
					42.77	94.32	18.1		
					42.77	94.32	31.99		
					42.77	94.32	18.1		
	4600 (100%/0%/0%)	4600	0	0	153.22	0	42.19	155.46	4.168
					153.22	0	39.11		
					153.22	0	42.19		
					153.22	0	39.11		

Table 4.6 – Neutral Currents, VUF and Phase Currents at the Most Sensitive Nodes of the Test Feeder with 200% PV Penetration

PV penetration(%)	**PV penetration (kW)**	**Per phase (kW)**			**Currents (Amps)**			**Neutral currents(A)**	**VUF (%)**
		A	**B**	**C**	A	B	C		
200	9200 (20%/60%/20%)	1840	5520	1840	63.18	183.7	32.36	159.58	3.4
					63.18	183.7	34.18		
					63.18	183.7	32.36		
					63.18	183.7	34.18		
	9200 (100%/0%/0%)	9200	0	0	295.35	0	42.35	287.66	7.9
					295.35	0	39.26		
					295.35	0	42.35		
					295.35	0	39.26		

Table 4.7 – Maximum VUF for Various Case Studies

Set	**Nodes**	**PV penetration (kW) 50 % penetration**	**Maximum VUF (%)**
Most sensitive nodes	0x008d8b88	2300(100%/0%/0%)	2.195
	0x008d8d40		
	0x008c4688		
	0x008c9598		
Intermediary sensitive nodes	0x008e8ea0	2300(100%/0%/0%)	1.714
	0x008c2120		
	0x008dcd80		
	0x008da7a8		
Least sensitive nodes	0x008b87e8	2300(100%/0%/0%)	1.357
	0x008d3fe8		
	0x008d9f10		
	0x008cf420		

4.4 Mitigation of Phase Unbalance in Distribution Feeders

Phase unbalance leads to various problems in the operation of power distribution systems, including overcurrents in neutral conductors and unequal loading of transformer windings and distribution cables. This section focuses on some of the common mitigation methods. Mitigation strategies for phase unbalance caused by PV generators include:

- Rephasing the laterals
- Adding voltage regulators
- Switching capacitor banks
- Using power electronics based devices

Rephasing the laterals is one of the options for solving phase unbalance problems [58]. The main barrier to rephasing existing distribution system laterals is revealed through cost-benefit analysis. After considering the cost and time to rephase the laterals, one can conclude this method is not suitable for mitigating the unbalance caused by PV generators. Additionally, rephasing the laterals cannot handle the varying unbalance conditions, such as solar irradiation changes that occur during the day.

Adding voltage regulators is a traditional option to mitigate the voltage unbalance in a distribution system [59]. The voltage ratio of the voltage regulators can be adjusted to balance the three-phase voltages for certain nodes. However, the smallest tap-changing step of the voltage regulator limits the accuracy of adjusting the voltage ratio, thus affecting the accuracy of the voltage balancing. Another disadvantage of the voltage regulator is that the current unbalance is exacerbated when voltage regulators are being used to balance the voltages.

Voltage unbalance caused by reactive power can be mitigated by switching capacitor banks in the network [60]. However, most of the PV systems generate power at nearly unity power factor. To mitigate the phase unbalance caused by distributed PV generators, active power instead of reactive power should be compensated, which could not be provided by capacitor banks.

The neutral currents and unbalanced voltage components in the system can be actively compensated using a three-phase switched-mode power converter. This power electronics-based solution with an advanced closed-loop control is capable of injecting any desired current within its ratings to compensate harmonics, reactive power, and load unbalance.

The active power filter with voltage source converter is a widely used method to compensate the current harmonics, increase power factor, and compensate neutral currents. Figure 4.7 shows a simple schematic of a shunt-type active power filter in a three-phase, four-wire network [61]. A step-up transformer may be needed to connect the power converter to a medium-voltage network. The active power filter injects a compensating current equal in amplitude but opposite in phase with the target components in load current (can be harmonics, reactive current, negative sequence current, and zero sequence current) to achieve the function, such as filtering for the target components.

Ideally, the active power filter does not consume power for current conditioning; except for the power lost in the hardware. The semiconductor switching devices are key components of the active power filter. The insulated-gate bipolar transistor (IGBT) is the most popular choice for medium power-rating active power filters for its ability to maintain high efficiency when switching. High switching frequency can reduce the size of the passive filter at the converter output for attenuating switching frequency current ripple. Higher switching frequency also allows higher control

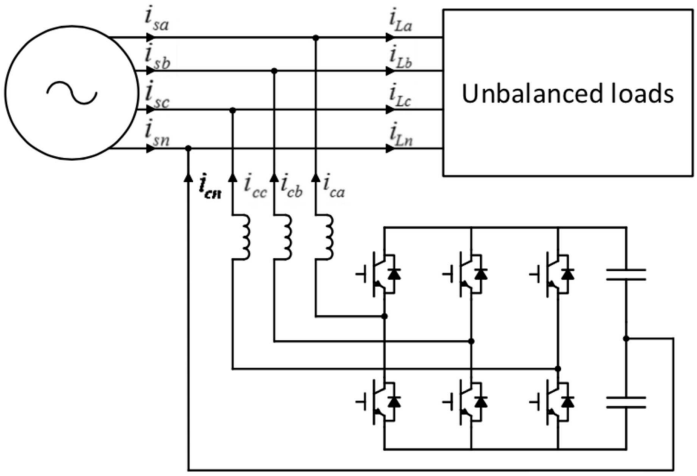


Figure 4.7 – A Simple Schematic of the Active Power Filter with Voltage Source Converter

bandwidth of the active power filter. The inductors between the supply system and switches act as a filter for the switching frequency components in the converter output current.

4.4.1 Active Power Filter Design to Mitigate Phase Unbalance in OpenDSS

To establish the functionality of the active power filters, a user-defined model was developed in OpenDSS. The native tool of OpenDSS does not include a model of an active power filter. Hence, a user-defined model of an active power filter capable of supporting the quasi-static analysis was developed. The functionality of the active power filter is described in Figure 4.8.

The process started with measuring the currents at the node of interest, followed by extracting the symmetrical components for the measured currents. The

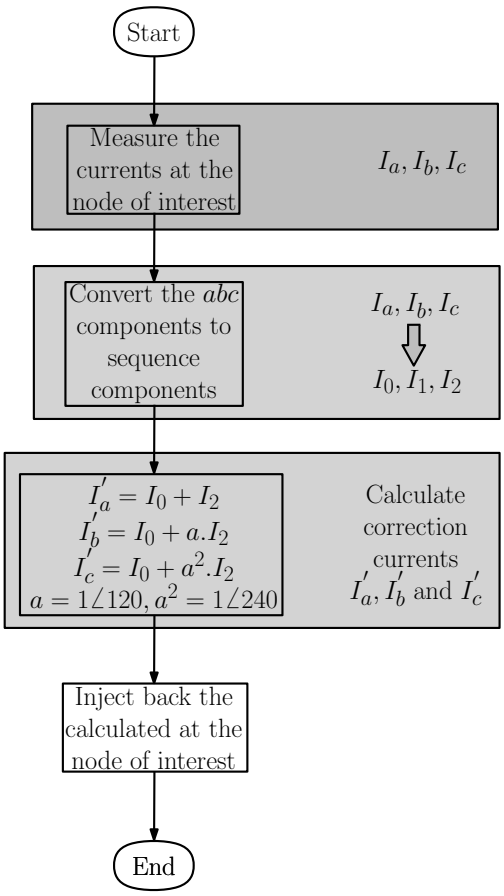


Figure 4.8 – A Flowchart of the Process Involved for the Calculation of Correction Currents

symmetrical components were extracted using Equation (4.6).

$$\begin{bmatrix} I_0 \\ I_1 \\ I_2 \end{bmatrix} = \frac{1}{3} \begin{bmatrix} 1 & 1 & 1 \\ 1 & a & a^2 \\ 1 & a^2 & a \end{bmatrix} \begin{bmatrix} I_a \\ I_b \\ I_c \end{bmatrix} \tag{4.6}$$

where I_a, I_b, and I_c were the phase currents in the abc domain, I_0, I_1, and I_2 were the symmetrical components. Using the previously calculated negative-sequence and the zero-sequence components the correction currents were calculated. Because the active power filter is not intended to provide any real power support, the positive sequence component was not considered when calculating the correction currents, as

shown in Equation (4.7).

$$\begin{bmatrix} I_a^{'} \\ I_b^{'} \\ I_c^{'} \end{bmatrix} = \begin{bmatrix} 1 & 1 & 1 \\ 1 & a^2 & a \\ 1 & a & a^2 \end{bmatrix} \begin{bmatrix} I_0 \\ 0 \\ I_2 \end{bmatrix} \tag{4.7}$$

where $I_a^{'}$, $I_b^{'}$, and $I_c^{'}$ are the correction currents injected back to the feeder at the node of interest.

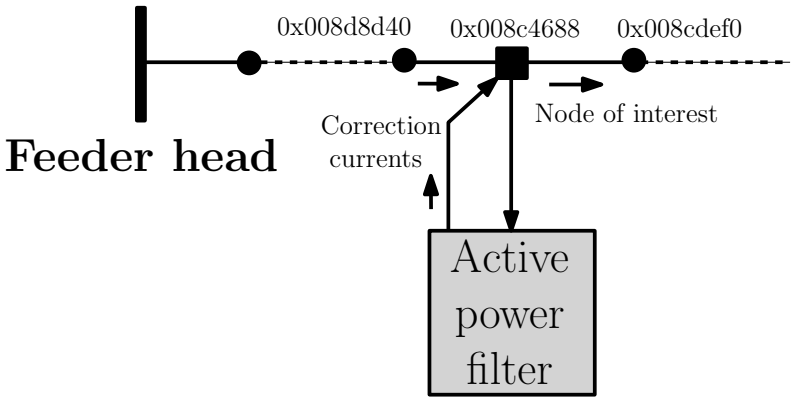


Figure 4.9 – Active Power Filter Implemented as a Controlled Current Source in OpenDSS

The active power filter was placed at the most sensitive node in the test distribution feeder. The node had the highest VUF and the largest neutral current magnitude. The details of the connection are visually depicted in Figure 4.9. The correction currents was calculated and injected back at the node, following the flow chart shown in Figure 4.8. A time-series simulation for an entire year with hourly load data was carried out in OpenDSS, and currents were captured at various locations on the test feeder. Figures4.10 through 4.13 present the currents before and after the operation of the active power filter at various locations on the test feeder.

Figure 4.10 and Figure 4.11 show the phase currents at the feeder head before and after the application of the correction currents at the most sensitive node,

respectively. The correction currents injected at the node of interest are shown in Figure 4.12. After applying the correction currents at the most sensitive node, the active power filter ensured zero neutral currents at the most sensitive node, as shown Figure 4.13. However, the neutral currents at the feeder head were reduced by 40% due the active power filter, as shown in Figure 4.14.

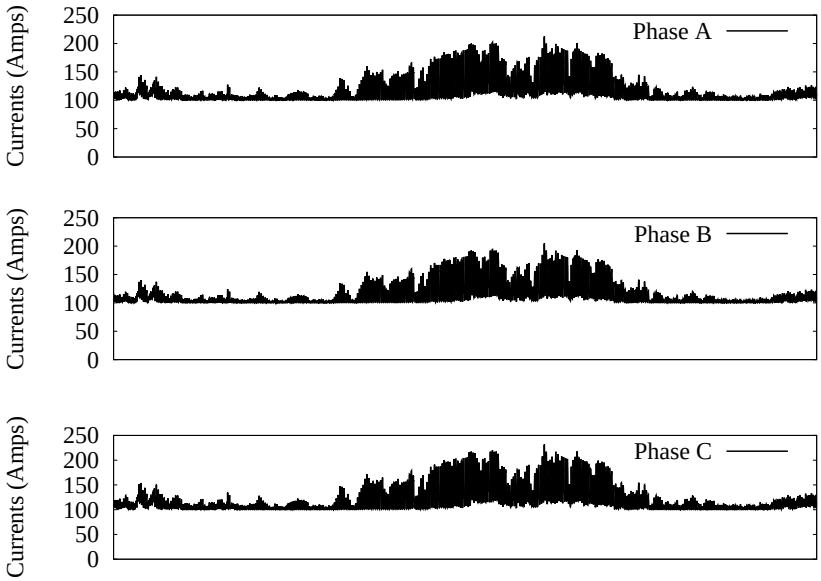


Figure 4.10 – Phase Currents at the Feeder Head with the Proposed Active Power Filter in Operation

An important advantage of power electronic converter-based active solutions, especially for PV induced unbalance, is that the unbalance is not fixed but varies continuously in time in response to the solar output and load. Other mitigation methods are either fixed or cannot follow this variation continuously. As seen in this study, the neutral current at the most sensitive node was brought close to zero for the entire year after the correction currents were applied. The power rating of the active power filter was calculated based on the maximum value of the correction current required at the node of interest. The maximum value of the correction currents

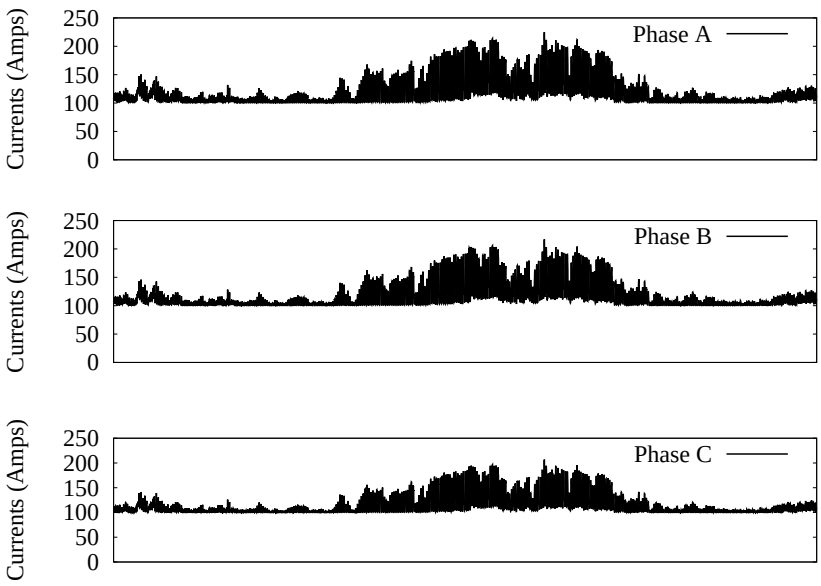


Figure 4.11 – Phase Currents at the Feeder Head Without the Proposed Active Power Filter

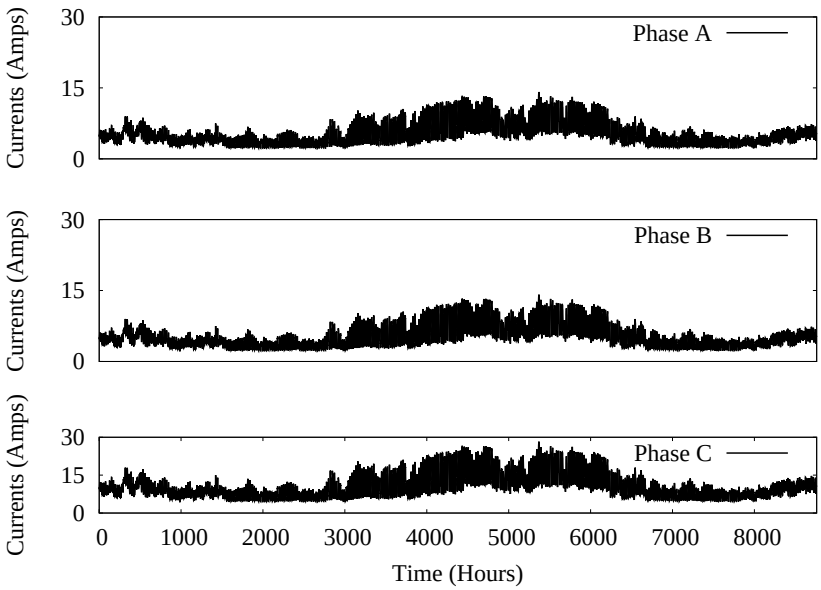


Figure 4.12 – Correction Currents Injected by the User-defined Active Power Filter Model in OpenDSS

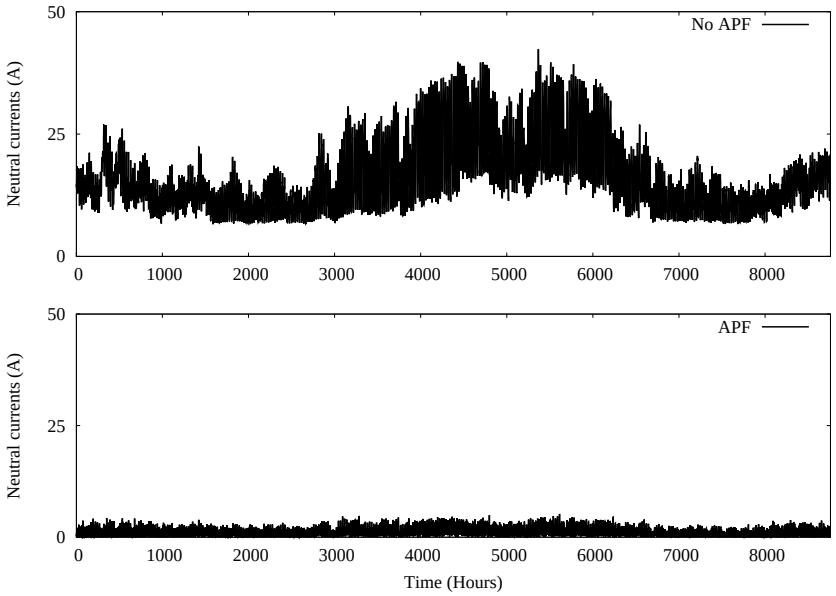


Figure 4.13 – Neutral Currents at the Most Sensitive Node Before and After Realizing the Active Power Filter

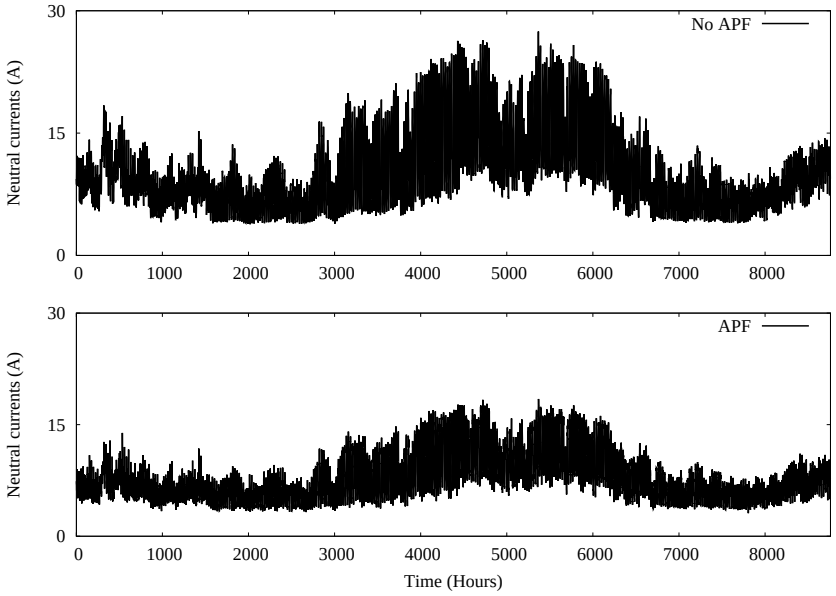


Figure 4.14 – Neutral Currents at the Feeder Head Before and After Realizing the Active Power Filter

among all the phases at the most sensitive node was 28.4 Amps, connected to a medium voltage line with 7.2 kV as line-neutral voltage. Hence, the rating of the device required was 604.8 kVA.

Chapter 5

DEPLOYMENT OF ENERGY STORAGE SYSTEMS IN A DISTRIBUTION FEEDER

5.1 Introduction

Technical advances over the last few years in the development of the lithium-ion batteries have substantially improved the prospects for the application in distribution systems. Lithium-ion based energy storage is a unique technology in this area, as it has the potential to meet many of the objectives relevant to distribution systems. Significant progress in lithium-ion battery chemistries and technology now permits them to be used for meeting the performance, life, and safety requirements of grid and utility related applications [62].

This study provides a generalized framework for strategic operation of the lithium-ion based battery energy storage system (BESS) to increase the benefits in a distribution feeder. This study proposes the use of convex optimization to enhance the value of the lithium-ion based energy storage system. An optimal schedule for the BESS is proposed based on the technical and economic variables using a novel quadratic objective convex optimization problem. The multiple objectives of the proposed optimization problem are as follows :

- Reduce substation transformer losses
- Reduce the cost of energy delivered from the grid
- Reduce life cycle costs of the energy storage system
- Accommodate the variability of renewable energy resources

A lithium-ion based energy storage system of 1,500 kWh, 500 kW was chosen for this study. Although this work was specifically developed to exploit the energy price arbitrage along the optimization time horizon, this study served the following applications: electric supply capacity, substation transformer congestion relief, electric service reliability, electric service power quality, and ancillary services.

Other than the energy price arbitrage, and substation distribution transformer (SDT) loss reduction, the capability of BESS to accommodate the PV variability was studied. The study for accommodating the PV variability consisted of a PV generation site with a 400 kW three-phase PV solar system interconnected to the primary distribution system. The cost incentive and substation transformer loss reduction were studied with and without the PV solar generation. The convex optimization model of the BESS was extended to accommodate the variability of the PV generation. The complete study presented in this work was based on the historically measured field data from the years 2009 to 2013. The mitigation of the intermittent nature of the PV source was studied under two scenarios:

- Energy shifting scenario - this mode was designed to focus on storing energy during the periods of high solar PV generation or low cost time-of-use power from the grid, and shifting the energy delivery to periods of the day that provide the best benefits
- Solar smoothing scenario - this mode was designed to allow the BESS to monitor the solar PV output and react immediately to accommodate the rapid changes in PV output caused by the clouds

In order to quantify the benefits of BESS in a distribution feeder, a test distribution system was chosen. The details of the test distribution feeder are presented in Section 5.3. The open source distribution system analysis tool from EPRI, OpenDSS

was used for this study [54]. The model of the distribution feeder in OpenDSS was validated with the field measured data from the support of local utility. The formulated problem was implemented in IBM ILOG CPLEX optimization studio (CPLEX) [63].

5.2 Detailed List of Data Required for Modeling

Modeling the energy storage system along with the substation in OpenDSS and CPLEX required a multitude of data. The framework of the data gathered from multiple sources are as listed below:

- Data specific to the substation -
  - Historical load data (August 2009 - July 2012)
  - One-line diagram of the substation (Figure 5.2)
  - Transformer parameters (three transformers)
  - Thevenin equivalent of the source at the substation
  - Time-of-use tariff (normalized) for delivering the power
  - Power system parameters at the feeder head, BESS and the substation transformer
  - Substation source voltage variation
- Data specific to the BESS -
  - Nominal DC voltage
  - Limits on charging and discharging rates
  - Charging and discharging efficiency
  - Recommended maximum depth of discharge
  - Plot of number of charge cycles versus battery life

  - Plot of battery voltage versus state of charge
  - Idling losses - energy required by internal controls, heaters and coolers

- Data specific to the inverter -
  - Converter topology
  - Specifications and datasheets - continuous and short term ratings
  - Limits on maximum charge and discharge rates
  - Operating modes
  - Reactive power capability
  - Efficiency
  - Anti-islanding scheme

Historical load data was used to model the load at the substation. Load data with a resolution of 10 seconds from August 2009 to July 2013 was shared by the utility for calculating the charge/discharge schedule of the energy storage system. Hence an algorithm was developed to extract 15 minute data from the provided 10 seconds data. A detailed tool chain is presented in Figure 5.1. Step 1 through step 3 made use of MATLAB programming tool. The program developed in MATLAB realized an algorithm to extract 15 minute data from the input file with 10 seconds resolution.

Averaged values of the loads for weekdays and weekends for all the months were arranged in a specific format required for the optimization tool (CPLEX). The load profiles for weekdays and weekends specific to each month were generated using this approach. Holidays coinciding on weekdays were considered as weekends. The data specific to the characteristics of the battery system and the inverter are listed in Table 5.1 and Table 5.2 respectively.

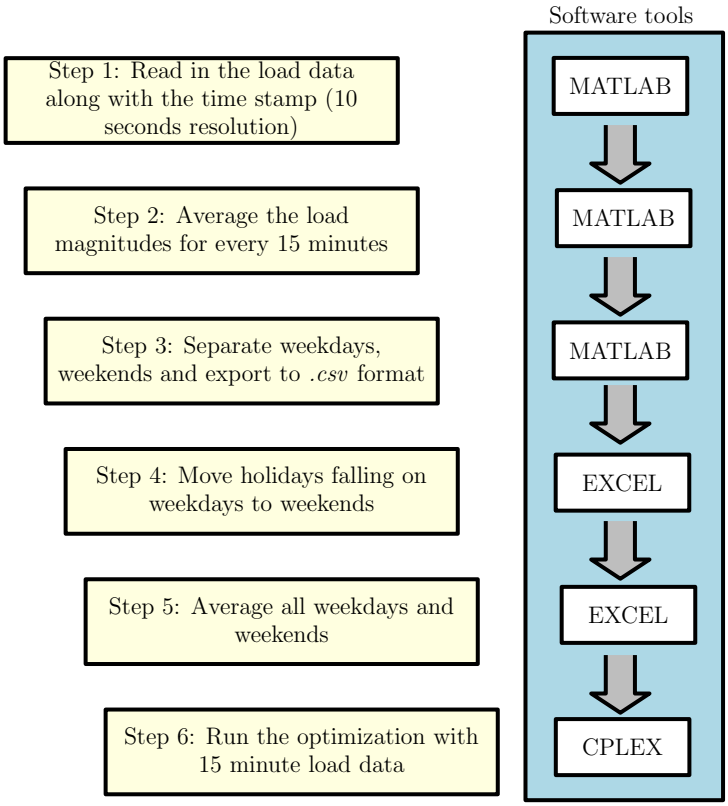


Figure 5.1 – Tool Chain at a Detailed Level

Table 5.1 – Details of the Energy Storage System

Nominal DC voltage	555 V (DC) - 685 V(DC)
Limits on charging and discharging rate	Limited by the inverter (0 - 500 kW)
Charging and discharging efficiency	90%
Recommended bounds on depth of discharge and charge	300 MWh/1.333 MWh

Table 5.2 – Details of the Grid Interface Inverter

Active power limit	500 kW+/-
Reactive power limit	400 kVAr+/-
Speed of response	step response (0%-100%) in 30ms - 40ms
Switching frequency	2kHz
Efficiency	97%
Overload capability	10 min 120% 30 sec 150% 2 sec 200%
Compliance with IEEE 1547	Yes[64]

5.3 Model of the Test Distribution Feeder

The basic one-line diagram of the test substation along with the storage system and PV solar generator is as shown in Figure 5.2. The main motivation behind this study was to reduce the SDT loading (69kV/12.47kV) and model the BESS life cycle costs. Historical load data from August 2009 to July 2013, shared by the utility, was used for fixed scheduling of the energy storage system operation. The models are developed through a combination of manufacturer data and the available models in the simulation tools such as OpenDSS.

A detailed view of the test substation is presented in Figure 5.3. The distribution feeder with 738 nodes, 1,142 sections, 174 distribution transformers, 287 loads was considered in OpenDSS. Three spots referred to as Spot 1 (at the feeder head), Spot 2 (at the middle of the feeder), and Spot 3 (at the tail of the feeder) are identified

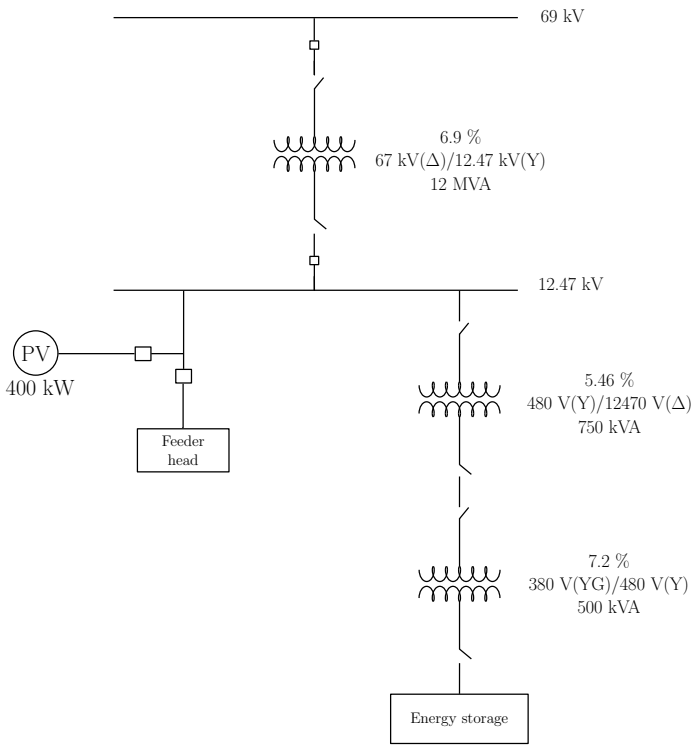


Figure 5.2 – One Line Diagram of the Test Substation with the Energy Storage System

for placing the BESS while conducting the study. The aggregated weekday load profiles from the historical data for summer months and winter months were shown in Figure 5.4 and Figure 5.5 respectively.

The distribution feeder presented in Figure 5.3 was modeled in a distribution system analysis tool (OpenDSS) and validated with the field measured data. The variation in the source voltage was considered while modeling the feeder in OpenDSS. In order to vary the source voltage an additional voltage source was modeled along with the slack bus with a high impedance. Due to the high impedance of the slack bus the load was catered from the additional constant power-voltage source following the varying voltage specified by the user. The voltage profile at the feeder head obtained from the field measured data was used to compare the simulated results.

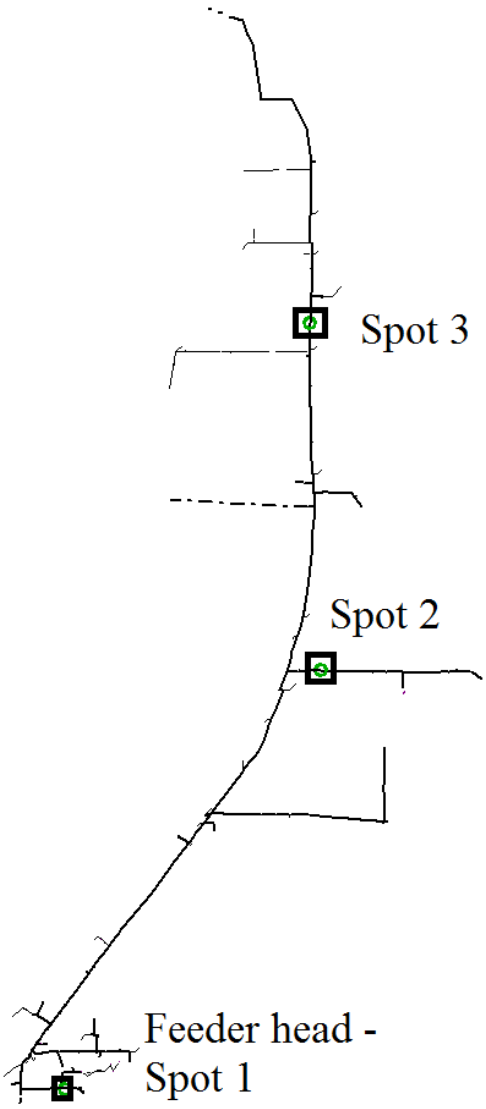


Figure 5.3 – View of the Feeder in OpenDSS Highlighting the Spots for Studying the Impact of the Reactive Power Support from BESS

A specific scenario in the field, where the BESS discharged at a rate of 500 kW, was chosen to validate the OpenDSS simuation. Figure 5.6 and Figure 5.7 shows the voltage and active power at various points of the one line diagram (Fig. 5.2) as the BESS starts to discharge at the 72nd minute. Figure 5.6 furnishes the data obtained from the field. The voltages obtained from the simulation tool is compared

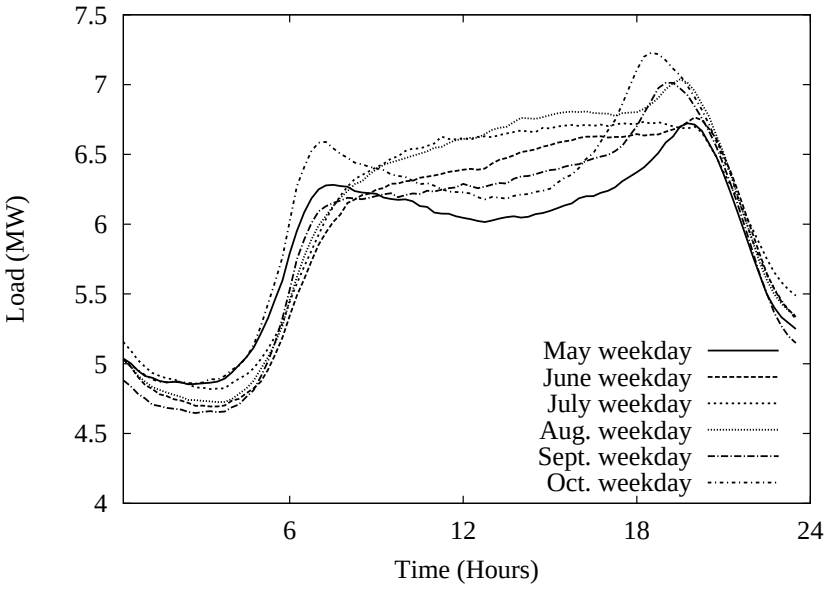


Figure 5.4 – Load Profile for a Typical Weekday in the Months of May, June, July, August, September, and October

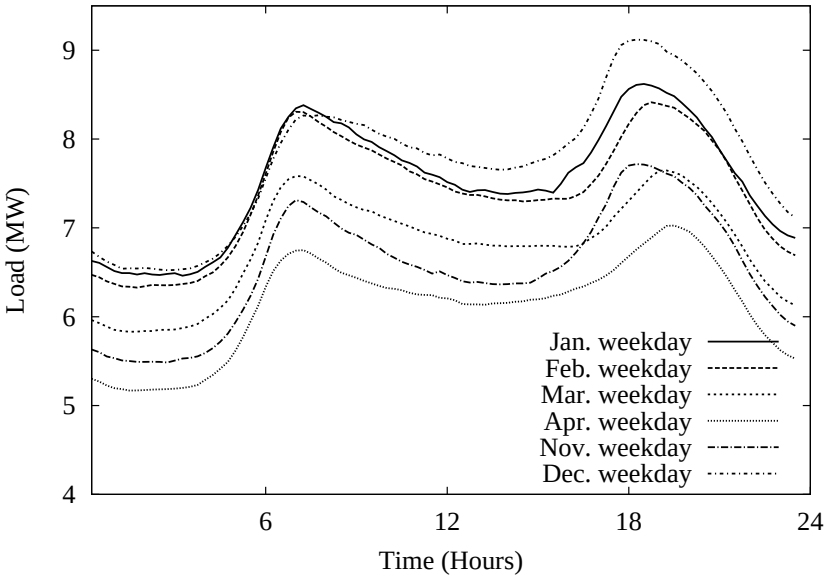


Figure 5.5 – Load Profile for a Typical Weekday in Months of January, February, March, April, November, and December

with the field measured data in Figure 5.7 as the BESS starts discharging at its full capacity. From Figure 5.7, it can be observed that the measured data closely matches the simulation data . For further clear comparison the voltage variation from the 50th minute until the 81st minute in Figure 5.7 is magnified and inserted in their respective plots.

With reference to Figure 5.6, at the 72nd minute the BESS starts to discharge at its full rate of 500 kW. Since at the 72nd minute an apparent step change in the voltage at the feeder head was not observed (Figure 5.7), it can be inferred that the impact of active power support on the voltage at the feeder head is negligible.

Reactive power support from the energy storage system was not implemented in the field. However, to understand the impacts of reactive power support from the BESS, previously validated OpenDSS model (Figure 5.3) was used.

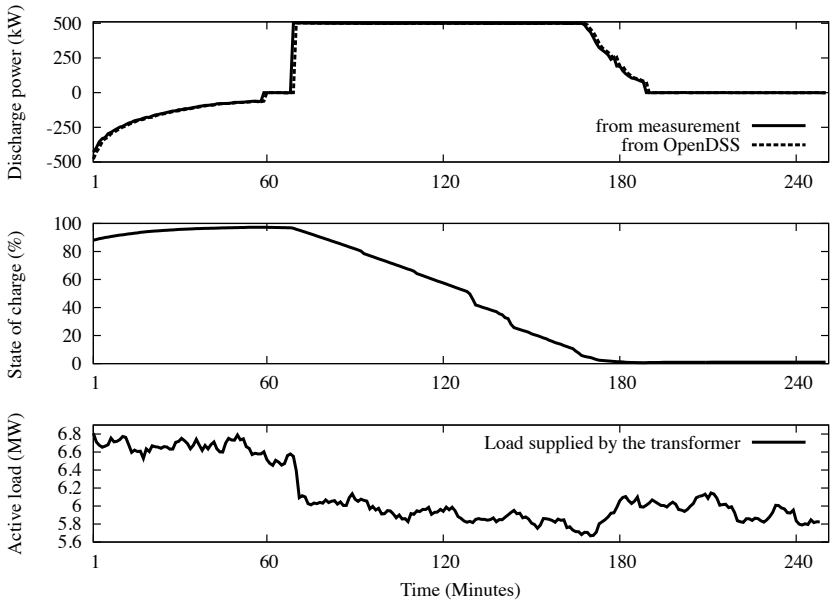


Figure 5.6 – Waveforms of Power Supplied by BESS, the Reduction in SOC of BESS, and the Load Supplied Through the Transformer

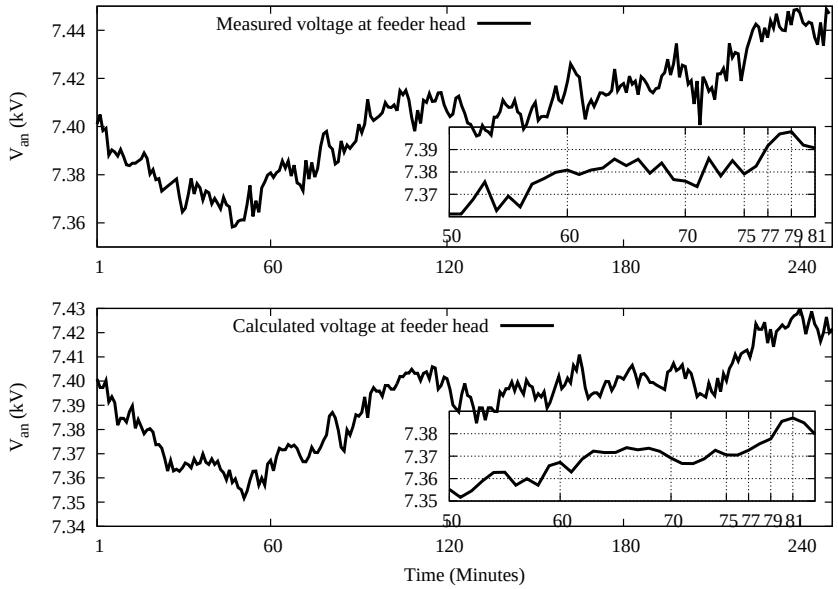


Figure 5.7 – Plot Presenting the Line-neutral Voltage of Phase A at the Feeder Head While the BESS is Discharged

5.4 Description of the Optimization Model

This study proposes the use of multiobjective optimization to dispatch the BESS with a goal of minimizing the following objectives:

- Loading of the substation transformer (Figure 5.2)
- Cost incurred for delivering power from the substation
- Life cycle costs associated with BESS

The objectives were combined to frame a convex optimization problem with a quadratic objective and linear constraints. Generation costs were modeled as costs incurred by the utility to deliver the power from the substation. Grid operation costs, shared by the utility, was used for optimal scheduling of the energy storage system. The cost reduction due to BESS was studied with and without the PV solar

generation. This section highlights on the cost incentives and the reduced substation transformer loading due to BESS without PV solar generation.

5.4.1 Minimization of Transformer Losses Based on Power Drawn from the Grid

Although the losses in a transformer are of multiple types, only the resistive loss (copper losses) was minimized. Considering a constant power factor operation the transformer losses and the active power was related by a constant. Hence the copper losses were considered to be proportional to the square of the active power transferred through the transformer, instead of the rms current in the windings. The power drawn from the grid was considered as a decision variable through which the transformer loss was calculated in the objective function.

5.4.2 Life Cycle Costs Associated with the BESS

Energy storage systems deteriorate in their operation capacity due to the cumulative changes in structure and composition of the key battery cell components caused by the charge discharge cycle. Battery cycle life thus can be defined as the number of cycles after which the battery performance has degraded to a predetermined level. Hence every charge or discharge cycle accumulates an additional cost.

The additional cost, added per charge or discharge of the energy storage system, depends on the depth of discharge and frequent variation in the rate of charge/discharge. Hence the formulated optimization problem avoids the charging and discharging of the BESS at higher rates as much as possible; as well as avoids variation in the charging and discharging rates.

The formulated problem was implemented in IBM ILOG CPLEX optimization studio (CPLEX). All the constraints were linear and the objective is a quadratic function.

5.4.3 Model Formulation

The optimal dispatch of the BESS refers to a strategy for timing the charge and discharge the BESS. The bounds for the dispatch problem were the capacity limitations on the equipment including the BESS capacity and the DC/AC converter rating. The objective function which was minimized is as presented below.

$$C = \sum_{t=1}^{T} (k\ r_{xfmr} P_t^{grid} P_t^{grid} + C_t^{grid} P_t^{grid} + C_t^z [Z_t]^+) \tag{5.1}$$

Load balance constraint

$$D_t = P_t^{grid} + (\eta_{ds} ds_t - ch_t/\eta_{ch}) \qquad \forall\ t \in T \tag{5.2}$$

Updating the SOC constraint

$$SOC_t = SOC_{t-1} - ds_t + ch_t \qquad \forall\ t \in T \tag{5.3}$$

Associated lower and upper bounds

$$\underline{h} \leq SOC_t \leq \bar{h} \qquad \forall\ t \in T \tag{5.4}$$

$$0 \leq ds_t \leq S \qquad \forall\ t \in T \tag{5.5}$$

$$0 \leq ch_t \leq S \qquad \forall\ t \in T \tag{5.6}$$

Decision variable associated with the life cycle costs

$$Z_t \geq ch_{t-1} - ch_t + ds_t - ds_{t-1} \qquad \forall\ t \in T \tag{5.7}$$

$$Z_t \geq ch_t - ch_{t-1} + ds_{t-1} - ds_t \qquad \forall\ t \in T \tag{5.8}$$

The description of the symbols used in (6.20) through (6.26) are listed in Table 5.3. The formulated problem was solved over a day horizon, with 15 minute time intervals. The defined feasibility constraints included the supply-demand balance (Equation (6.21)), calculation of the new state of charge (Equation (6.22)), and calculation of the expected battery replacement cost as a function of the depth of discharge (Equation (6.25) and Equation (6.26)). Energy storage units had two constraints on their dispatch, the energy storage limit of the battery and the power transfer capacity of the grid interface inverter.

5.4.4 Calculation of Penalty Factors k and C_t^z

The parameters k and C_t^z were the pseudo-costs used in selectively opting between minimizing the substation transformer losses and minimizing the battery life cycle costs. Between the two parameters the value of C_t^z was chosen to be unity and the value of the k was calculated based on the assumptions as follows:

- Avoid the BESS charging/discharging at high rates
- Avoid frequent variation of the rate of charge/discharge

The value of k was finalized based on an algorithm presented in Figure 5.8. The algorithm reduced the value of k and iterated until the constraint was satisfied.

5.4.5 Results of the BESS Schedule

The optimal schedule of the BESS was derived by solving the formulated quadratic program. Figure 5.9 exhibits the optimal schedule obtained for a winter weekday system without the PV penetration. Normalized fuel costs were used and hence has been considered as unit-less (without SI units). It can be observed that the BESS gets charged when the fuel cost is low and discharges when the fuel cost is at its

Table 5.3 – List of Parameters and Decision Variables

Parameters used in the optimization	
T	complete set of 15 minute intervals in a day
t	particular 15 minute interval during a day
$\underline{h}$, $\bar{h}$	minimum and maximum SOC of the BESS respectively - 300 kWh and 1200 kWh respectively
D_t	system load at 15 minute interval t
η_{ch}, η_{ds}	charge and discharge efficiencies of BESS - 90% each
C_t^{grid}	cost of power from the grid
k	cost coefficient associated with the transformer losses - varied based on the need
r_{xfrm}	resistance of the transformer windings - 1.54 Ω (0.414 pu)
C_t^z	cost coefficient associated with the life cycle costs of the battery - varied based on the requirement
S	DC/AC converter rating in kW - 500 kW
Decision variables used in the optimization	
P_t^{grid}	power drawn from the grid in kW
ds_t	rate at which the battery will be charged (kW/h)
ch_t	rate at which the battery will be discharged (kW/h)
SOC_t	state of charge of the battery calculated from ch_t and ds_t (kWh)
$[Z_t]^+$	expected battery replacement cost as a function of depth of discharge from time t-1 to t in kW; calculated from the ch_t and ds_t

maximum. Since the life cycle costs of the BESS was included in the objective the variation in the charge/discharge rate was minimized.

Data: k=1; C_t^z=1

Result: Updated value of the parameter k

Run the optimization code with the values of k and C_t^z

if *[MAX(ch_t) > 400]* or *[MAX(ds_t) > 400]* or *[MAX(ds_t) - AVERAGE(ds_t) >= 50]* $\forall\ t \in T$ **then**

  Run the optimization code with the values of k and C_t^z

  $k = \frac{k}{10}$

else

  break

end

Figure 5.8 – Algorithm Used to Identify the Value of the Parameter k in C++ Programming Language

5.5 Cost Savings as a Result of BESS

This study used optimization to enhance the benefits of an energy storage system. One of the goals was to minimize the cost incurred for delivering the power by the utility. The time-of-use tariff shared by the utility was a normalized quantity. The cost savings were calculated and measured as units (instead of $/hour) as well as a percentage of the total cost. The equations (5.9) and (5.10) are used to calculate the values in Table 5.4. Table 5.4 presents the cost savings as a result of active power support from the BESS without PV solar generation.

$$Costsavings \text{ in units} = \sum_t (C_t^{grid}\ D_t) - \sum_t (C_t^{grid}\ P_t^{grid}) \tag{5.9}$$

$$Costsavings \text{ in } \% = \frac{\sum_t (C_t^{grid}\ D_t) - \sum_t (C_t^{grid}\ P_t^{grid})}{\sum_t (C_t^{grid}\ D_t)} \tag{5.10}$$

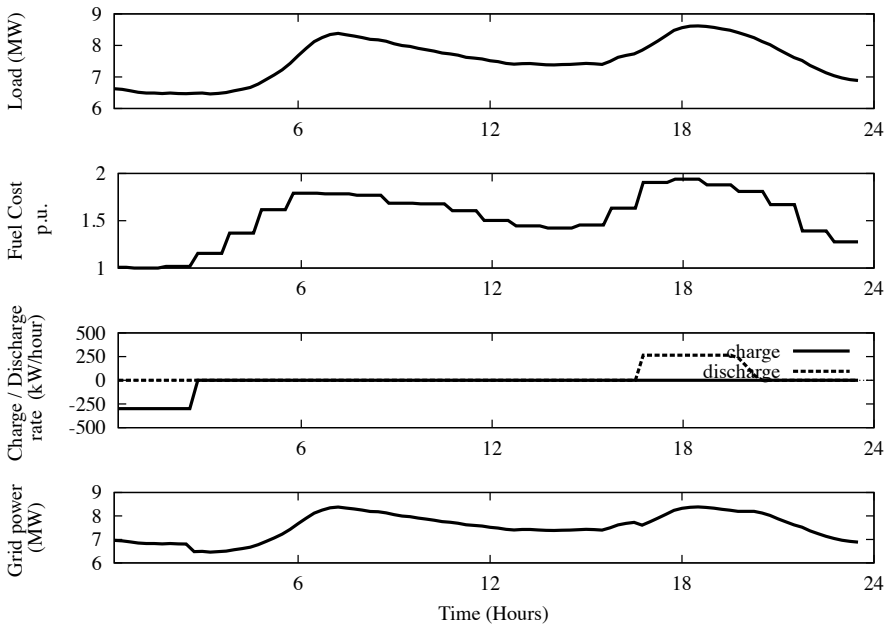


Figure 5.9 – Load at the Substation, Fuel Cost, Charge Rate and Discharge Rate of BESS, and Power Drawn from the Grid on a Typical Weekday in the Month of January

The values in Table 5.4 display a pattern, that the savings from BESS during a typical summer month is high when compared with a typical winter month. The transitions from summer to winter (November) displayed low gains from the BESS.

5.6 Impact of BESS Dispatch on Substation Transformer Losses

This section studies the impact of the energy storage system dispatch on the SDT losses. Moreover, impact of the reactive power support from the BESS on the distribution feeder at multiple points on the feeder was studied.

Table 5.5 presents the reduction of the substation transformer losses as a consequence of optimally dispatching the energy storage system. The variation in the reduction of substation transformer losses as the BESS was placed at different spots was observed.

Table 5.4 – Cost Savings as a Result of Active Power Support from BESS

Month	**Weekday**		**Weekend**	
	Units	**%**	**Units**	**%**
January	2111	0.18	2114	0.20
February	1335	0.12	1334	0.13
March	1776	0.19	1785	0.2
April	1860	0.2	1883	0.21
May	3818	0.35	3814	0.36
June	5365	0.46	5346	0.48
July	4775	0.44	4785	0.46
August	4297	0.42	4310	0.44
September	3360	0.35	3325	0.36
October	1484	0.18	1472	0.18
November	1152	0.14	1140	0.14
December	1694	0.20	1694	0.20

The study was performed on August weekday profile. The variation in the substation transformer losses for various levels of active power and reactive power dispatch is presented in Table 5.5. Table 5.5 shows that, as anticipated, the substation transformer losses reduce with economically dispatching the energy storage system. The differing levels of the active power and reactive power dispatch were obtained by multiplying the values recommended by the optimization problem. The active power multiplier and the reactive power multiplier are the factors by which the schedule recommended by the optimization problem was multiplied (0 corresponds to the base case with no BESS). The critical observation, that the reactive power support further

aids in reducing the substation transformer losses was made. The column with the title percentage in Table 5.5 furnishes the energy loss reduction as a percentage (with the kWh losses) of the transformer loss without any support from the energy storage system. The conclusion reached from the values in Table 5.5 is that, increased performance can be obtained by providing reactive power support from the BESS with the BESS situated closer to the feeder head.

Table 5.5 – Values of Energy Loss at the Substation Transformer Over a Day (August Weekday Profile)

Active power multiplier	**Reactive power multiplier**	**Location**					
		Spot 1		**Spot 2**		**Spot 3**	
		kWh	**%**	**kWh**	**%**	**kWh**	**%**
0	0	766	-	766	-	766	-
1	0	758	1.04	760	0.7	762	0.5
1	1	754	1.6	757	1.1	760	0.7
1	2	751	2.0	754	1.6	758	1.04

5.7 Optimal Dispatch of BESS with PV Solar Generation

This section accommodates the PV variability by utilizing the energy capacity of BESS. The PV generation site with a capacity of 400 kW was chosen. Figure 5.10 furnishes the PV generation profile at two points in a year - June represents a summer month, and December represents a winter month, from a geographical location Flagstaff, AZ. A specific day in December was chosen such that the PV variation was high. This section proposes the use of BESS for accommodating the PV variability.

The economic dispatch of the BESS with PV solar generation was studied under two scenarios - energy shifting scenario and solar smoothing scenario.

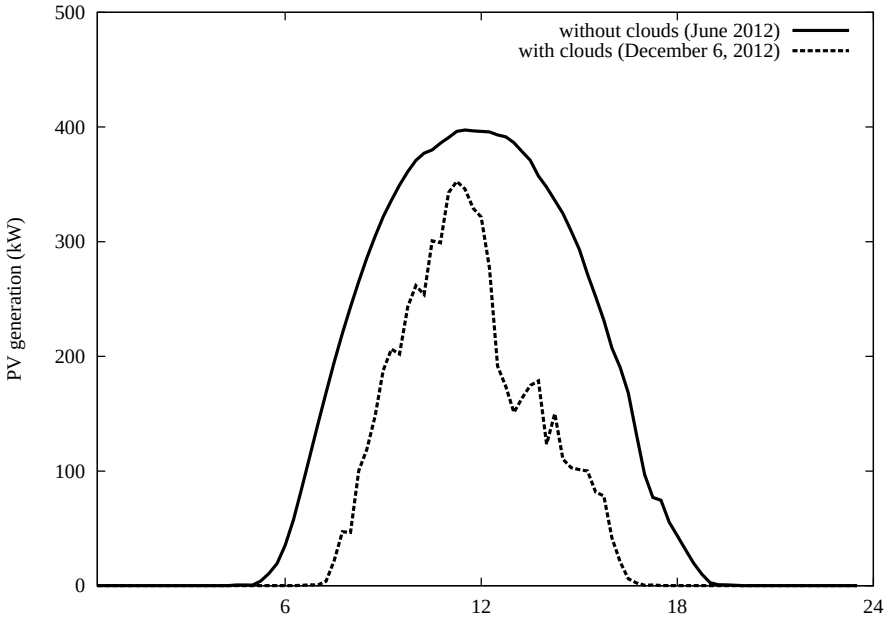


Figure 5.10 – PV Generation Profiles on the Two Days with Different Levels of Clouds

5.7.1 Energy Shifting Scenario

Energy shifting scenario was designed to provide an optimal dispatch of the BESS along with the PV generation in the distribution feeder. However, the variability of the PV generation was accommodated by the main grid. Energy shifting scenario was expected to guarantee minimal variation in the charge/discharge rate for the BESS, thus leading to a longer life-time. The PV generation profile for this study is chosen from Dec 6th, 2012, since large variation in the PV insolation was observed. The emphasis was on utilizing the PV generation to charge the BESS at a fixed rate during peak generation and serve the load during the peak conditions. A typical winter load (December) along with the variable PV generation was chosen for the study. Figure 5.11 presents the optimal dispatch of the BESS with the proposed

energy shifting scenario. With reference to Figure 5.11, it can be clearly observed that energy shifting scenario effectively assists in reducing the peak load served by the grid. Besides, the BESS is charged from the PV generation source at a fixed rate assuring longer life-time. With the PV solar generation in the energy shifting scenario the cost savings raised to 1.5% in comparison with 0.2% (Table 5.4).

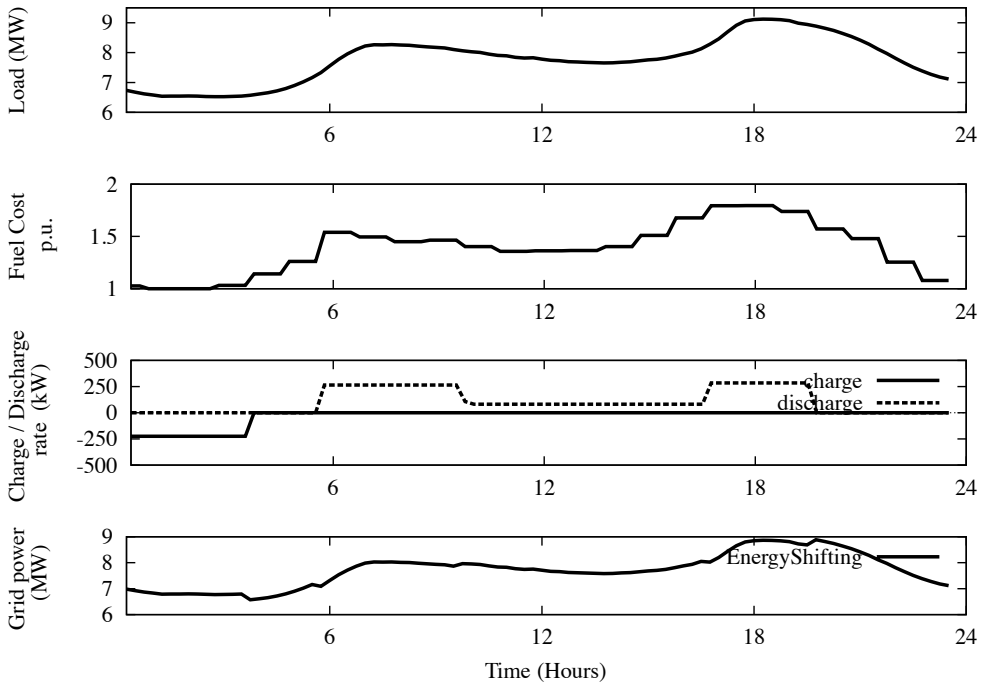


Figure 5.11 – Load at the Substation, Fuel Cost, Charge Rate and Discharge Rate of BESS, and Power Drawn from the Grid on a Typical Weekday in the Month of December with Energy Shifting Scenario

5.7.2 Solar Smoothing Scenario

Solar smoothing scenario was designed to allow the BESS to monitor the solar PV output and react immediately for the variation in the PV generation. The PV generation profile for the study was chosen from Dec 6th, 2012, since large variation in PV insolation was observed. Figure 5.12 presents the load profile, time-of-use fuel

costs, charge/discharge profile, and the grid power with and without solar smoothing. As the difference between grid power with and without solar smoothing cannot be distinctly observed in Figure 5.12 additional figure has been included (Figure 5.13). Figure 5.13 presents a much clear view of the PV generation profile, power drawn from the grid, and SOC of BESS with solar smoothing and energy shifting scenario. During the peak of the PV generation (11th hour of the day) BESS charged from the PV source and started discharging during the rapid changes in the PV output caused by the clouds. The variation in the grid power drawn to cater the load was minimized. BESS accommodated the PV variability in solar smoothing, whereas during energy shifting scenario grid fulfilled the PV variability.

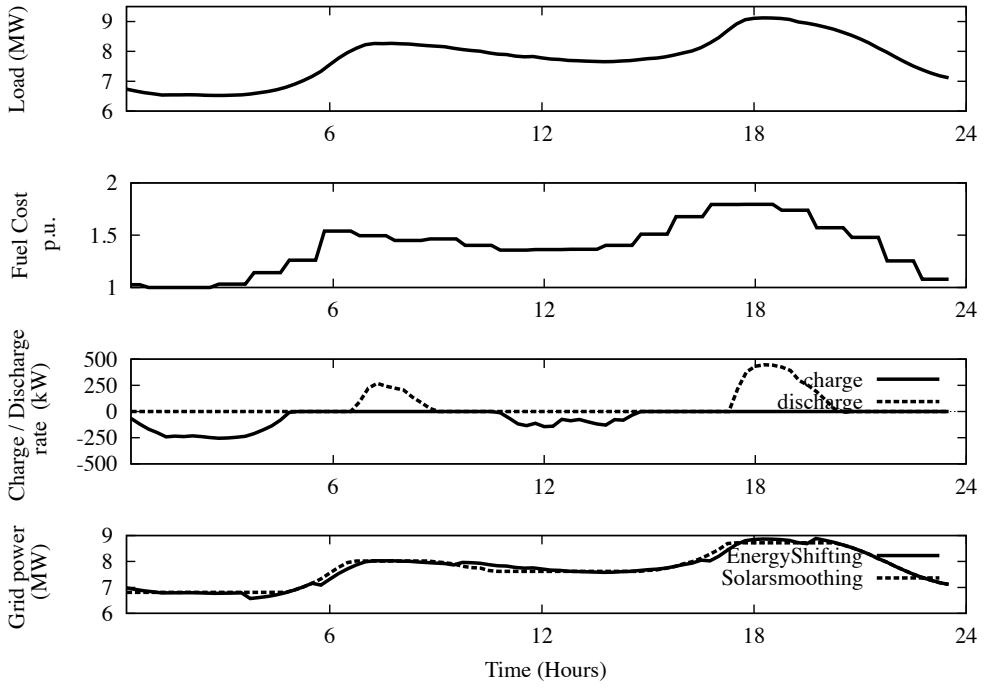


Figure 5.12 – Load at the Substation, Fuel Cost, Charge Rate and Discharge Rate of BESS, and Power Drawn from the Grid on a Typical Weekday in the Month of December with Solar Smoothing Scenario

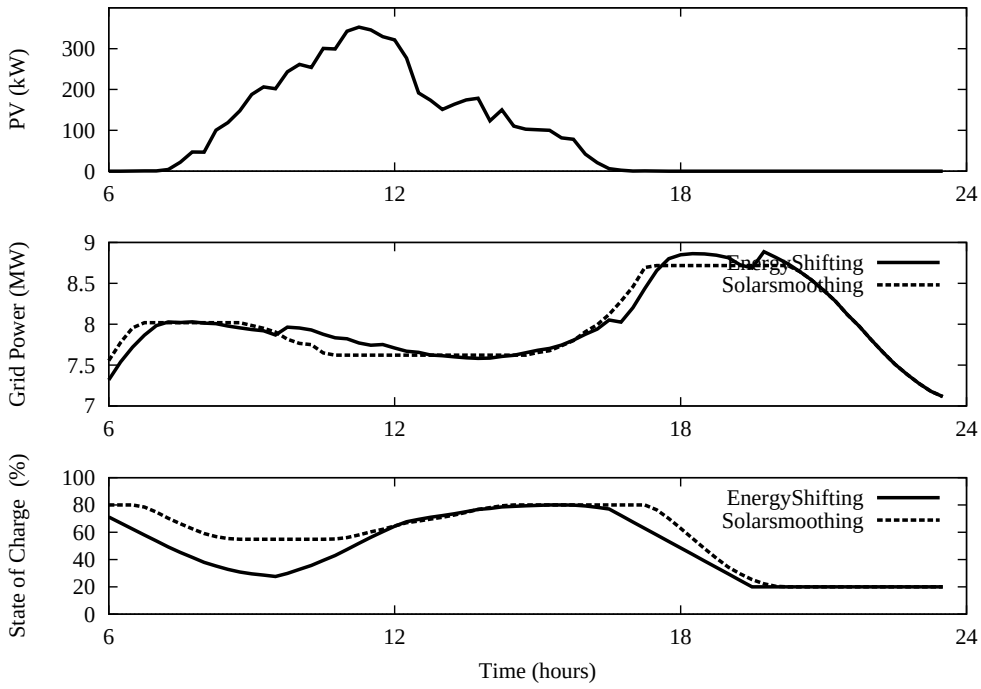


Figure 5.13 – Plot Comparing the Grid Power and the SOC for the BESS of the Solar Smoothing Scenario with that of the Energy Shifting Scenario

Chapter 6

DESIGN AND SCHEDULING OF MICROGRIDS

6.1 Introduction

A microgrid consists of a cluster of generators, loads, an energy storage system, and control devices that can operate either connected or isolated from the traditional centralized grid [65]. In a microgrid, the load is usually served by a combination of micro resources, such as renewable resources (PV generator, wind turbine) and microturbines (gas/diesel). Renewable resources are intermittent and stochastic in nature. A potential solution to accommodate the variability of the renewable resources is to utilize an energy storage system. Energy storage systems play a major role in the operation of microgrids.

Energy storage systems are fast response devices capable of supporting the microgrids and providing economic benefits. Additionally, they can store energy at times of low electric prices and use the stored energy at times of high electric prices. Further, energy storage systems can be used for load following, peak load management, power quality improvement, and deferral of upgrade investments. However, it is necessary to size the systems optimally in order to prevent over or under utilization.

Optimal sizing of an energy storage system depends on various components, as shown in Figure 6.1. The sizing of the energy storage system and the microturbine were performed based on the historical load data, PV generation data, and time-of-use component fuel costs. The objective of resource planning in this study was to minimize the investment and operation cost while satisfying the requirement for system reliability.

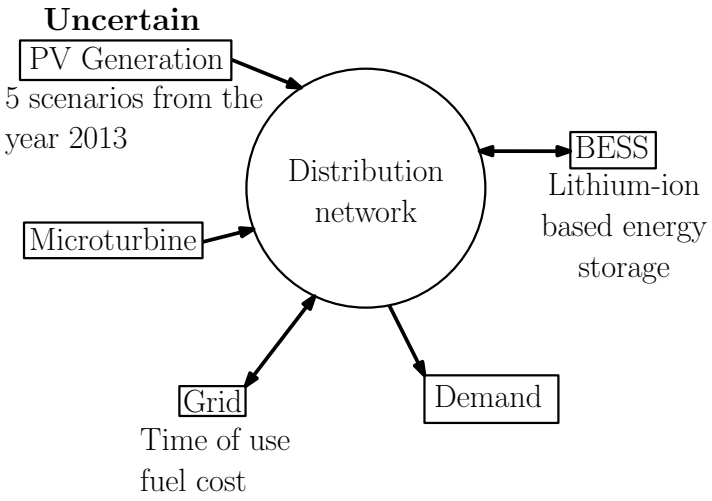


Figure 6.1 – View of the Components Involved in the Sizing of the Energy Storage System

Figure 6.2 shows the lateral from the test feeder chosen for the study of microgrid. The microgrid has a utility-scale three-phase PV generator with a maximum capacity of 400 kW, and winter peaking load with a maximum of 350 kW for the month of January. A detailed view of the microgrid is as shown in Figure 6.3 having a load profile as shown in Figure 6.4. The energy storage system and microturbine are sized for a typical summer (June) and winter (January) months.

However, the sizing of the energy storage system mainly depended on the variability of the renewable resource; thus, the stochasticity of the renewable resource was considered. Figure 6.2 shows the lateral from the test feeder of the microgrid chosen for the study. The microgrid had a utility-scale three-phase PV generator with a maximum capacity of 400 kW and a winter peaking load maximum of 350 kW for the month of January. A detailed view of the microgrid is shown in Figure 6.3, and a load profile is shown in Figure 6.4. The energy storage system and microturbine were sized for typical summer (June) and winter (January) months.

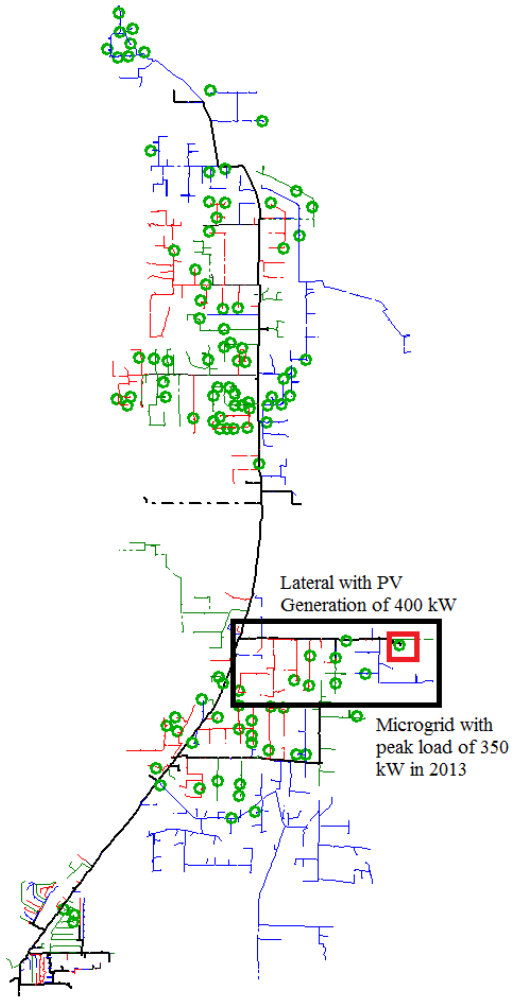


Figure 6.2 – View of the Chosen Microgrid from the Test Feeder

A mathematical approach based on optimization was used for this purpose. The entire problem of unit sizing and unit scheduling was decomposed into three stages. The first two stages involved sizing the kW/kWh rating of the energy storage system and the kW rating of the microturbine. In order to manage the computational complexity, the first two stages were coupled using Benders decomposition. The third stage provided the optimal schedule for the microturbine and the energy storage system. The optimization problem in the third stage considered the life-cycle costs to determine the optimal schedule. Based on the outputs of the first two stages,

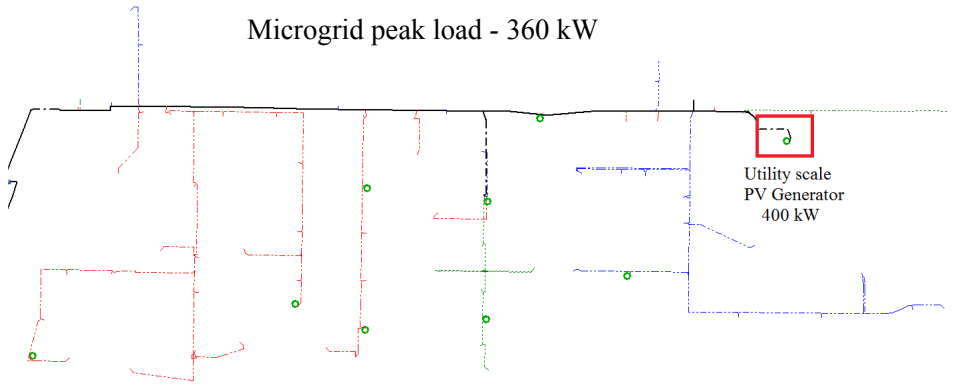


Figure 6.3 – Detailed View of the Chosen Microgrid from the Test Feeder

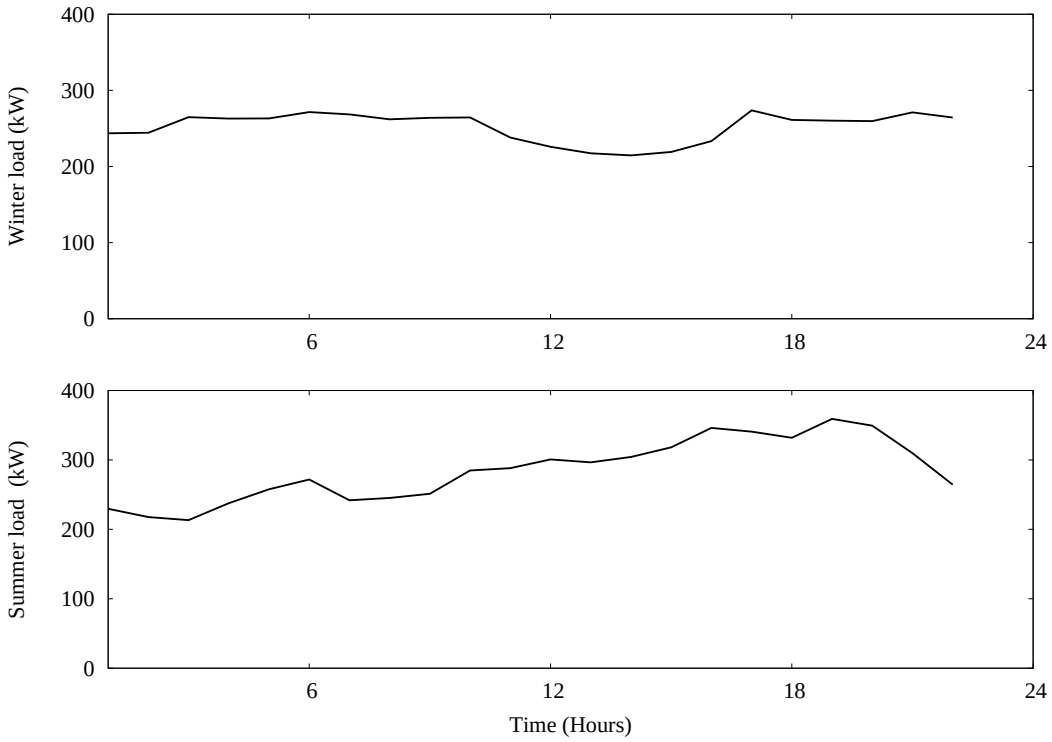


Figure 6.4 – Load Profile of the Microgrid for a Typical Winter Month and Typical Summer Month

the third stage was solved as an independent problem. The formulated problem was implemented in the IBM ILOG CPLEX optimization studio (CPLEX).

6.1.1 PV Generation as Stochastic Resource

PV generation was treated as a stochastic resource in the formulation of the optimization problem. Five scenarios from the year 2013 for the geographical location of Flagstaff, AZ, were considered. Figure 6.5 presents the five scenarios considered for the stochastic optimization. The scenarios are numbered from PV scenario 1 to scenario 5, representing the best to the worst generation scenarios, respectively.

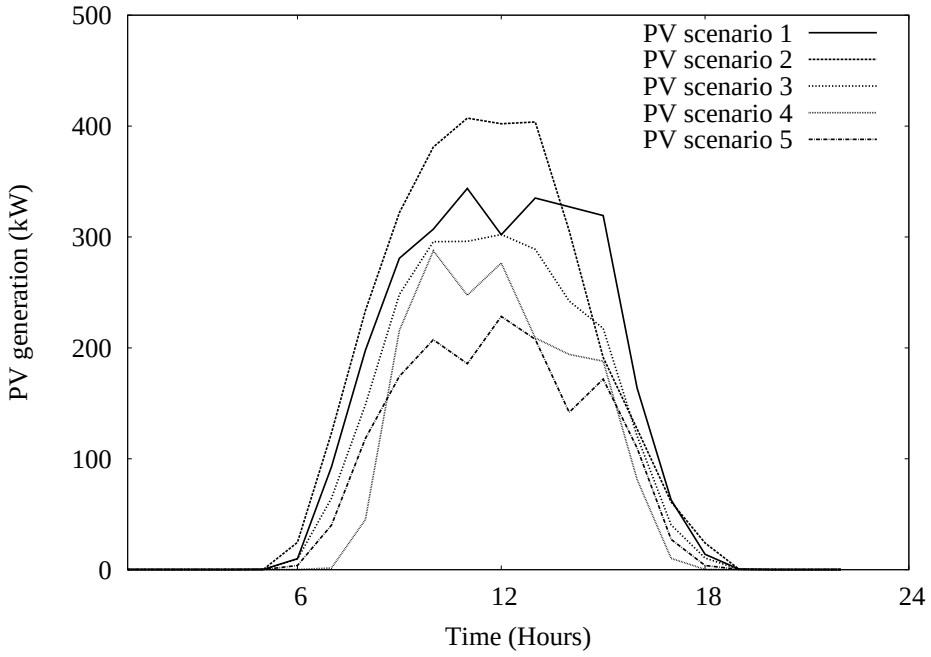


Figure 6.5 – Measured PV Generation Corresponding to the Five PV Scenarios Used in the Study

6.1.2 Microturbines

A microturbine engine is a combustion turbine that includes a compressor, a combustor, a turbine, a generator, and a recuperator. The cross-sectional view of a typical microturbine is available in the reference [66]. The rotating components

are mounted on a single shaft supported by air bearings and spin at a maximum speed of 60,000 RPM. The permanent magnet generator is cooled by the airflow into the microturbine. The output of the generator can be variable voltage and variable frequency AC.

The microturbine can efficiently use a wide range of approved hydrocarbon-based gaseous fuels, depending on the model. The standard system is designed for pressurized hydrocarbon-based gaseous fuels. Other models are available for low-pressure gaseous fuels, gaseous fuels with lower heat content, gaseous fuels with corrosive components, and biogas (landfill and digester gas) fuels.

Power electronic components control and condition the electrical output of the microturbine. The power electronic components change the variable frequency AC power from the generator to DC voltage, and then to constant frequency AC voltage as required at the grid terminal. During start-up, the microturbine is operated as a variable frequency drive, and motors the generator until the microturbine has reached ignition, and electrical power is available from the microturbine. The power electronic components again operate as a drive for cooling to remove heat stored in the recuperator and within the microturbine engine.

6.1.3 Energy Storage Systems

This work incorporated the use of Li-ion battery-based energy storage systems (BESS). Li-ion batteries are versatile in module size and discharge time, compared to other technologies. Additionally, the Li-ion battery technology is widely implemented in various areas of grid services. The operation capacity of batteries deteriorates with time. This process occurs due to cumulative changes of the structure and composition of key battery cell components caused by the chargedischarge cycle. Thus, battery life cycle can be defined as the number of cycles after which the battery performance has

degraded to a predetermined level. Hence, every charge or discharge cycle accumulates an additional cost. The additional cost, added per charge or discharge of the energy storage system, depends on the depth of discharge and the frequency variation in the rate of charge or discharge. Thus, in addition to the $/kW and $/kWh, the life-cycle cost was considered.

6.1.4 Grid Support and Demand

Grid support was treated as a slack source for the mathematical formulation of the problem. The operational costs of the grid were assumed to have a time-of-use profile. Normalized fuel costs were used, formulated as unitless (without SI units). The sizing and dispatch of the energy storage system were individually studied for a typical winter month (January) and for a typical summer month (June). The values for the power demand and the time-of-use operational costs for each month of the year were obtained from the local utility. Figure 6.6 furnishes the typical summer/winter load profiles and time-of-use operational costs for the electric power drawn from the grid.

6.2 Case Studies

This research focused on examining the sizing and scheduling of an energy storage system and a microturbine for three cases. A diagrammatic view of the cases is presented in Figure 6.7. The details of the cases are listed below:

- Case 1 - Energy storage sizing for 24 hours of microgrid operation without support from the grid
- Case 2 - Energy storage sizing for microgrid operation during peak hours of the test feeder

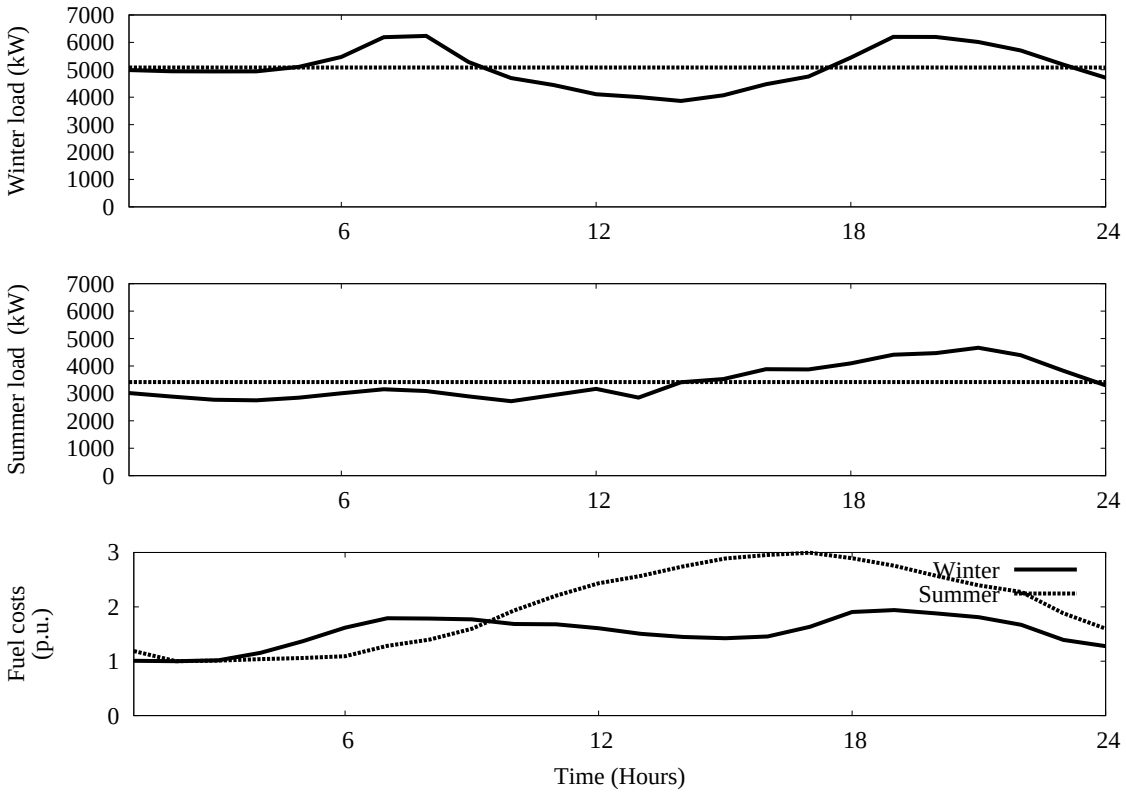


Figure 6.6 – Typical Load Profiles for the Entire Feeder and Time-of-use Operational Costs for the Electric Power Drawn from the Grid

- Case 3 - Energy storage sizing based on the mean outage reported from the historical data

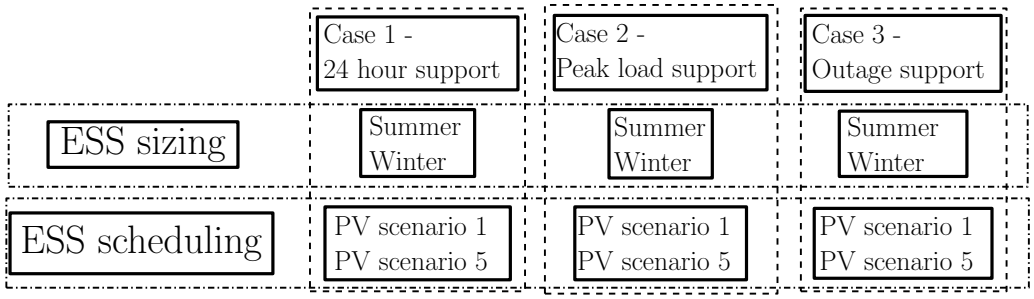


Figure 6.7 – Overview of Case Studies Performed

Case 1 modeled the worst-case scenario in which the support from the main grid was unavailable for 24 hours. Case 2 involved the operation of the microgrid specifically during the peak hours of the main grid. Trading was allowed between the main grid and the microgrid in Case 2. Trading could be nonfirm, which allowed the sender to interrupt the power delivery if needed. With this ability, the microgrid was able to disrupt the power being sent to the main grid during PV contingency, avoiding the turn-on of an emergency generator or the occurrence of a blackout.

Case 3 considered mean outage duration and mean time of outages from the five years of historical data. Figure 6.8 presents the histogram of the duration of sustained faults with a mean of 2 hours. Figure 6.9 shows the histogram of the time of sustained faults with a mean of 3:00 PM.

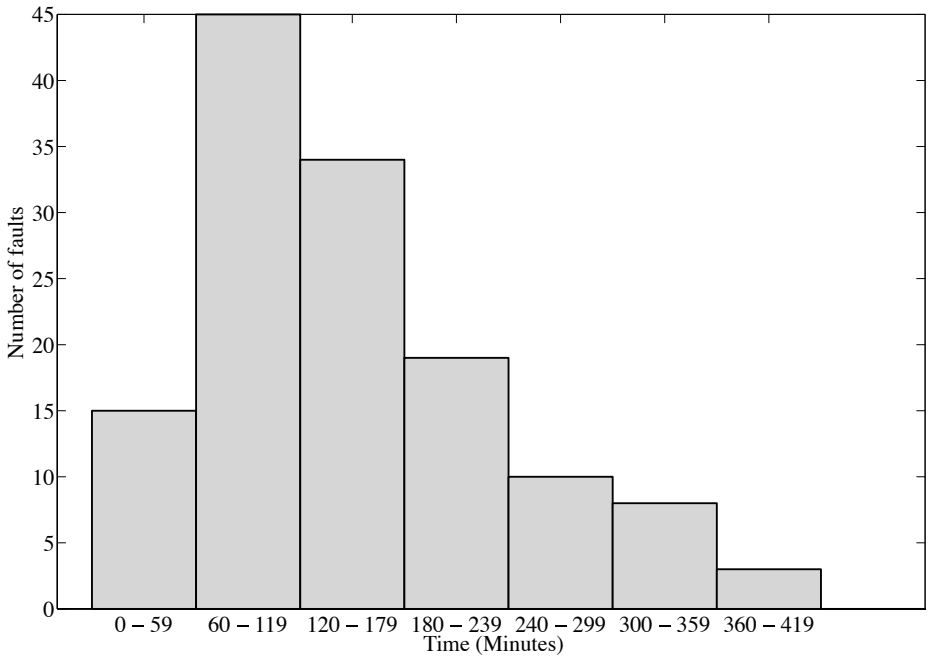


Figure 6.8 – Histogram of the Duration of Sustained Faults from Five Years of Historical Data

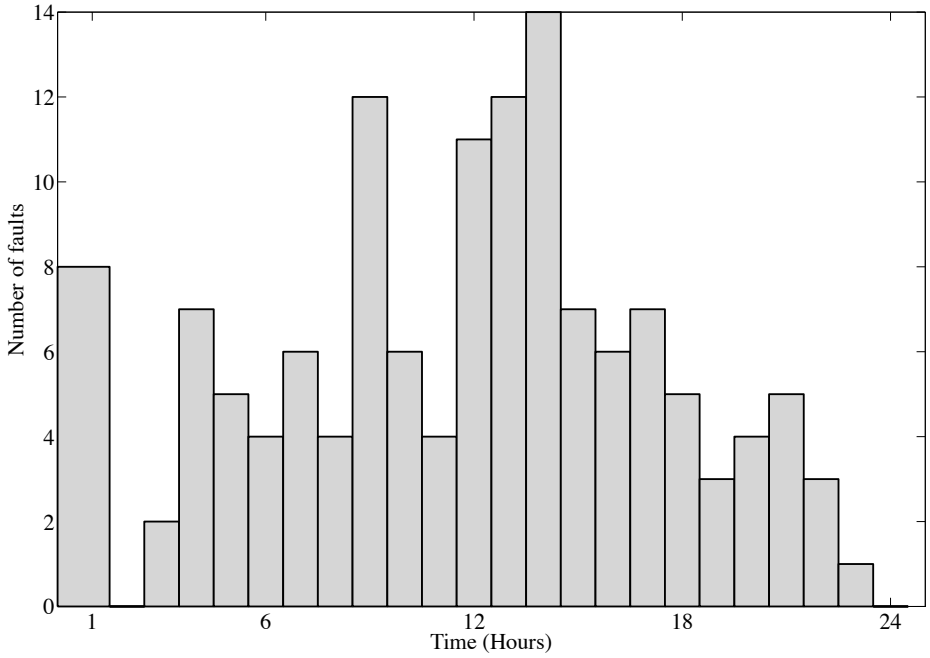


Figure 6.9 – Histogram of the Time of the Sustained Fault Events from Five Years of Historical Data

6.3 Description of Problem Formulation

The goal of this model was to address the increased uncertainty involved in solar power generation and to demonstrate how a microgrid can increase reliability and decrease costs associated with solar power generation. This problem was focused on sizing the energy storage system and the microturbines. Additionally, scheduling of the associated units was considered. A mathematical approach based on optimization was used for this purpose. The full problem of unit sizing and unit scheduling was decomposed into three stages. The first two stages involved sizing the kW/kWh rating of the energy storage system and the kW rating of the microturbine. In order to manage the computational complexity, the first two stages were coupled using Benders' decomposition. Based on the outputs of the first two stages, the third stage was solved as an independent problem.

Benders' decomposition is a well-researched and often utilized decomposition technique for integer and mixed integer linear programs [37]. Instead of solving one large complex problem, the problem is broken into smaller parts to be solved individually. The goal of such an approach is to ease the computational burden; however, depending on the problem, this may not always be the outcome. In Benders approach, the problem is split into a master problem and a subproblem. The master problem is an integer or mixed integer problem, which fixes particular variables for the subproblem. The subproblem then solves a linear program (LP) using the fixed variables and adds constraints to the master problem to reflect the added complexity of the subproblem. This process then iterates back and forth until the convergence criteria is reached.

The basic premise of Benders' decomposition is that a mixed integer problem can be reformulated into a problem that is easier to solve than the original. What follows is a simple statement of the reformulation.

Overall problem

$$Minimize \quad z = c^T\ x + d^T\ y \tag{6.1}$$

$$\text{s.t.} \qquad Ay \geq b \tag{6.2}$$

$$Ex + Fy \geq h \tag{6.3}$$

$$x \geq 0,\ y \in S \tag{6.4}$$

where y was a vector of integer variables, x was a vector of continuous variables, A, E, F were matrices and c, d, b, h were vectors with complementary dimensions. The problem was reformulated as

Master problem

$$Minimize \quad Z_{lower} \tag{6.5}$$

$$\text{s.t.} \qquad Z_{lower} \geq d^T y \tag{6.6}$$

$$Ay \geq b \tag{6.7}$$

$$y \in S \tag{6.8}$$

Subproblem

$$Minimize \quad c^T x \tag{6.9}$$

$$s.t. \qquad Ex \geq h - F\widehat{y} \tag{6.10}$$

$$x \geq 0 \tag{6.11}$$

where Z_{lower} was a dummy variable included to aid the solution of the master problem, $\widehat{y}$ was the parameter for the subproblem which was fixed by the master problem, with rest of the variables remained the same as previously described. The dual variable of (6.10), referred to as $\widehat{u}^p$, was used for formulating the optimality cuts for the master problem.

As part of Benders' decomposition, the problem was decomposed into a master problem and a subproblem. Equations (6.5)-(6.11) present the decomposed problem. The complete proof for this is available in [37]. There are two primary types of cuts for Benders decomposition: feasibility cuts and optimality cuts. In this problem, feasibility in the LP was ensured through slack variables for the grid support. Optimality cuts were applied after each iteration of the problem through the dual formulation of the LP (master problem). Essentially, these cuts added a cost to the master problem for the complexity in the LP. The cut was composed of the dual variable for each constraint in the LP multiplied by the right-hand-side (parameters) of the constraint.

Sometimes, the right-hand-side values in the subproblem contained fixed values from the master. Therefore, when applied back to the master, the value became unfixed and could take a new value. The steps for solving the Benders decomposition are listed below:

- Step 1 - Solve the master problem
- Step 2 - Solve the subproblem
- $Z_{upper} = d^T \hat{y} + c^T x$
- If $|Z_{upper} - Z_{lower}| \leq \epsilon$
- Otherwise generate a feasibility constraint $Z_{lower} \geq d^T y + (h - Fy)^T \hat{u}^p$ or $Z_{lower} \geq d^T y + c^T x - (y - \hat{y})\hat{u}^p$

Figure 6.10 presents the stages involved in sizing and scheduling the energy storage system. The master problem, which is a mixed integer program, considered an investment plan for the power conversion system (PCS) of the energy storage unit and the power rating of the microturbines. Once the candidate units were identified by the master problem, the energy rating of the energy storage unit was identified by the subproblem. If the load curtailment violations persisted, the subproblem was developed with the corresponding Benders cut, based on the dual multipliers from the subproblem, which were added to the master problem. The iterative solution created a Benders cut for the next iteration of the optimal operation to the master problem by using dual multipliers of the subproblem. The iteration process continued until a converged optimal solution was found.

The set of planning constraints in the master problem included the availability of capital investment, limited by the number of microturbines and the system capacity

requirement. The master problem was a mixed integer program, while the solution to the master problem was required to satisfy the reliability requirement. An infeasible cut was included in the master problem, provided that the solution to the master problem was either infeasible for the primal subproblem or unbounded for the dual subproblem.

The optimization problem formulated in stage 3 identified the BESS charge/discharge and microturbine schedule, whereas stages 1 and 2 identified the kW/kWh rating of the BESS and kW rating of the microturbine. The purposes of the problem formulated in stage 3 were as follows:

- To check the feasibility of the solution obtained from the Benders' decomposition (Stages 1 and 2) for the best and the worst PV scenarios (PV scenario 1 and PV scenario 5 respectively).
- To Model the life-cycle costs for the Li-ion based energy storage system.
- To maximize the trade of electric power to the grid from PV generation resource (Case 2).

6.3.1 Mathematical Formulation of Master Problem

Stage 1 of the process was intended to solve the master problem, which was a mixed integer program (MIP). The objective of the master problem was to minimize the kW rating of the ESS and the microturbine. Equation (6.12) presents the objective of the master problem. Equations (6.13) and (6.14) show the constraints associated with the master problem. After every iteration, a new optimality constraint was appended to the existing master problem. Table 6.1 furnishes the list of parameters and decision variables associated with the master problem.

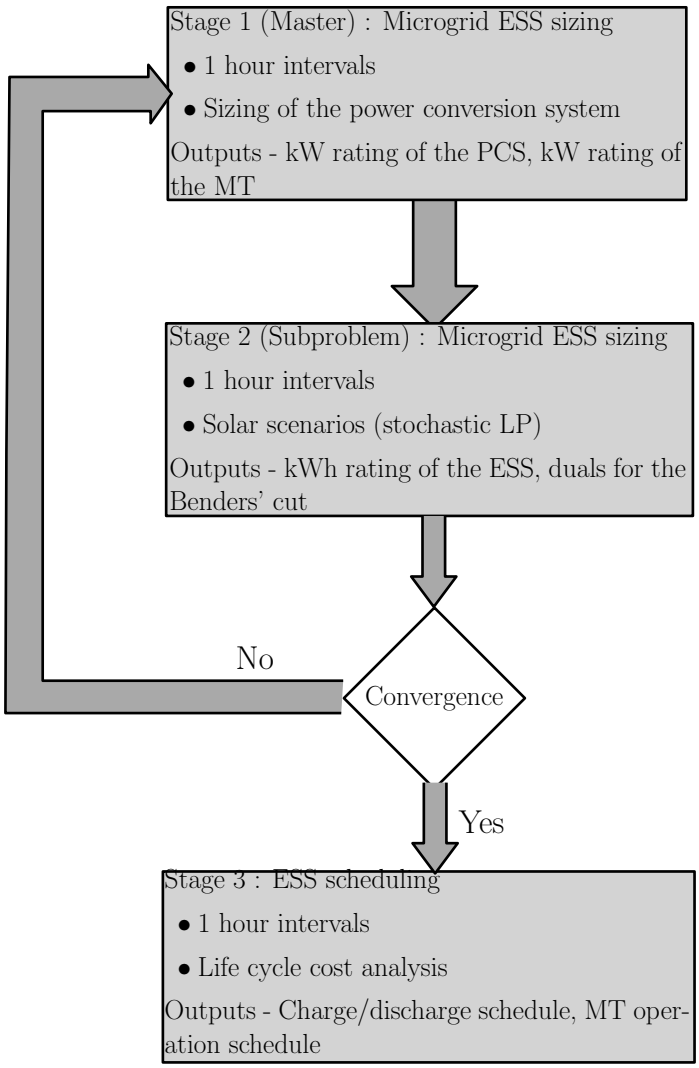


Figure 6.10 – Flowchart of the Steps Involved in Sizing the ESS and Microturbine

$$\text{min.} \quad Z_{lower} \tag{6.12}$$

The constraints are

$$Z_{lower} \leq \sum_{n} C^{ESS}_{\$/kW} \; B^{ESS}_{kW} \; x_n + \sum_{m} C^{MT}_{\$/kW} \; B^{MT}_{kW} \; x_m \tag{6.13}$$

$$\sum_{n} x_n \; B^{ESS}_{kW} + \sum_{m} x_m \; B^{MT}_{kW} \geq peakload \tag{6.14}$$

Table 6.1 – List of Parameters for the Master Problem

Parameter	Details	Units	Value
$C^{ESS}_{\$/kW}$	cost of power conversion system for the ESS	\$/kW	492 [62]
$C^{MT}_{\$/kW}$	cost of microturbine	\$/kW	3000 [67]
B^{ESS}_{kW}	individual block sizes chosen for ESS to decide the best mix of units	kW	100
B^{MT}_{kW}	individual block sizes chosen for MT to decide the best mix of units	kW	50
n	number of B^{ESS}_{kW} required	-	6
m	number of B^{MT}_{kW} required	-	6
Decision variables	Details	Units	Value
x_m	binary variable to choose the block n of the ESS	-	{0,1}
x_n	binary variable to choose the block m of the microturbine	-	{0,1}

6.3.2 Mathematical Formulation of Subproblem

The subproblem calculated the kWh rating of the energy storage system, treating the PV generation as a stochastic resource. The kW rating of the PCS and microturbine were obtained from the master problem. The objective value of the subproblem was included in the optimality cut for the following iterations of the

Benders decomposition. Equation (6.15) presents the objective of the subproblem. Equations (6.16) and (6.19) show the constraints associated with the subproblem. After each iteration, a new optimality constraint was appended to the existing master problem. Table 6.2 furnishes the list of parameters and decision variables associated with the subproblem.

Table 6.2 – List of Parameters for the Subproblem

Parameters	Details	Unit	Value
$C^{ESS}_{\$/kWh}$	cost of energy storage system installation costs without the power conversion system	\$/kWh	902
$C^{gas}_{\$/kW}$	cost of natural gas	\$/kW	0.1375
$PV_{\omega}[t]$	PV generation as a stochastic variable $\omega \in \{5scenarios\}$	kW	-
$load[t]$	load profile for the microgrid	kW	-
$y[t]$	used to connect/disconnect the grid	-	[0,1]
M	Big M value for P_{grid}	-	10000

$$min\ w = \sum_{t} \Bigg[C^{ESS}_{\$/kWh} \sum_{n} (BESSkW_n[t]) + C^{gas}_{\$/kW} \sum_{m} (MT_m[t]) + C^{grid}_{\$/kW}[t]\ P_{grid}[t] \Bigg] \tag{6.15}$$

Constraints are

$$BESSkW_n[t] + MT_m[t] + PV_\omega[t] + P_{grid}[t] \geq load[t] \qquad \forall \quad t,\ n,\ m,\ \omega \quad (6.16)$$

$$BESSkW_n[t] \leq B_{kW}^{ESS}\ \widehat{x_n} \qquad \forall \quad n,\ t \quad (6.17)$$

$$MT_m[t] \leq B_{kW}^{MT}\ \widehat{x_m} \qquad \forall \quad m,\ t \quad (6.18)$$

$$P_{grid}[t] \leq M\ y[t] \qquad \forall \quad t \quad (6.19)$$

The sizing and scheduling of the energy storage system was studied as three individual cases. A single mathematical formulation of the MILP presented in this chapter was capable of capturing the results for all three cases. The results for the cases was obtained by simply changing the vector $y[t]$ specific to each case. The $y[t]$ used for all the cases are listed below:

- $y[t]$ for Case 1 - [0,0,0,0,0,0,0,0,0,0,0,0,0,0,0,0,0,0,0,0,0,0,0,0]
- $y[t]$ for Case 2 winter month - [1,1,1,1,0,0,0,0,0,1,1,1,1,1,1,1,1,0,0,0,0,0,0,1]
- $y[t]$ for Case 2 summer month - [1,1,1,1,1,1,1,1,1,1,1,1,1,1,0,0,0,0,0,0,0,0,0,1]
- $y[t]$ for Case 3 - [1,1,1,1,1,1,1,1,0,0,0,0,1,1,1,1,1,1,1,1,1,1,1,1]

6.3.3 Energy Storage System Scheduling

The optimal dispatch of the BESS and microturbine refers to a strategy for timing the charge and discharge of the BESS along with the microturbine. The bounds for the dispatch problem were the capacity limitations on the equipment, including the BESS capacity and the DC/AC converter rating. The objective function that needed to be minimized is shown in (6.20).

Table 6.3 – List of Parameters and Variables in the ESS Scheduling Problem

Parameters used in the optimization	
T	complete set of 1 hour intervals in a day
t	particular 1 hour interval during a day
$\underline{h}$, $\bar{h}$	minimum and maximum SOC of the BESS respectively
$load[t]$	system load at 1 hour interval t
η_{ch}, η_{ds}	charge and discharge efficiencies of BESS - 90% each
C_t^{grid}	cost of power from the grid
S	DC/AC converter rating in kW
Decision variables used in the optimization	
P_t^{grid}	power drawn from the grid in kW
ds_t	rate at which the battery will be discharged (kW)
ch_t	rate at which the battery will be charged (kW)
SOC_t	state of charge of the battery calculated from ch_t and ds_t (kWh)
Z_t^+	expected battery replacement cost as a function of depth of discharge from time t-1 to t in kW; calculated from the ch_t and ds_t

$$min.\ c = \sum_t \left(C_{\$/kW}^{gas}\ P_t^{MT} + C_t^z\ Z_t^+ + C_{\$/kW}^{grid}[t] P_t^{grid} \right) \tag{6.20}$$

Load balance constraint

$$load_t = (P_t^{MT} + PV_t + \eta_{ds} \quad ds_t - ch_t/\eta_{ch} + P_t^{grid}) \qquad \forall\ t \in T \tag{6.21}$$

Updating the SOC constraint

$$SOC_t = SOC_{t-1} - ds_t + ch_t \qquad \forall\ t \in T \qquad (6.22)$$

Associated lower and upper bounds

$$\underline{h} \leq SOC_t \leq \bar{h} \qquad \forall\ t \in T \qquad (6.23)$$

$$0 \leq ds_t \leq S, 0 \leq ch_t \leq S \qquad \forall\ t \in T \qquad (6.24)$$

Decision variable associated with the life cycle costs

$$Z_t \geq ch_{t-1} - ch_t + ds_t - ds_{t-1} \qquad \forall\ t \in T \qquad (6.25)$$

$$Z_t \geq ch_t - ch_{t-1} + ds_{t-1} - ds_t \qquad \forall\ t \in T \qquad (6.26)$$

Choosing the P_t^{grid}

$$P_t^{grid} \leq M\ y_t \qquad \forall\quad t \in T \qquad (6.27)$$

Either charge or discharge

$$ch_t \leq S\ y_t^{ch} \qquad \forall\quad t \in T \qquad (6.28)$$

$$ds_t \leq S\ y_t^{ds} \qquad \forall\quad t \in T \qquad (6.29)$$

$$y_t^{ch} + y_t^{ds} \leq 1 \qquad \forall\quad t \in T \qquad (6.30)$$

6.4 Results of Case Studies

The optimal size and schedule of an energy storage system and the microturbine is presented in this section. The energy storage system was assumed to be based on Li-ion technology. The sizing and scheduling of the energy storage system was performed in three stages (objectives). The first two stages, coupled with Benders' decomposition, calculated the kW/kWh rating of the ESS and kW rating of the microturbine. The third stage provided the optimal schedule of the generation resources.

6.4.1 Energy Storage System and Microturbine Sizing for All Cases

The mathematical formulation of the Benders' decomposition presented in section 6.3 was solved for all the cases mentioned in Figure 6.7. The size of the energy storage system involved the kW (active power) and kWh (energy) ratings, whereas the microturbine involved only the kW rating. The first two stages presented in Figure 6.10 were coupled using the Benders decomposition technique. The results obtained from solving the Benders decomposition for all the three cases were tabulated in Table 6.4, which also includes the associated cost for installation.

Table 6.4 – Power Rating of the Energy Storage System and Microturbine for All the Three Cases

Cases		ESS		Microturbine	Investment
		kW	kWh	kW	$
Case 1	Summer	200	1745	100	1,736,870
	Winter	200	2322	100	2,238,690
Case 2	Summer	300	1453	150	1,503,070
	Winter	200	1695	100	1,670,950
Case 3 (mean)	Summer	100	100	100	251,939
	Winter	100	75	100	144,172
Case 3 (longest)	Summer	1508	100	100	1,553,280
	Winter	200	1031	100	1,072,520

The results from the Table 6.4 were used to generate Figure 6.11. Figure 6.11 displays the entire size of the energy storage system and microturbine. It can be clearly observed that the sizing of the kWh rating of the energy storage system was

specific to a month of study in the year. The kWh rating of the energy storage system was large for a typical winter month, compared to the rating for a summer month. The historic load profiles and the PV generation profiles were chosen from the geographic location of Flagstaff, AZ, for the analysis. This observation can also be seen in Figure 6.6.

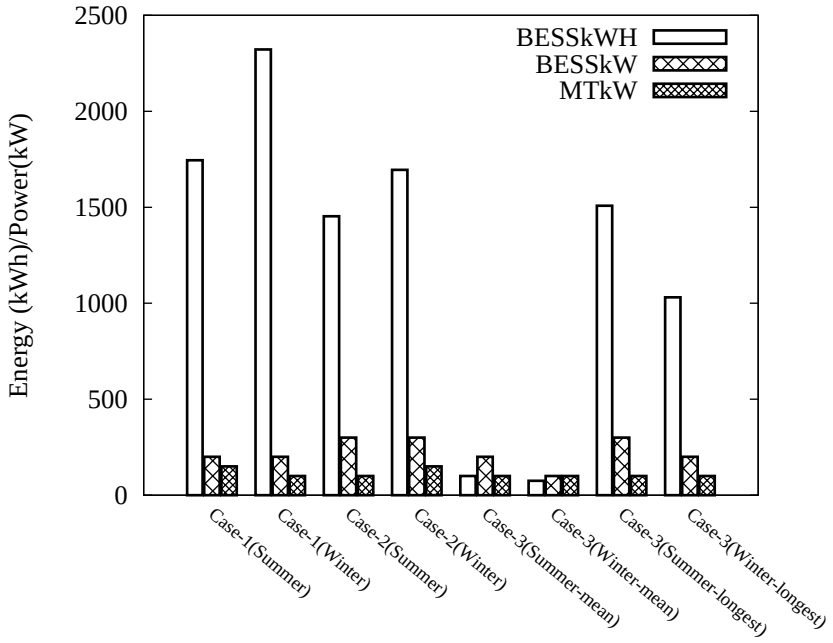


Figure 6.11 – Results of the Energy Storage Sizing for Each of the Cases Listed

The energy storage system and the microturbine needed to be optimally scheduled to minimize the operation and life-cycle costs of the energy storage system. The mathematical formulation of optimal scheduling problem is presented in section 6.3.3. The optimal scheduling was performed based on the results obtained from the Benders decomposition. The results tabulated in Table 6.4 were used to decide the optimal schedule. The following sections furnish the optimal schedule of all the generation components of the microgrid for all the cases.

6.4.2 Case 1 - Energy Storage Scheduling for 24 Hours of Microgrid Operation without Support from the Grid

Figures 6.12 and 6.13 present the optimal schedule of the generation resources of the microgrid without support from the main grid for a period of 24 hours. The optimal schedule for case 1 was presented for a typical summer month (Figure 6.12) and winter month (Figure 6.13). Further, scheduling was performed for the best and worst PV generation scenarios to study the impact of PV variability on the optimal schedule. Figures 6.12 and 6.13 present the schedule of the microturbine, the charge/discharge profile of the energy storage system, and the state of charge of the energy storage system.

From Figures 6.12 and 6.13 the following observations can be made:

- To maximize the life time of the energy storage system, the variability in PV generation was accommodated using the microturbine
- The excess PV generation was used to charge the energy storage system

6.4.3 Case 2 - Energy Storage for Microgrid Scheduling during Peak Hours of the Feeder

Figures 6.14 and 6.15 present the optimal schedule of the generation resources of the microgrid with support from the main grid for a period of 24 hours. The support for the microgrid was expected only during the peak hours. For a summer load profile, the duration between 1:00 PM and 11:00 PM constituted peak hours. For a winter month, the durations between 5:00 AM and 9:00 AM and between 4:00 PM and 11:00 PM were considered peak hours. The cost of power from the grid was

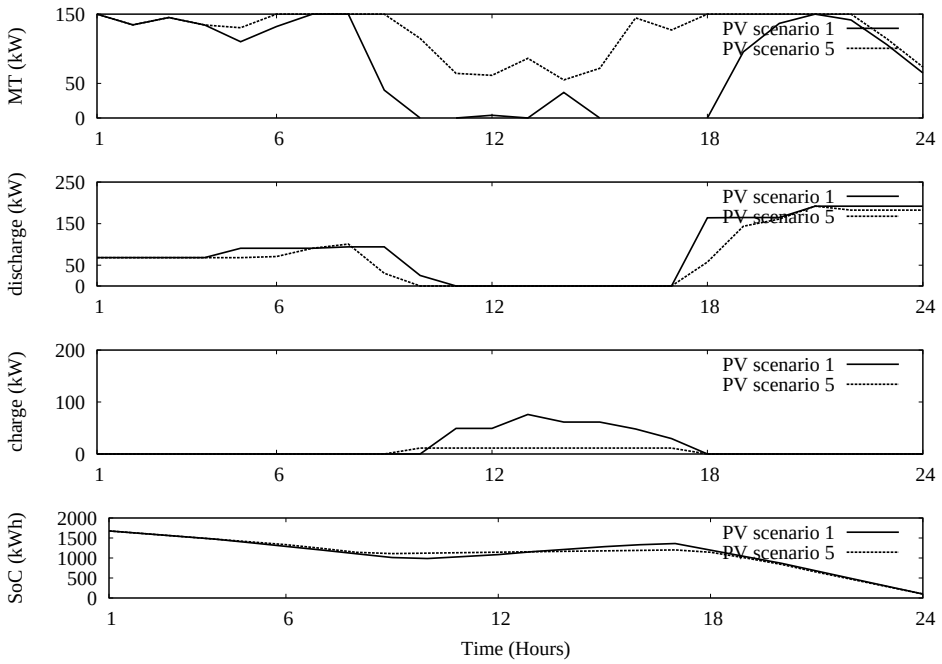


Figure 6.12 – Optimal Schedule of the Generation Resources of the Microgrid without the Main Grid (Case 1) for a Typical Summer Month (June)

assumed to follow a time-of-use profile. The time-of-use cost profiles for the power from the grid are presented in Figure 6.6.

The optimal schedule for case 2 was presented for a typical summer month (Figure 6.14) without any trade with the grid. Figure 6.15 presents the optimal scheduling scenario with nonfirm trade. Further, scheduling was performed for the best and worst PV generation scenarios to study the impact of PV variability on the optimal schedule and the nonfirm trade. Figures 6.14 and 6.15 present the schedule of the main grid, the microturbine, the charge/discharge profile of the energy storage system, and the state of charge of the energy storage system.

From Figures 6.14 and 6.15 the following observation can be made:

- To maximize the life time of the energy storage system variability in PV generation was accommodated using microturbines

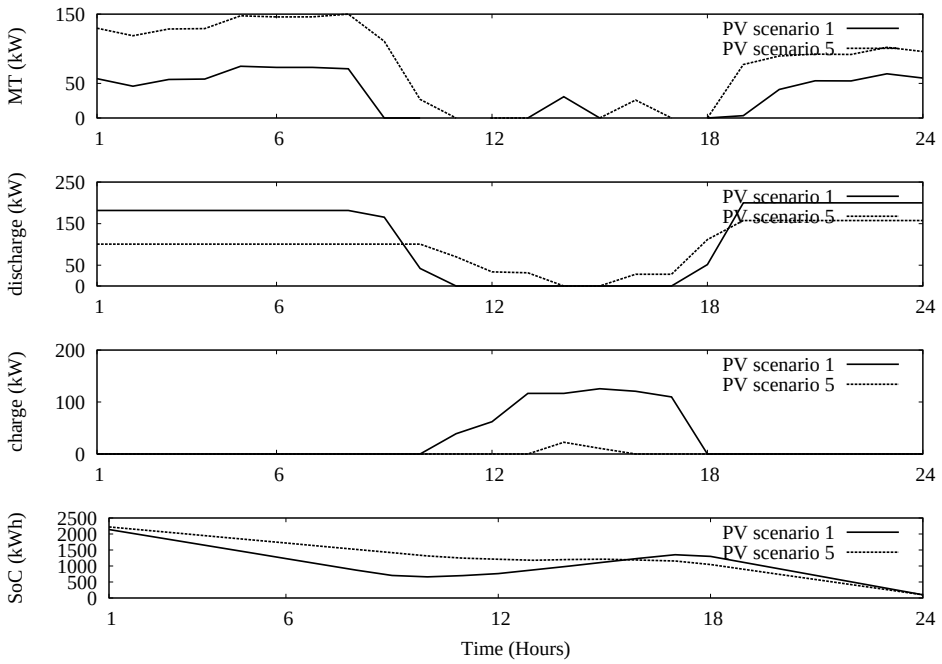


Figure 6.13 – Optimal Schedule of the Generation Resources of the Microgrid without the Main Grid (Case 1) for a Typical Winter Month (January)

- The excess PV generation was used to charge the energy storage system
- The energy storage system was charged partially from the main grid only specifically when the grid costs were low
- With high PV generation (PV scenario 1) the energy storage system was charged largely from the PV source, whereas with low PV generation (PV scenario 5) the main grid was used
- With non-firm trade to the grid (Figure 6.15) instead of charging the energy storage system the excess PV generation was traded to the main grid.

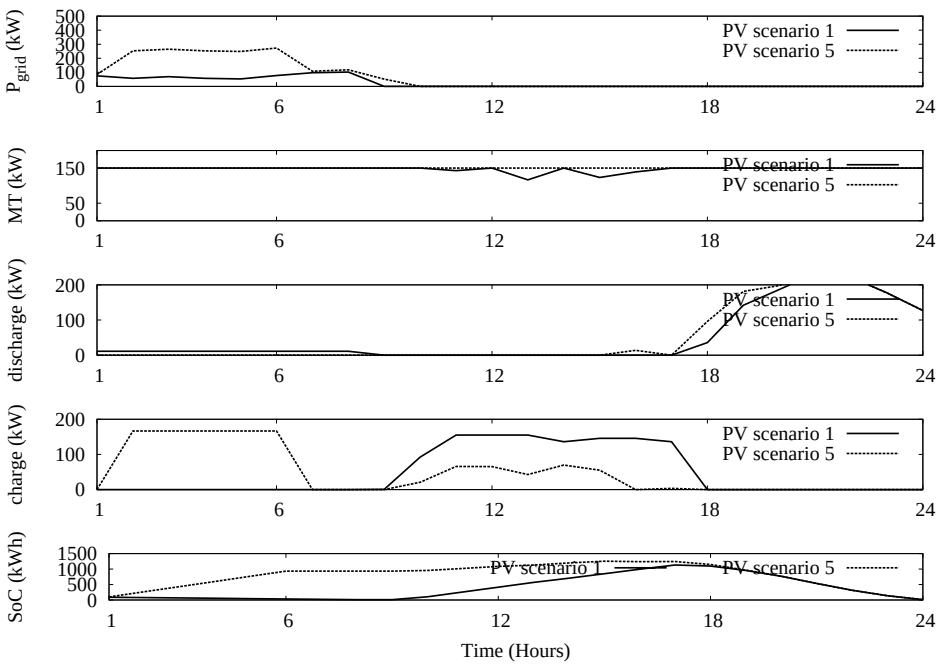


Figure 6.14 – Optimal Schedule of the Generation Resources of the Microgrid with the Main Grid (Case 2) for a Typical Summer Month (June)

6.4.4 Case 3 - Energy Storage Scheduling Based on the Mean Outage Reported from the Historical Data

Based on outage reports from the previous five years, the mean duration of sustained outage was identified (Figure 6.8). Further, the historical data for the mean time of the sustained fault events from the past five years were identified (Figure 6.9). Based on the mean values, the obtained optimal schedule is presented in Figure 6.16. The energy storage system and the microturbine adequately supplied the load during the outage of the substation.

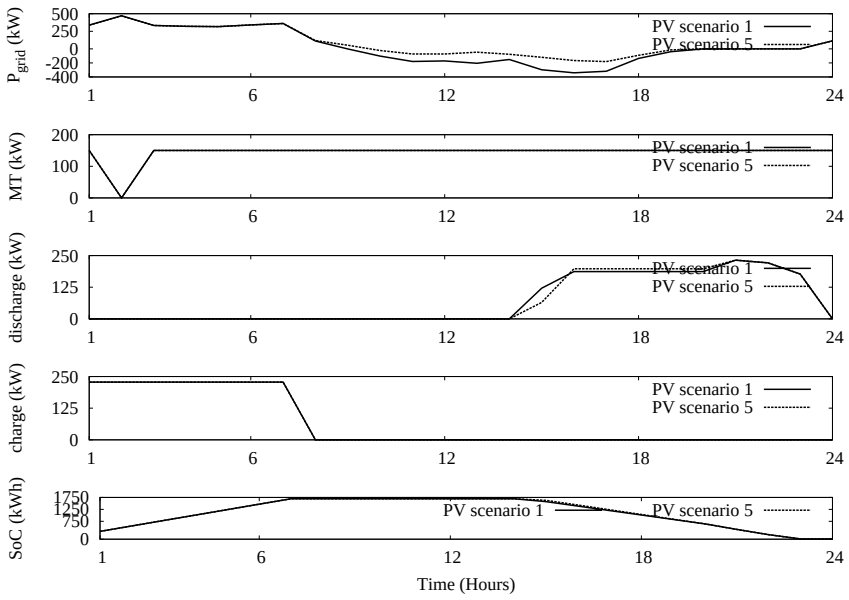


Figure 6.15 – Optimal Schedule of the Generation Resources of the Microgrid without the Main Grid (Case 2) with Non-firm Trade for a Typical Summer Month (June)

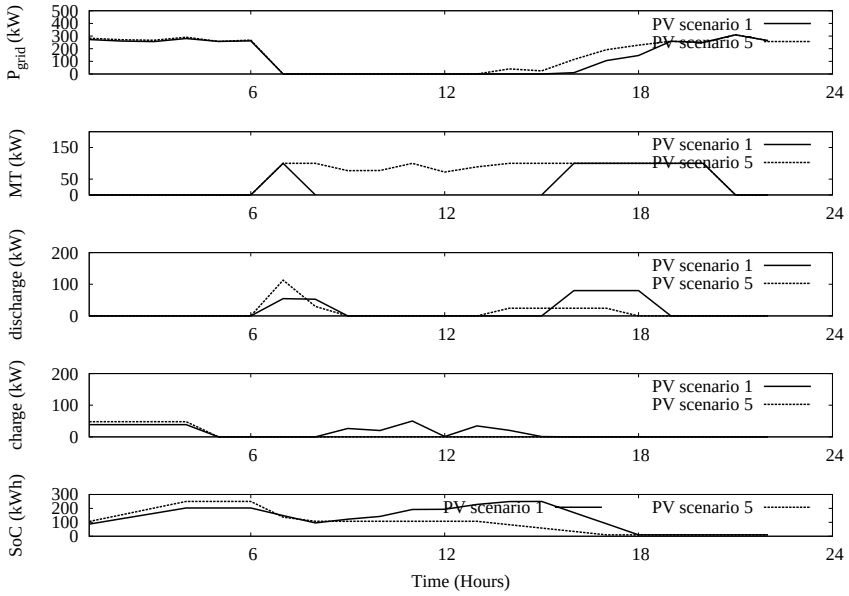


Figure 6.16 – Optimal Schedule of the Generation Resources to Support the Outages in the Microgrid for a Typical Summer Month (June)

Chapter 7

SUMMARY AND CONCLUSIONS

This work was motivated from ongoing installations of PV generators on existing distribution feeders. A detailed study on multiple topics of interest relevant to distribution systems with high penetration of PV generation was conducted. The topics included methods for distribution system analysis, unbalance induced by roof-top PV generation, use of energy storage systems as bulk storage devices, and microgrid design. All the analyses and results presented corresponded to two test feeders chosen as test beds. The primary contributions of this work are as follows.

- Demonstrated the possibility of performing long-term transient analysis using the dynamic phasors and DAE
- Proposed and validated the use of active power filters for mitigating the effects of unbalanced PV generators
- Proposed and implemented optimization methods for sizing and scheduling BESS and microturbines using Benders' decomposition

7.1 Distribution System Modeling and Analysis

As a part of the distribution system analysis, the test feeder was modeled in CYMDIST, OpenDSS, and MATLAB/Simulink. At every step of the modeling process, multiple levels of verification were carried out. The DAE were verified with dynamic phasors, which were in turn verified with results of the time-series analysis. The results from OpenDSS aligned well with the field measurements, with an RMS error of approximately 2% in the voltages and currents at multiple points along

the feeder. The model of the test feeder in MATLAB/Simulink, compared with the OpenDSS test feeder, was observed to deviate 1.5% at the feeder head and 3.4% at the end of the feeder. The performance of the dynamic analysis in OpenDSS was also verified with dynamic phasor performance.

This work demonstrated the possibility of performing long-term transient analysis using the dynamic phasors and DAE. This is one of the first works to apply the theory of dynamic phasors and DAE for solving large distribution feeders with high penetration of PV generators. To summarize, distribution system analysis for impact of high penetration involves:

- Snapshot analysis - static voltage profile, active power profile, reactive power profile, typical scenario analysis
- Time-series analysis - capacitor bank operation/regulator switching/PV generation profies/load profiles
- Transient analysis - study of fast PV ramp rates, grid transients, interaction of control devices with high bandwidth control

This work presented three methodologies for transient analysis suitable for different study objectives. The intent of the study was not to choose the best among these approaches, rather to propose novel mathematical techniques to efficiently perform the distribution system analysis.

- Time domain transient analysis - anti-islanding operation/switching transients
- Dynamic phasor transient analysis - cloud transients/voltage sags/controller interaction

- DAE-based transient analysis - cloud transients/voltage sags/controller interaction

All the mathematical techniques involving dynamic simulations have been compared in Tables 7.1 and 7.2.

7.2 Analysis and Mitigation of Phase Unbalance

The voltage unbalance induced by PV generators further aggravates the existing unbalance caused by load mismatch. The impact of the unbalanced PV penetrations on the VUF largely depends on the selection of nodes in a distribution feeder. In this research, the sensitivity of each node to unbalanced PV generators varied based on the loading of the distribution feeder. A systematic approach was taken to categorize the nodes as most sensitive, intermediary sensitive, and least sensitive nodes based on their VUFs.

In order to study the unbalance induced by the PV generators various case studies were performed. The level of PV penetration was increased in steps and the corresponding increase in the VUF and neutral currents were studied. The PV penetration was raised as a percentage of the maximum load (4600 kW) from 25% to as high as 200% to understand the effects at very high penetration levels. Choosing the most sensitive nodes for installing the PV generators resulted in a violation of the VUF limit (2%) at 50% PV penetration. In comparison, a 40% reduction in the VUF was observed by placing the identical PV generators at less sensitive nodes. This study clearly shows the importance of choosing an appropriate node for installing the PV generators in a distribution feeder. The distribution feeder can accommodate much higher penetration levels when installed at less sensitive nodes.

A power electronics converter based solution was proposed to mitigate the identified impacts. A model of the active power filter was realized to validate the effec-

tiveness of the proposed methodology on the test feeder in OpenDSS. An user-defined model of the active power filter was placed at the most sensitive node for the purpose of analysis. After applying the correction currents at the most sensitive node, the active power filter ensured zero neutral current at the node of interest. The neutral currents at the feeder head were reduced by 42% due the active power filter at the most sensitive node.

An important advantage of power electronic converter based active solutions, especially for mitigating PV induced unbalance, is that the correction currents vary continuously in time following the solar output and load. Other mitigation methods are either fixed or cannot follow this variation continuously. As seen, the neutral current at the most sensitive node was brought close to zero for the entire year after the correction currents were applied. The power rating of the active power filter was calculated based on the maximum value of the correction current required at the node of interest. The maximum value of the correction currents among all the phases at the most sensitive node was 28.4 A, connected to a medium-voltage line at 7.2 kV as line-neutral voltage, corresponding to a rating of 604.8 kVA.

7.3 Microgrid Analysis and Design

Furthermore, microgrid design and analysis were considered. This study concentrated on sizing the energy storage system, and the microturbines. Additionally, the associated units were scheduled using the formal mathematical optimization techniques. The entire problem of unit sizing and scheduling was decomposed into three stages. The first two stages involved sizing of the kW/kWh rating of the energy storage system and the kW rating of the microturbine. In order to manage the computational complexity the first two stages were coupled using Benders' decompo-

sition. Based on the outputs of the first two stages the third stage was solved as an independent problem.

The sizing was performed based on the historical load and PV generation data. The results illustrated that in order to minimize the life cycle costs of the energy storage systems the microturbines should be employed to mitigate the variability of PV generation. Moreover, excess generation from the PV resource was primarily stored in the energy storage system and traded to the main grid during the peak hours.

7.4 Deployment of Energy Storage Systems in a Distribution Feeder

An approach based on convex optimization was proposed to schedule the charging and discharging of the lithium-ion based battery energy storage system. The objectives included reduction of the substation transformer losses, savings on the cost of energy delivered from the grid and reducing the life cycle cost of the battery storage system. The resulting cost reduction was also determined. The developed tools can be used for analyzing and optimizing different sets of operating conditions, penalty factors or different distribution systems. The impact of the reactive power support from the energy storage system on the voltage at the feeder head was studied. Additionally the BESS optimal dispatch was used to study the impact on the substation transformer losses. A reduction in the substation transformer losses was observed.

A PV generation source of 400 kW was considered at the feeder head and the impact of cloud transients on the system operation was studied. The economic dispatch of the BESS with PV solar generation was studied under two scenarios - energy shifting scenario and solar smoothing scenario.

Table 7.1 – Detailed Comparison of the Proposed Methodologies for Distribution System Analysis - Part 1

Study	**Time-series**	**Time-domain**	**Dynamic phasor**	**DAE**
Time scope of analysis	day, month, year	few 60 Hz cycles	$\leq$ 60 minutes	$\leq$ 10 minutes
Simulation time	1/5/15 minutes	5 days	3 hours	15 minutes
Frequency of the transients	-	No limit	$\leq$ 60 Hz	$\geq$60 Hz
Limitation on the size of feeder	No limit	$\leq$ 50 nodes	$\leq$ 2000 nodes	No limit

Table 7.2 – Detailed Comparison of the Proposed Methodologies for Distribution System Analysis - Part 2

Study	**Time-series analysis**	**Time-domain**	**Dynamic phasor**	**DAE**
Time step	$\geq$ 1 sec	$\leq$ 100 μsec	$\leq$ 100 μsec	$\leq$ 1 m sec
Solvers	Newton-raphson powerflow solvers	Fixed step and variable step solvers (Runge-Kutta, Euler, Adams-Bashforth)	Fixed step and variable step solvers (Runge-Kutta, Euler, Adams-Bashforth)	Fixed step (improved Euler-Cauchy predictor-corrector)
Existing tools with capability	CYMDIST, OpenDSS, GridLab-D	Simulink, PSCAD	Simulink, Opal-RT	OpenDSS

REFERENCES

[1] Institute for sustainable energy solution in collaboration with Arizona corporation commission; Available at: http://nau.edu/CEFNS/Centers-Institutes/Sustainable-Energy-Solutions/, 2014.

[2] California public utility commission; Available at: http://www.cpuc.ca.gov/PUC/energy/Renewables/, 2014.

[3] CYME by Cooper power systems; Available at: http://www.cyme.com/software/cymdist/, 2013.

[4] R. F. Arritt and R. Dugan, "Distribution system analysis and the future smart grid," *IEEE Transactions on Industry Applications*, vol. 47, pp. 2343–2350, Nov. 2011.

[5] S. Sanders and G. Verghese, "Synthesis of averaged circuit models for switched power converters," in *IEEE International Symposium on Circuits and Systems*, pp. 679–683, May 1990.

[6] S. Sanders, J. Noworolski, X. Liu, and G. Verghese, "Generalized averaging method for power conversion circuits," *IEEE Transactions on Power Electronics*, vol. 6, pp. 251–259, Apr. 1991.

[7] V. Venkatasubramanian, H. Schattler, and J. Zaborszky, "Fast time-varying phasor analysis in the balanced three-phase large electric power system," *IEEE Transactions on Automatic Control*, vol. 40, pp. 1975–1982, Nov. 1995.

[8] A. Nagarajan and R. Ayyanar, "Dynamic phasor model of single-phase inverters for analysis and simulation of large power distribution systems," in *Power Electronics for Distributed Energy Systems*, pp. 1–8, July 2013.

[9] J. B. Ward, "Equivalent circuits for power-flow studies," *Transactions of the American Institute of Electrical Engineers*, vol. 68, pp. 373–382, July 1949.

[10] J. Yang, G. Cheng, and Z. Xu, "Dynamic reduction of large power system in PSS/E," in *Transmission and Distribution Conference and Exhibition*, pp. 1–4, Mar. 2005.

[11] H. Oh, "A new network reduction methodology for power system planning studies," *IEEE Transactions on Power Systems*, vol. 25, pp. 677–684, May 2010.

[12] C. Coulston and R. Weissbach, "Routing transmission lines via Steiner trees," in *Power Engineering Society General Meeting*, vol. 3, p. 4, July 2003.

[13] A. Ishchenko, A. Jokic, J. Myrzik, and W. Kling, "Dynamic reduction of distribution networks with dispersed generation," in *International Conference on Future Power Systems*, pp. 7–15, Nov. 2005.

[14] T. L. Le, Q. T. Tran, O. Devaux, O. Chilard, and R. Caire, "Reduction and aggregation for critical and emergency operation of distribution network in presence of distributed generators," in *20th International Conference and Exhibition on Electricity Distribution - Part 1*, pp. 1–4, June 2009.

[15] H. Oh, "Aggregation of buses for a network reduction," *IEEE Transactions on Power Systems*, vol. 27, pp. 705–712, May 2012.

[16] S.-Y. Yun, C.-M. Chu, S.-C. Kwon, and I.-K. Song, "A reduction method of distribution network for smart distribution operation system," in *Integration of Renewables into the Distribution Grid, CIRED Workshop*, pp. 1–4, May 2012.

[17] X. Mao and R. Ayyanar, "Average and phasor models of single phase PV generators for analysis and simulation of large power distribution systems," in *Applied Power Electronics Conference and Exposition*, pp. 1964–1970, July 2009.

[18] W. D. Humpage and B. Stott, "Predictor-corrector methods of numerical integration in digital-computer analyses of power-system transient stability," *Proceedings of the Institution of Electrical Engineers*, vol. 112, pp. 1557–1565, Aug. 1965.

[19] H. Dommel and N. Sato, "Fast transient stability solutions," *IEEE Transactions on Power Apparatus and Systems*, vol. PAS-91, pp. 1643–1650, July 1972.

[20] M. Adibi, P. Hirsch, and J. Jordan, J.A., "Solution methods for transient and dynamic stability," *Proceedings of the IEEE*, vol. 62, pp. 951–958, July 1974.

[21] Delphi Embarcadero Delphi XE5; Available at: http://www.embarcadero.com/products/delphi, 2013.

[22] C. Vartanian and N. Bentley, "A123 systems advanced battery energy storage for renewable integration," in *Power Systems Conference and Exposition (PSCE)*, pp. 1–6, Mar. 2011.

[23] A. Nourai, R. Sastry, and T. Walker, "A vision and strategy for deployment of energy storage in electric utilities," in *Power and Energy Society General Meeting*, pp. 1–4, July 2010.

[24] M. Brandao, H. Johal, and L. Ion, "Energy storage for LV grid support in Australia," in *Innovative Smart Grid Technologies Asia (ISGT)*, pp. 1–8, Nov. 2011.

[25] J. Eyer and G. Corey, "Energy storage for the electricity grid: Benefits and market potential assessment guide," tech. rep., 2010.

[26] J. Eyer, J. Iannucci, and P. Butler, "Estimating electricity storage power rating and discharge duration for utility transmission and distribution deferral a study for the DOE energy storage program," tech. rep., Sandia National Laboratories-Energy Storage Program, Office of Electric Transmission and Distribution, U.S. Department of Energy, 2004.

[27] H. Saboori and H. Abdi, "Application of a grid scale energy storage system to reduce distribution network losses," in *Electrical Power Distribution Networks (EPDC)*, pp. 1–5, Apr. 2013.

[28] N. Rau and B. Tayor, "A central inventory of storage and other technologies to defer distribution upgrades-optimization and economics," *IEEE Transactions on Power Delivery*, vol. 13, pp. 194–202, Jan. 1998.

[29] E. Troster, T. Ackermann, and B. Betz, "Using storage to integrate renewables into the distribution system ; a case study," in *Electricity Distribution (CIRED)*, pp. 1–4, June 2013.

[30] W. Kempton and J. Tomić, "Vehicle-to-grid power fundamentals: Calculating capacity and net revenue," *Journal of Power Sources*, vol. 144, no. 1, pp. 268–279, 2005.

[31] R. Sioshansi and P. Denholm, "The value of plug-in hybrid electric vehicles as grid resources," *The Energy Journal*, vol. 31, no. 3, pp. 1–23, 2010.

[32] M. Duvall and M. Alexander, "Batteries for electric drive vehicle status 2005: Performance, durability, and cost of advanced batteries for electric, hybrid electric, and plug-in hybrid electric vehicles," tech. rep., EPRI, 2005.

[33] S. Shao, F. Jahanbakhsh, J. R. Aguero, and L. Xu, "Integration of PEVs and PV-DG in power distribution systems using distributed energy storage; dynamic analyses," in *Innovative Smart Grid Technologies (ISGT)*, pp. 1–6, 2013.

[34] S. Lin, M. Han, R. Fan, and X. Hu, "Configuration of energy storage system for distribution network with high penetration of PV," in *IET Conference on Renewable Power Generation*, pp. 1–6, Mar. 2011.

[35] Y. Xu and C. Singh, "Multi-objective design of energy storage in distribution systems based on modified particle swarm optimization," in *Power and Energy Society General Meeting*, pp. 1–8, July 2012.

[36] G. Li, Z. Bie, B. Hua, and X. Wang, "Reliability evaluation of distribution systems including micro-grids considering demand response and energy storage," in *Universities Power Engineering Conference (UPEC)*, pp. 1–6, 2012.

[37] J. F. Benders, "Partitioning procedures for solving mixed-variables programming problems," *Numerische mathematik*, vol. 4, no. 1, pp. 238–252, 1962.

[38] M. Caramanis, J. P. Stremel, and L. Charny, "Modeling generating unit size and economies of scale in capacity expansion with an efficient, real, number representation of capacity additions," *IEEE Transactions on Power Apparatus and Systems*, vol. PAS-103, pp. 506–515, Mar. 1984.

[39] M. V. F. Pereira, L. M. V. G. Pinto, S. H. F. Cunha, and G. Oliveira, "A decomposition approach to automated generation/transmission expansion planning," *IEEE Transactions on Power Apparatus and Systems*, vol. PAS-104, pp. 3074–3083, Nov. 1985.

[40] J. Yellen, T. Al-Khamis, S. Vemuri, and L. Lemonidis, "A decomposition approach to unit maintenance scheduling," *IEEE Transactions on Power Systems*, vol. 7, pp. 726–733, May 1992.

[41] S. H. Alawaji and K. Lo, "A new approach for solving the problem of unit commitment," in *2nd International Conference on Advances in Power System Control, Operation and Management*, pp. 571–577, Dec. 1993.

[42] H. Ma and S. M. Shahidehpour, "Decomposition approach to unit commitment with reactive constraints," *IEE Proceedings - Generation, Transmission and Distribution*, vol. 144, pp. 113–117, Mar. 1997.

[43] Y. Gu, J. McCalley, and M. Ni, "Coordinating large-scale wind integration and transmission planning," *IEEE Transactions on Sustainable Energy*, vol. 3, pp. 652–659, Oct. 2012.

[44] J. Barton and D. Infield, "Energy storage and its use with intermittent renewable energy," *IEEE Transactions on Energy Conversion*, vol. 19, pp. 441–448, June 2004.

[45] B. Borowy and Z. Salameh, "Methodology for optimally sizing the combination of a battery bank and PV array in a wind/PV hybrid system," *IEEE Transactions on Energy Conversion*, vol. 11, pp. 367–375, June 1996.

[46] Z. Qing, Y. Nanhua, Z. Xiaoping, Y. You, and D. Liu, "Optimal siting and sizing of battery energy storage system in active distribution network," in *Innovative Smart Grid Technologies Europe*, pp. 1–5, Oct. 2013.

[47] A. Barnes, J. Balda, A. Escobar-Mejia, and S. Geurin, "Placement of energy storage coordinated with smart PV inverters," in *Innovative Smart Grid Technologies*, pp. 1–7, Jan. 2012.

[48] Y. Tang, X. Mao, and R. Ayyanar, "Distribution system modeling using CYMDIST for study of high penetration of distributed solar photovoltaics," in *North American Power Symposium*, pp. 1–6, Sept. 2012.

[49] T. H. Cormen, C. E. Leiserson, R. L. Rivest, and C. Stein, *Introduction to algorithms*. Cambridge: MIT press, 2001.

[50] J. Nesetril, E. Milkova, and H. Nesetrilova, "Otakar boravka on minimum spanning tree problem translation of both the 1926 papers, comments, history," *Discrete Mathematics*, vol. 233, pp. 3–36, 2001.

[51] M. Mares, "The saga of minimum spanning trees," *Computer Science Review*, vol. 2, no. 3, pp. 165–221, 2008.

[52] W. Kersting, "Radial distribution test feeders," *IEEE Transactions on Power Systems*, vol. 6, no. 3, pp. 975–985, 1991.

[53] R. Dugan and T. McDermott, "An open source platform for collaborating on smart grid research," in *Power and Energy Society General Meeting*, pp. 1–7, July 2011.

[54] OpenDSS Repository of source code for OpenDSS; Available at: http://svn.code.sf.net/p/electricdss/code/trunk/Source/, 2013.

[55] "Motors and generators," *ANSI/NEMA Standards Publication MG 1-1993, Rev. 4*, June 1997.

[56] "IEEE standard test procedure for polyphase induction motors and generators," *IEEE Standard 112*, 1991.

[57] R. C. Dugan, M. F. McGranaghan, and H. W. Beaty, eds., *Electrical power systems quality*. New York, NY: McGraw-Hill, 1996.

[58] C. Lin, C.-S. Chen, T. Ku, and C. Ho, "Mitigation of three-phase unbalancing for distribution feeders by rephasing of laterals and distribution transformers," in *IEEE PES Transmission and Distribution Conference and Exposition*, pp. 1–6, April 2010.

[59] T. A. Short, *Electric power distribution handbook*. Boca Raton, FL: CRC press, 2014.

[60] B. Singh, K. Al-Haddad, and A. Chandra, "A review of active filters for power quality improvement," *IEEE Transactions on Industrial Electronics*, vol. 46, pp. 960–971, Oct. 1999.

[61] P. Enjeti, W. Shireen, P. Packebush, and I. Pitel, "Analysis and design of a new active power filter to cancel neutral current harmonics in three-phase four-wire electric distribution systems," *IEEE Transactions on Industry Applications*, vol. 30, pp. 1565–1571, Nov. 1994.

[62] DOE/EPRI 2013 electricity storage handbook in collaboration with NRECA, Prepared by Sandia National Laboratories; Available at: http://www.sandia.gov/ess/pubs_tech.html, 2013.

[63] IBM ILOG CPLEX optimization studio; Available at : http://www-03.ibm.com/software/products/en/ibmilogcpleoptistud/.

[64] "IEEE application guide for IEEE std. 1547(tm), IEEE standard for interconnecting distributed resources with electric power systems," *IEEE Std. 1547.2-2008*, pp. 1–217, Apr. 2009.

[65] C. Marnay, F. Robio, and A. Siddiqui, "Shape of the microgrid," in *Power Engineering Society Winter Meeting*, vol. 1, pp. 150–153 vol.1, Jan 2001.

[66] Capstone C200 microturbine technical reference; Available at: http://www.capstoneturbine.com/prodsol/products/, 2013.

[67] Characterization of the installed costs of prime movers using gaseous opportunity fuels, Prepared by Oak Ridge National Laboratory; Available at: https://www1.eere.energy.gov/manufacturing/distributedenergy/pdfs /characterization_installed_costs.pdf, 2013.